

**POLITECNICO  
DI TORINO**

Master Thesis in Aerospace Engineering

# Modeling, Dynamics, and Control of Orbiting Distributed Systems

*Supervisor:*

**Prof. Lorenzo CASALINO**

Politecnico di Torino

*Mentor:*

**Dr. Marco B. QUADRELLI**

Jet Propulsion Laboratory, California Institute of Technology

*Candidate:*

**Riccardo APA 258613**



*This research was carried out at Jet Propulsion Laboratory, California Institute of Technology, during an internship sponsored by JVSRP (JPL Visiting Student Research Program) and NASA (National Aeronautic and Space Administration).*



# Acknowledgments

I would like to thank my supervisor at Politecnico di Torino, Prof. Lorenzo Casalino and my JPL mentor, Dr. Marco Quadrelli, who both inspired and supported me during my research.

To my dear friends and to all those who have believed in me and whose esteem for me has always given me the strength and determination to always go forward to the best of my ability.

To my grandparents who taught me to never stop in front of difficulties and to always face them with tenacity and sense of sacrifice.

To my father, my mother and my brother, who have made me what I am, who have given me a happy and light-hearted life, who have always taught me what are the most important things in life, who have supported me in every choice I have made, who have always made me feel loved and who have always believed in me even when I didn't. To them I mainly dedicate this work because without them I would have never reached this goal, because without them nothing would make sense.

*"That lies in space which I in time must come to, ineluctably."*

JAMES JOYCE



# Abstract

The macro topic treated in this thesis is the analysis of the feasibility and problems related to the operation of autonomous and re-configurable satellite formations. The main objective is to model and control with great precision the relative 6DoF dynamics of the followers with respect to a leader satellite in order to allow a correct taking of the data required by the mission.

The differential accelerations to which the formation satellites are subjected (drift) make it necessary to implement control techniques for their re-positioning. To ensure a long mission duration, the number of such correction maneuvers should be minimized. In an autonomous formation perspective, such corrections are computed by the spacecraft itself, which therefore need to be equipped with sufficient computational resources. In this paper the problems just presented are described in detail and some techniques to mitigate their effects are described. In order to have results more similar to reality, a high precision dynamic propagation model has been created and validated with the NASA General Mission Analysis Tool (GMAT). This model includes harmonics of the gravitational potential up to order 21, drag, solar pressure and third-body perturbation (Moon and Sun).

After defining the external environment in which the satellites operate, the problem of maintaining the desired configuration of the system is addressed through two different analyses: uncontrolled dynamics stability analysis and active formation control. The study of uncontrolled formation stability aims to derive the initial conditions of the formation satellites that most closely minimize the relative *drift* between followers and leader. This allows to reduce the number of maneuvers required to maintain the formation given a fixed interval of time. Despite the careful choice of initial conditions, this *drift*, although minimal, will tend to alter the initial configuration until the formation is no longer operational. For these reasons, two types of closed-loop active control have been implemented. The first type consists of a proportional derivative controller. The quantities to be controlled and their derivatives are measured so that a control command can be generated. This methodology is simple to implement and requires limited computational resources.

The second control methodology aims to minimize the amount of fuel used to perform the correction maneuver. The optimal control is presented in different variants, in particular two strategies, centralized and decentralized, have been implemented in the context of *Sequential Convex Programming (SCP)*. Both types of control were analyzed considering unmodeled external factors.

Finally, the possibility of total or partial reconfiguration of the formation is analyzed through the description of the algorithm that allows to assign to each satellite of the old configuration its place in the new one in such a way that the cost to perform this maneuver is minimized.

Some test cases are discussed so that discussion and conclusions can be made regarding the limitations and issues associated with the methodologies implemented.

# Sommario

Il macro argomento trattato in questa tesi é l'analisi di fattibilità e delle problematiche legate alle operazioni di formazioni di satelliti autonome e riconfigurabile. L'obiettivo principale é quello di modellizzare e controllare con molta precisione la dinamica 6DoF relativa dei spacecrafts followers rispetto ad un satellite leader in modo tale da permettere una corretta presa dei dati richiesti dalla missione.

Le accelerazioni differenziali a cui sono sottoposti i satelliti della formazione (drift) rendono necessaria l'implementazione di tecniche di controllo per il loro riposizionamento. Per garantire una lunga durata della missione, il numero di tali manovre di correzione dovrebbe essere minimizzato. In un'ottica di formazione autonoma, tali correzioni sono calcolate dagli spacecrafts stessi che quindi devono essere dotati di sufficienti risorse computazionali. In questo lavoro i problemi appena presentati sono descritti nel dettaglio e alcune tecniche per poterne mitigare gli effetti sono descritte. Per poter avere dei risultati più simili alla realtà, un modello di propagazione dinamica ad alta precisione é stato creato e validato con il General Mission Analysis Tool (GMAT) della NASA. Tale modello include armoniche del potenziale gravitazionale fino ad ordine 21, resistenza aerodinamica, pressione solare, perturbazione del terzo corpo (Luna e Sole).

Dopo aver definito l'ambiente esterno in cui i satelliti operano, il problema del mantenimento della configurazione desiderata del sistema viene affrontato attraverso due analisi differenti: analisi di stabilità della dinamica incontrollata e controllo attivo della formazione. Lo studio della stabilità della formazione incontrollata ha l'obiettivo di derivare le condizioni iniziali dei satelliti della formazione che più minimizzano il *drift* relativo tra followers e leader. Questo permette di ridurre in numero di manovre necessarie per mantenere la formazione dato un intervallo di tempo fissato. Nonostante l'accurata scelta delle condizioni iniziali, tale *drift*, seppur minimo, tenderà ad alterare la configurazione iniziale fino a quando la formazione non sarà più operativa. Per tali motivi due tipologie di controllo attivo ad anello chiuso sono state implementate. La prima tipologia consiste in un controllore proporzionale derivativo. Le quantità da controllare e le loro derivate sono misurate in modo tale

da poter generare un comando di controllo. Tale metodologia risulta semplice da implementare e richiede limitate risorse computazionali. La seconda metodologia di controllo ha invece lo scopo di minimizzare la quantità di carburante utilizzato per effettuare la manovra di correzione. Il controllo ottimale viene presentato in diverse varianti, in particolare due strategie, centralizzata e decentralizzata, sono state implementate nel contesto della *Sequential Convex Programming (SCP)*. Entrambe le tipologie di controllo sono state analizzate considerando fattori esterni non modellizzati.

Infine, la possibilità di riconfigurazione totale o parziale della formazione viene analizzata attraverso la descrizione dell'algoritmo che permette di assegnare ad ogni satellite della vecchia configurazione il suo posto in quella nuova in modo tale che il costo per effettuare tale manovra sia minimizzato.

Alcuni test cases vengono discussi in modo tale da poter effettuare delle conclusioni critiche riguardanti i limiti e le problematiche legate alle metodologie implementate.

# Contents

|   |             |
|---|-------------|
| <b>Acknowledgments</b>  | <b>IV</b>   |
| <b>Abstract</b>   | <b>VI</b>   |
| <b>Sommario</b>   | <b>VIII</b> |
| <b>1 Introduction</b>   | <b>1</b>    |
| 1.1 What is Spacecraft Formation Flying? . . . . .                | 1           |
| 1.2 Features and Properties of Formation Flying . . . . .         | 2           |
| 1.3 Potentialities and Problems . . . . .                         | 4           |
| 1.4 Possible Applications and Formation Flying Missions . . . . . | 6           |
| 1.5 Work Subdivision . . . . .                                    | 12          |
| <b>2 Theoretical background</b>                                   | <b>14</b>   |
| 2.1 Notation . . . . .  | 14          |
| 2.2 Reference Frames . . . . .                                    | 17          |
| 2.2.1 ECI Frame . . . . .   | 17          |
| 2.2.2 LVLH Frame . . . . .  | 18          |
| 2.2.3 BF frame . . . . .  | 19          |
| 2.3 Description of the Motion . . . . .                           | 20          |
| 2.3.1 Translational Motion . . . . .                              | 20          |
| 2.3.2 Rotational Motion . . . . .                                 | 21          |
| <b>3 High-Fidelity Orbital Mechanics Propagation Model</b>        | <b>24</b>   |
| 3.1 Force Modeling . . . . .                                      | 24          |
| 3.1.1 Gravity Potential Perturbation . . . . .                    | 25          |
| 3.1.2 Drag Perturbation . . . . .                                 | 27          |
| 3.1.3 Solar Pressure Perturbation . . . . .                       | 29          |
| 3.1.4 Third-body Perturbation . . . . .                           | 32          |
| 3.1.5 Propagation of the Orbit . . . . .                          | 32          |

|          |   |            |
|----------|---|------------|
| <b>4</b> | <b>Relative motion</b>  | <b>33</b>  |
| 4.1      | Relative Translational Dynamics Modeling . . . . .                        | 35         |
| 4.2      | Rotational Dynamics Modeling . . . . .                                    | 36         |
| 4.3      | Non-Linear Complete State Space Representation . . . . .                  | 38         |
| <b>5</b> | <b>Configurations and Stability</b>                                       | <b>41</b>  |
| 5.1      | Clohessy-Wiltshire IRC . . . . .  | 42         |
| 5.2      | Remote Sensing Configurations . . . . .                                   | 44         |
| 5.2.1    | Interferometric Cartwheel (IC) Configuration . . . . .                    | 47         |
| 5.2.2    | Cross-Track Pendulum (CTP) Configuration . . . . .                        | 49         |
| 5.2.3    | Cartwheel-Pendulum (CP) Configuration . . . . .                           | 51         |
| 5.2.4    | Helix Configuration . . . . .   | 53         |
| 5.2.5    | Stability of the CW Initial Conditions . . . . .                          | 55         |
| 5.2.6    | IC free-flying CW Initial Conditions stability . . . . .                  | 56         |
| 5.2.7    | CTP free-flying CW Initial Conditions stability . . . . .                 | 58         |
| 5.2.8    | CP free-flying CW Initial Conditions stability . . . . .                  | 60         |
| 5.2.9    | Helix free-flying CW Initial Conditions stability . . . . .               | 62         |
| 5.3      | Energy Matching (EM) Initial Conditions Method . . . . .                  | 64         |
| 5.3.1    | Linear Energy Matching . . . . .  | 64         |
| 5.3.2    | Non-Linear Energy Matching . . . . .                                      | 66         |
| 5.3.3    | Energy Matching including $J_2$ perturbation . . . . .                    | 68         |
| 5.3.4    | Stability of the EM including $J_2$ Initial Conditions . . . . .          | 72         |
| <b>6</b> | <b>Formation Control and Reconfigurability</b>                            | <b>79</b>  |
| 6.1      | Proportional Derivative (PD) Control Method . . . . .                     | 80         |
| 6.2      | Optimal Control Method . . . . .  | 82         |
| 6.2.1    | Definition of the General Optimal Control Problem . . . . .               | 83         |
| 6.2.2    | Convexification of the Optimal Control Problem . . . . .                  | 84         |
| 6.3      | Sequential Convex Programming (SCP) . . . . .                             | 90         |
| 6.4      | Closed Loop Control with Sequential Convex Programming (CL-SCP) . . . . . | 92         |
| 6.5      | Reconfigurability . . . . .   | 94         |
| <b>7</b> | <b>Numerical Results and Discussion</b>                                   | <b>100</b> |
| 7.1      | Common Parameters . . . . .   | 100        |
| 7.2      | Drift Correction . . . . .  | 102        |
| 7.2.1    | PD Controller . . . . .   | 102        |
| 7.2.2    | Optimal Controller de-centralized SCP . . . . .                           | 111        |
| 7.2.3    | Optimal Controller centralized SCP . . . . .                              | 114        |
| 7.2.4    | Optimal Controller de-centralized CL-SCP . . . . .                        | 116        |

|          |  |            |
|----------|--|------------|
| 7.3      | Discussion . . . . .   | 123        |
| 7.4      | Closed-Loop Partial reconfiguration . . . . .                          | 125        |
| <b>8</b> | <b>Conclusions and Future Work</b>                                     | <b>129</b> |
| 8.1      | Research Outcome and Discussion . . . . .                              | 129        |
| 8.2      | Future Works . . . . .   | 130        |
|          | <b>Appendices</b>  | <b>137</b> |
|          | <b>Appendix A Model Validation</b>                                     | <b>137</b> |
|          | <b>Appendix B Relative Motion under <math>J_2</math> perturbation</b>  | <b>143</b> |
|          | <b>Appendix C Centralized Optimal Problem</b>                          | <b>145</b> |
|          | <b>Appendix D Test case: Optimal control high-number of satellites</b> | <b>147</b> |

# List of Figures

|      |   |    |
|------|---|----|
| 1.1  | PRISMA possible scenario for Autonomous Formation Flying, [42] . . .  | 7  |
| 1.2  | Artist’s view of the LISA space mission, [47] . . . . .   | 8  |
| 1.3  | Artist’s view of the MMS space mission, [51] . . . . .  | 9  |
| 1.4  | 3D CAD model of star-shade spacecraft, [6] . . . . .  | 10 |
| 1.5  | Nominal configuration of NWO mission, [6] . . . . .   | 10 |
| 1.6  | Initial orbits design for TanDEM-X mission, [13] . . . . .  | 11 |
| 1.7  | MASSIM spacecrafts operating scenario, [15] . . . . .   | 12 |
| 2.1  | ECIJ2000 Frame, [5] . . . . .   | 18 |
| 2.2  | LVLH Frame, [52] . . . . .  | 19 |
| 2.3  | Keplerian elements, [2] . . . . .   | 21 |
| 3.1  | Conical shadow model, [33] . . . . .  | 30 |
| 3.2  | Apparent disks for $\nu$ computation, [33] . . . . .  | 31 |
| 4.1  | Chief and deputy LVLH frame description, [7] . . . . .  | 34 |
| 5.1  | Bistatic radar working principle, [37] . . . . .  | 45 |
| 5.2  | Multistatic radar working principle. <i>Left:</i> Fully-active configuration.<br><i>Right:</i> Semi-active configurations, [37] . . . . . | 46 |
| 5.3  | Representation of radar <i>Baseline</i> , [23] . . . . .  | 46 |
| 5.4  | 3D representation of IC configuration . . . . .   | 48 |
| 5.5  | Time-evolution of IC configuration, [37] . . . . .  | 49 |
| 5.6  | 3D representation of CTP configuration . . . . .  | 50 |
| 5.7  | Time-evolution of CTP configuration, [37] . . . . .   | 51 |
| 5.8  | 3D representation of CP configuration . . . . .   | 52 |
| 5.9  | Time-evolution of CP configuration, [37] . . . . .  | 53 |
| 5.10 | 3D representation of Helix configuration . . . . .  | 54 |
| 5.11 | Time-evolution of Helix configuration, [37] . . . . .   | 55 |
| 5.12 | IC relative dynamics propagation, CW Initial Conditions . . . . .   | 57 |
| 5.13 | CTP relative dynamics propagation, CW Initial Conditions . . . . .  | 59 |

|      |  |     |
|------|--|-----|
| 5.14 | CP relative dynamics propagation, CW Initial Conditions . . . . .                                    | 61  |
| 5.15 | Helix relative dynamics propagation, CW Initial Conditions . . . . .                                 | 63  |
| 5.16 | IC relative dynamics propagation, EM $J_2$ Initial Conditions . . . . .                              | 74  |
| 5.17 | CT relative dynamics propagation, EM $J_2$ Initial Conditions . . . . .                              | 75  |
| 5.18 | CP relative dynamics propagation, EM $J_2$ Initial Conditions . . . . .                              | 76  |
| 5.19 | Helix relative dynamics propagation, EM $J_2$ Initial Conditions . . . . .                           | 77  |
| 6.1  | <i>Left</i> Non-convex CA constraint, <i>Right</i> Convex CA constraint, [44] . . . . .              | 88  |
| 6.2  | <i>Left</i> : Trajectory given by SCP . <i>Right</i> : Trajectory given by CL-SCP,<br>[44] . . . . . | 94  |
| 7.1  | Trajectories drift correction PD controller . . . . .  | 103 |
| 7.2  | Position errors history drift correction PD controller . . . . .                                     | 104 |
| 7.3  | Velocity errors history drift correction PD controller . . . . .                                     | 104 |
| 7.4  | Actuation Forces drift correction PD controller . . . . .  | 106 |
| 7.5  | $\hat{z}_{BF}$ field drift correction PD controller . . . . .  | 107 |
| 7.6  | $\hat{z}_{BF}$ field drift correction PD controller (detail) . . . . .                               | 108 |
| 7.7  | Quaternion errors history drift correction PD controller . . . . .                                   | 108 |
| 7.8  | Angular velocity errors history drift correction PD controller . . . . .                             | 109 |
| 7.9  | Actuation Torques drift correction PD controller . . . . .   | 110 |
| 7.10 | Trajectories drift correction Optimal controller de-centralized SCP . . . . .                        | 112 |
| 7.11 | Actuation Forces drift correction Optimal controller de-centralized SCP                              | 113 |
| 7.12 | Trajectories drift correction Optimal controller centralized SCP . . . . .                           | 114 |
| 7.13 | Actuation Forces drift correction Optimal controller centralized SCP . . . . .                       | 115 |
| 7.14 | Trajectories drift correction Optimal controller de-centralized CL-SCP . . . . .                     | 117 |
| 7.15 | Actuation Forces drift correction Optimal controller de-centralized<br>CL-SCP . . . . .              | 118 |
| 7.16 | $xy$ trajectories comparison between SCP and CL-SCP . . . . .  | 119 |
| 7.17 | $xy$ trajectories comparison between SCP and CL-SCP (detail) . . . . .                               | 119 |
| 7.18 | $\hat{z}_{BF}$ field drift correction Optimal controller CL-SCP . . . . .                            | 120 |
| 7.19 | Quaternion errors history drift correction Optimal controller CL-SCP . . . . .                       | 121 |
| 7.20 | Angular velocity errors history drift correction Optimal controller CL-<br>SCP . . . . .             | 121 |
| 7.21 | Actuation Torques drift correction Optimal controller CL-SCP . . . . .                               | 122 |
| 7.22 | Trajectories partial re-configuration Optimal controller de-centralized<br>SCP . . . . .             | 126 |
| 7.23 | Actuation Forces partial re-configuration Optimal controller de-centralized<br>SCP . . . . .         | 127 |
| 7.24 | Trajectories drift correction non-optimal places assignation . . . . .                               | 128 |

|     |  |     |
|-----|--|-----|
| A.1 | GMAT comparison, Gravitational Potential (up to grade 4 order 4)                             | 138 |
| A.2 | GMAT comparison, Drag (Harris <i>priestervsJacchia</i> )                                     | 139 |
| A.3 | GMAT comparison, Solar Pressure  | 140 |
| A.4 | GMAT comparison, Third-body (Moon)   | 141 |
| A.5 | GMAT comparison, Third-body (Sun)  | 142 |
|     |  |     |
| D.1 | Trajectories 80 satellites Optimal controller de-centralized SCP                             | 148 |
| D.2 | Position errors history drift correction 80 satellites Optimal controller de-centralized SCP | 148 |
| D.3 | Velocity errors history drift correction 80 satellites Optimal controller de-centralized SCP | 149 |
| D.4 | Actuation Forces drift correction 80 satellites Optimal controller de-centralized SCP        | 150 |

# List of Tables

|      |   |     |
|------|---|-----|
| 5.1  | Initial Orbital Parameter of the Leader spacecraft . . . . .              | 55  |
| 5.2  | IC parameters for simulation. . . . .                                     | 56  |
| 5.3  | CTP parameters for simulation. . . . .                                    | 58  |
| 5.4  | CP parameters for simulation. . . . .                                     | 60  |
| 5.5  | Helix parameters for simulation. . . . .                                  | 62  |
| 7.1  | Initial Orbital Parameters of the Leader spacecraft, control simulations  | 100 |
| 7.2  | Initial inertial properties and dimensions . . . . .                      | 101 |
| 7.3  | Actuators properties . . . . .  | 101 |
| 7.4  | Helix final parameters for drift correction simulation. . . . .           | 102 |
| 7.5  | PD gains definition . . . . .   | 103 |
| 7.6  | SCP simulation paramters . . . . .  | 111 |
| 7.7  | Computational times comparison . . . . .                                  | 116 |
| 7.8  | Final position errors drift corrections simulations . . . . .             | 124 |
| 7.9  | Fuel consumption summary drift corrections simulations . . . . .          | 124 |
| 7.10 | $\mathbf{y}$ physical meaning . . . . .                                   | 125 |
| 7.11 | Fuel consumption partial re-configuration . . . . .                       | 128 |
| D.1  | SCP simulation paramters . . . . .  | 147 |
| D.2  | Helix final parameters for drift correction 80 satellites simulation. . . | 148 |
| D.3  | Fuel consumption summary drift corrections 80 satellites simulations      | 151 |

# Chapter 1

## Introduction

The purpose of this chapter is to introduce the concept of spacecraft formation flying giving a definition of it and to explain why there is an extensive research effort on this type of system, underlying its potentialities and the problems related to its operation. A brief overview of the concepts that are related to formation flying will be presented in order to have in mind what are the actors involved and the parameters of interest in the study of formations. In addition some possible applications of formation flying and representative missions effectuated by NASA and ESA will be reported in order to give an idea of the state of the art of this technology. Finally, last section outlines the general organization of this work, anticipating what are the main topics treated in the next chapters.

### 1.1 What is Spacecraft Formation Flying?

There are different opinions regarding the definition of *Spacecraft Formation Flying*. It is often confused with the more common definition of *Constellation*. In fact, the concept of formation flying is slightly different from it, and is a subclass of the broader category that goes by the name of *Distributed Space Systems*. Following the definitions given by NASA's Goddard Space Flight Center (GSFC) it is possible to distinguish:

- **Distributed Space Systems**

*An end-to-end system including two or more space vehicles and a cooperative infrastructure for science measurement, data acquisition, processing, analysis and distribution.*

- **Constellation**

*A collection of space vehicles that constitutes the space element of a distributed*

*space system.*

- **Space Formation Flying**

*The tracking or maintenance of a desired relative separation, orientation or position between or among spacecraft.*

It is then possible to conclude that the concept of space formation flying implies characteristics belonging to the class of *Distributed Space Systems* and expands the concept of *Constellation* referring rather to all the methodologies used to ensure that the system maintain or change the relative position and attitude between the spacecrafts that compose the formation. After these definitions, it is clear how Formation Flying operations are strictly related to those of the Guidance, Navigation, and Control (GN&C) system.

It is also important to define some of the aspects characterizing such a system which will be used extensively in the next sections. NASA GSFC also defines:

- **Virtual Platform**

*A spatially distributed network of individual vehicles collaborating as a single functional unit, and exhibiting a common system-wide capability to accomplish a shared objective.*

The definition subtends what is better explained in Section 1.4, i.e. it is that one of the main reasons for which the formations are used is their ability to achieve tasks through collaboration between the individual elements that a monolithic spacecraft can not achieve. No further details are given about the last two terms since their meaning will be more evident and clarified in the next sections.

## 1.2 Features and Properties of Formation Flying

This section aims at outlining what the main features of the Formation Flying are and what the main differences with respect to a single spacecraft approach exist. Some general aspects that can be referred to any Formation Flying are presented in the following list, even if the case of formation flying in Low Earth Orbit (LEO) will be treated with more attention in this work.

- **Orbit Tracking**

As an ensemble of single spacecrafts, it results possible to adopt a classical approach by considering the dynamics of the single spacecraft and imposing that its trajectory follows a target trajectory calculate by the preliminary study of the desired relative dynamics. This approach does not take into account the essential necessities of formation where rather the objective is to directly

impose the relative dynamics and act directly on it. The latter is in line with the fact that the formation will achieve its assigned goals if the relative position and attitude are correct, not being interested in the absolute position of the single spacecraft. From this new Orbit Tracking method it follows the relative dynamics description through a chief/deputy approach.

- **Chief/Deputy Approach**

In order to describe the relative motion, it is necessary to identify an object against which to describe this dynamics. This object is called the chief (or leader) spacecraft. The chief can be a real spacecraft belonging to the formation or a virtual one. The chief is also placed at the origin of a non-inertial reference frame wrt all the dynamics is described. The other spacecrafts of the formation will be named as deputies (or followers) and their motion will be described wrt the chief non-inertial reference frame. This approach will allow to control directly the relative dynamics.

- **Autonomous Property**

Because a great number of Formation Flying applications foresees a close-proximity motion between spacecrafts, such a system is often endowed with autonomous management of the relative dynamics. The higher the number of elements in the formation, the greater the need to make it autonomous as the potential risk of collision increases. We can also state that the greater the number of satellites in the formation, the greater the computational cost of recalculating the dynamics of an autonomous formation. This last aspect is closely related to the concept of formation architecture.

- **Architecture**

Another crucial aspect when dealing with Formation Flying is the Architecture of the system. According to the requirements of the mission in terms of precision of the relative dynamics control, different designs of the on-board systems such as inter-satellite communication system, metrology system, data handling system etc... can be envisaged. Two main categories of Architecture are present. The first is the so-called centralized Architecture, which foresees the chief spacecraft as the spacecraft deputed to perform the great majority of calculations, limiting the inter-satellite communications at the cost of a higher computational load. The second is the de-centralized Architecture which foresees distributed computational resources among the spacecrafts of the Formation but requiring a high performance inter-satellite communication system.

Having in mind these main features of Formation Flying, it is now possible to show

the potentiality and problems related to such a system.

### 1.3 Potentialities and Problems

It often happens that as the complexity of a system increases, there is greater difficulty in its management. This statement also applies in the case of Formation Flying. Both these aspects are a consequence of the main characteristic of the formation, that is the presence of a multiplicity of spacecrafts that collaborate to reach a common objective. It is evident that this multiplicity is the basis of the following advantages:

- **Reconfiguration Capacity**

Such a system is very flexible and allows to the possibility of re-configuring the formation. There is nothing to prevent the system from being able to change the relative position between individual spacecrafts so that a configuration can be obtained that is more suitable for obtaining a certain type of data rather than another. It is not only possible to change the shape of the Formation, but also the variation of its size can prove very useful in a multiple-objectives mission. This aspect is particularly useful in many applications as will be highlighted in the following section.

- **Fault-Tolerant System**

The greater the number of satellites that make up the formation, the more robust the system itself is against possible faults. In fact, in the event that a satellite is no longer active due to damage to their systems or other, it could be replaced by another satellite in the formation. Clearly this aspect also depends on the number of satellites present, which in turn affects the cost of the mission. The crucial consequence is that in any case the mission can be completed even with a decrease in performance.

- **Low-cost System**

Many applications of Formation Flying foresee the use of low-cost spacecrafts. This is an aspect of great relevance, in fact, space companies are always concerned with the cost of mission. So, the possibility of accomplishing tasks that a monolithic spacecraft can not achieve, united to the fault-tolerance aspect, makes this kind of system very attractive. Swarms take this concept to the extreme. One branch of research focuses on studying the control of thousands or even tens of thousands of inexpensive little robots that make up a "cloud." Such a system would present a very high fault-tolerance, making the replacement of a robot almost insignificant [32].

- **Light-Weight System**

Considering that Formation usually involves a relatively great number of units, the satellites composing the formation are usually small in size. This implies the system to be light-weight and results in a particular simplicity of space management inside the launcher. It is also evident how this aspect brings with it the concept of low-cost system just described.

As mentioned at the beginning of the section, the positive aspects are usually accompanied by the negative ones. It is always a matter of a trade-off that is most driven by mission requirements.

With this premise, it is also possible to present some possible disadvantages of a Formation Flying system compared to a single spacecraft so that we can better understand in which direction current research efforts are oriented and in which cases and to what extent it is possible to mitigate these problems. The most evident difficulties related to such a system are presented in the following list:

- **Computationally Expensive System**

A system consisting of a large number of satellites involves knowing the trajectories of each one. If to this aspect we add a requirement on the accuracy of the propagation of these orbits (since often, as mentioned above, Formation Flying presents close-proximity dynamics) it is clear that the system must be equipped with a high performance data handling system. This aspect is often not compatible with the dimensions usually employed for such a system. For these reasons a great effort of research towards high performance algorithms has been developed in recent years. Different solutions are applied depending on the architecture implemented.

- **Stability of the Formation**

Stability of the Formation refers to the self-maintaining of the relative positions when the system is not subject to control. All the perturbations to which the space environment is subject act on the system. These perturbations depend on the position and speed vectors of each spacecraft, which, being a priori different, give rise to differential accelerations that lead to a drift of the configuration. This concept is closely related to that of initial conditions which must be chosen in such a way as to minimize drift over time.

- **Fuel Consumption**

Another crucial aspect is fuel consumption. As mentioned earlier, relative drift involves a "break" in the initial formation configuration. In order to bring the system back to correct operation, it is necessary to carry out a check. In order to ensure a longer mission duration, and especially in case of satellites with

limited range, it is necessary to provide re-positioning algorithms that tend to minimize fuel waste.

- **Control and Task Assignment Complexity**

Formation Control is a complex task. In order to perform good data taking, the relative position must be controlled with high-precision. It is clear how this becomes more complex as the number of satellites in the formation increases. Moreover, the control methodology varies depending on the strategy adopted, i.e. on-board calculation control or ground-based control. Without going into detail, it is possible to imagine how these types of choices can give rise to a large number of cases and related design solutions.

Task Assignment problem is more related to reconfiguration capacity aspect. In case of reconfiguration of the system, an algorithm of Task Assignment which gives the single spacecraft the place it must occupy within the formation, must be provided. Such an algorithm must assign places in such a way as to avoid crossings between spacecrafts as much as possible and collisions. Further complications arise if a Task Assignment that includes cases where one or more satellites are no longer active (partial reconfiguration) is considered. These two aspect are correlated with the computational efficiency of the system and with fuel management, which are often limited for small satellites.

The majority of the problems presented can be mitigate adopting several solutions which depend on the particularities of the analysed system. In the following Chapters some of these solutions will be presented and analysed in detail in order to understand to what extent these problems can be solved. Ultimately, it is possible to state that the positive aspects justify the increment in complexity, so making Formation Flying a very promising system. The next section presents some possible applications of Formation Flying systems.

## 1.4 Possible Applications and Formation Flying Missions

There are many possible applications of Formation Flying system, they range from remote sensing of planets, measurements of gravity potential field, to the detection of gravitational waves etc... [20]. This section presents some real missions involving Formation Flying in order to show how wide their implementation is.

The first example is the Swedish-led technology ESA Prototype Research Instruments and Space Mission technology Advancement (PRISMA) mission which has been successfully launched on June 15, 2010. The purpose of this mission is to

demonstrate the feasibility and advantages of Formation Flying by implementing small-satellites endowed with advanced proximity ranging and propulsion systems. In particular, PRISMA was intended to perform GN&C demonstrations like autonomous Formation Flying, Homing and Rendez-Vous and to test technology as GPS-based navigation, RF metrology and star tracker-based vision navigation. Figure 1.1 show a possible scenario of Autonomous Formation Flying (AFF) of the PRISMA mission.

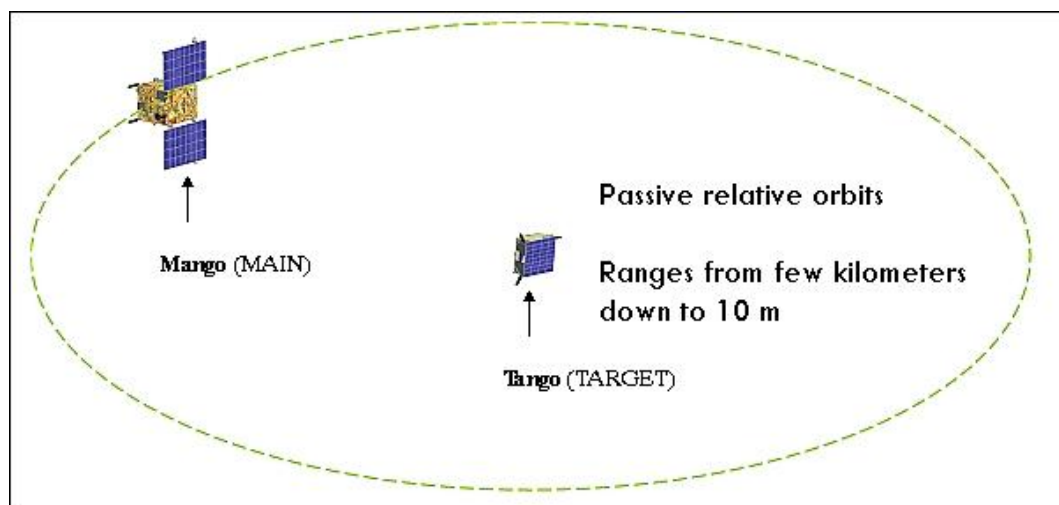


**Figure 1.1:** PRISMA possible scenario for Autonomous Formation Flying, [42]

Another important ESA mission which has analogous objectives is the PROBA-3 mission. It will be launched in 2023 into a highly elliptical orbit (600 x 60530 km at around 59 degree inclination). The formation is composed of two satellites which will be deployed in Tandem formation [13]. In order to avoid high fuel consumption the orbits followed by the spacecrafts will be divided into six hours of formation flying manoeuvres at apogee while the rest of the orbits will be traveled in passive safe drifting.

A very important mission involving a collaboration between ESA and NASA is the Laser Interferometer Space Antenna (LISA) whose launch is scheduled in the early 2030s. It is composed of three spacecrafts that form an equilateral triangle whose sides are approximately a million miles long. It aims at detecting gravitational waves (space-time distortions) produced by ultra-compact binaries in our Galaxy, supermassive black hole mergers, and/or extreme mass ratio inspirals. To do so, it measures relative position between the spacecrafts with laser technology, being the relative position sensitive to the gravitational waves which would cause a slight variation of it. The system will require a very high-stability in order to be able to

detect relative shifts in position that are less than the diameter of a helium nucleus over a distance of a million miles. A graphic representation of the LISA system is showed in Figure 1.2.

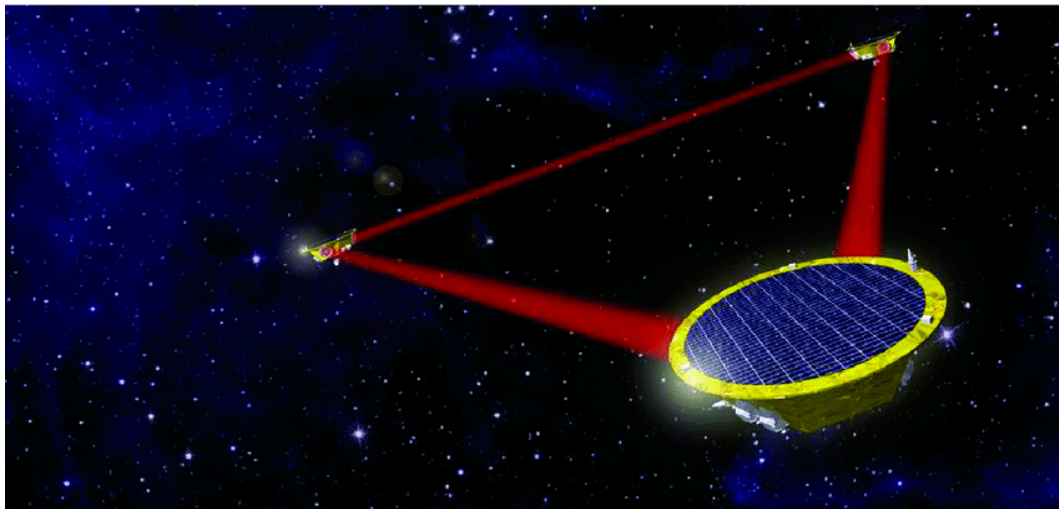


**Figure 1.2:** Artist's view of the LISA space mission, [47]

Another NASA mission which deserves to be mentioned is Magnetospheric Multiscale Mission (MMS) launched in 2015 and still operational (end of mission expected in 2040). MMS aims at studying the Earth's magnetosphere, using four identical spacecraft flying in a variable sides tetrahedral formation. To do so, the spacecrafts gather information about the microphysics of magnetic reconnection, energetic particle acceleration, and turbulence processes that occur in many astrophysical plasma. In order to take good measurements, the four satellites have to maintain their tetrahedral relative position when passing through regions of interest (the so-called dayside magnetopause and magnetotail). Spacecrafts are provided with an high-accuracy relative position measurements instrumentation based on high altitude rated GPS receiver, and are periodically corrected by maneuvers. An artistic depiction of the MMS system is given in Figure 1.3.

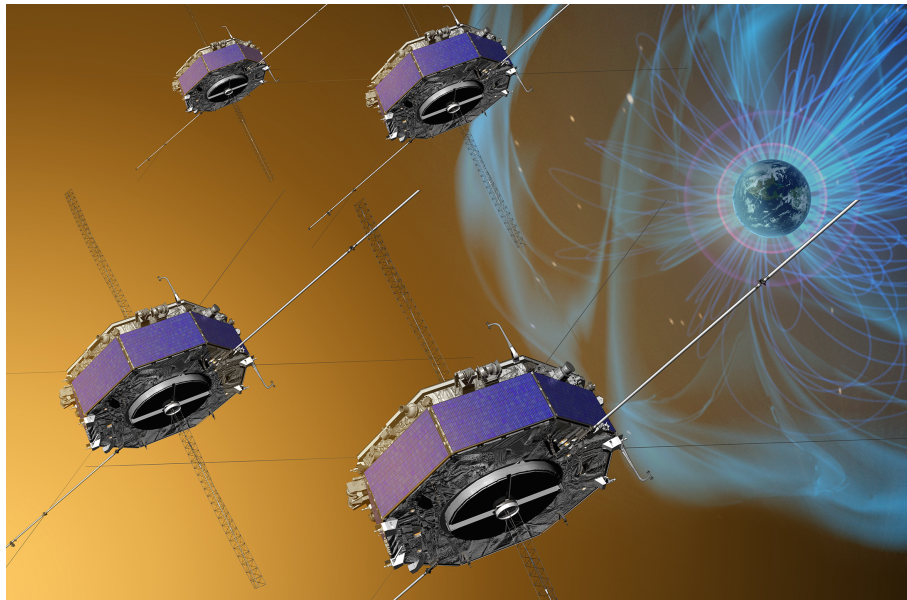


**Figure 1.3:** Artist's view of the MMS space mission, [51]

Regarding space exploration the NASA funded mission involving Formation Flying New World Observer (NWO) mission is of relevant importance for the innovative strategies implemented. NWO aims at characterizing extra-solar planets. The formation is made of two satellites , a large telescope and a star-shade spacecraft, flying at the Earth–Sun L2 (Lagrangian) point or in a drift-away solar orbit. In Figure 1.4 it is possible to visualize a 3D CAD model of the star-shade spacecraft. The problem with detection of exo-planets is the presence of light noise produced by the star the planet is orbiting around. NWO mission solves this issue suppressing the starlight before it enters the telescope.

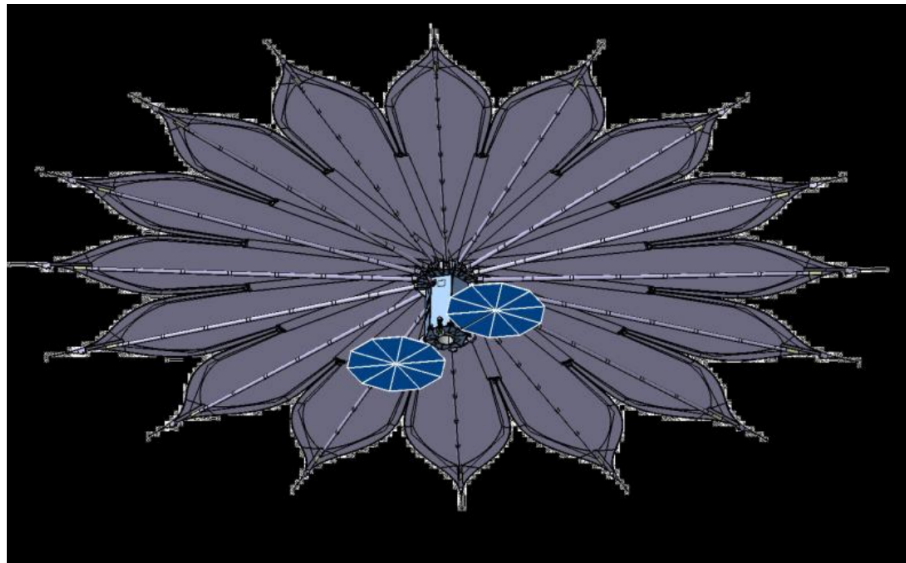


**Figure 1.4:** 3D CAD model of star-shade spacecraft, [6]

This task is achieved through a configuration which presents the star-shade spacecraft operating 70000 km from the telescope being maneuvered into the near line-of-sight of the telescope. A representation of this configuration is presented in Figure 1.5.

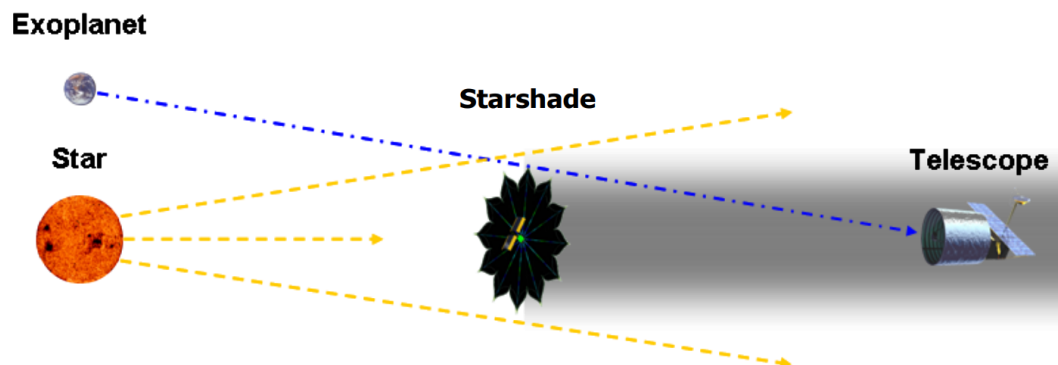


**Figure 1.5:** Nominal configuration of NWO mission, [6]

In regards to remote sensing, a very recent project is the TanDEM-X (TerraSAR-X add-on for Digital Elevation Measurements). The objective of the mission is the generation of a consistent global digital elevation model (DEM) with an unprecedented accuracy [13]. TanDEM-X is made of two radar satellite flying in close formation and provides a highly re-configurable platform for the demonstration of new radar imaging techniques and applications. The system is based on an innovative phase synchronization link through which bistatic data can be obtained. The orbits of the spacecrafts are initialized in order to obtain an helix configuration (Figure 1.6). The

helix configuration is widely used in Formation Flying for remote sensing purposes because it enables an interferometric mapping of the complete Earth surface [40].

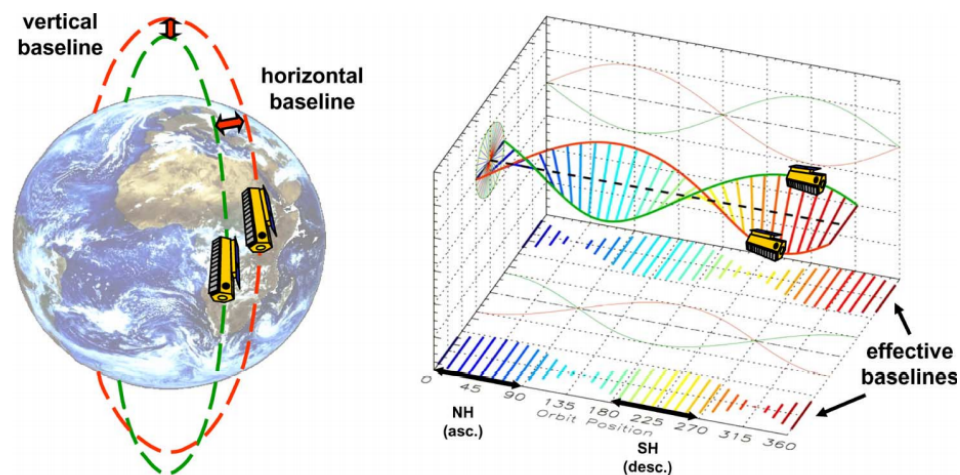
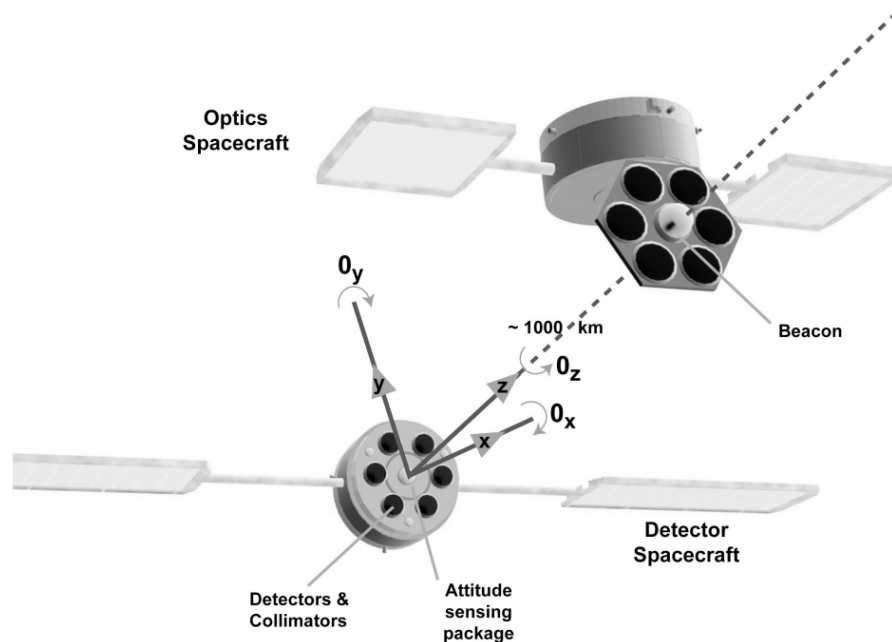


Figure 1.6: Initial orbits design for TanDEM-X mission, [13]

The last example is the NASA Milli-Arc-Second Structure Imager (MASSIM) mission. It aims at imaging the structure of astrophysical objects (like jets from black holes) with very accurate precision working in X-rays band. The formation presents two spacecrafts. In detail, an optics spacecraft carries simple large collecting area, light weight, refractive-diffractive X-ray lenses that focus radiation in the 4.5 to 11  $keV$  band upon detectors carried by a second spacecraft 1000  $km$  apart. A representation of an operating scenario of such a system is presented in Figure 1.7. Only some of the possible applications have been discussed, showing the potential of these kind of systems.



**Figure 1.7:** MASSIM spacecrafts operating scenario, [15]

This particular branch of aerospace engineering is in rapid development and continuous research. In the future, an equally wide range of applications is expected to make the Formation Flying one of the best performing system for obtaining data from satellites.

## 1.5 Work Subdivision

This last section aims at describing the organization of this work by reporting the main topics the Chapters deal with. The work can be divided into two main parts. A first part, whose purpose is to present basic concepts, which will be widely used in the second part, which represents the core and underlines the contribution given to the state of the art.

In particular, Chapter 2 focuses on the theoretical background which the following chapters are based on, by presenting the notation used in the work, the reference frames adopted for the description of the equations and the way the description of translational and relative motion is carried out.

Chapter 3 details the orbit propagation tool which has been developed for carrying out all the simulations. It describes in particular the choice of the forces modeling and the solution adopted for the integration of the differential equations.

Chapter 4 reports the main characteristics of relative dynamics, both for translational and rotational dynamics, by presenting the equations governing the relative motion description of a 6-DoF satellite wrt a chief spacecraft.

Chapter 5 presents one of the main issue related to Formation Flying, i.e. the stability of the formation. The topic is widely discusses by introducing principal configurations used for remote sensing purposes. These configurations will prove as practical test cases which will help showing the behaviours of free-flying formations subject to different relative initial conditions.

Chapter 6 two different types of controllers are presented: a proportional derivative controller and an optimal controller. In both cases the 6DoF dynamics is controlled. At the end of the chapter, partial or full optimal formation reconfiguration techniques are presented under a linear optimization perspective.

Chapter 7 presents test cases through which it is possible to analyze the performances of the different methodologies presented in the previous chapter.

Finally, in Chapter 8 a brief discussion on the results achieved by comparing the different solutions adopted for solving the problems stated in previous section is presented. In addition, possible future research which could represent an appropriate continuation of this work will be outlined.

# Chapter 2

## Theoretical background

### 2.1 Notation

When dealing with a multitude of reference frames, it becomes very useful to use a notation which makes visible to what frame the vectors are referred to. A vector is a mathematical object which possesses an amplitude and a direction in the 3D-space, so it exists independently from the way we describe it. In this work, a generic vector will be denoted by a bold letter  $\mathbf{v}$ . A vector which has unitary amplitude, so defining only a direction in space, is also called versor and it will be denoted by a symbol with a  $\hat{\mathbf{v}}$ . A generic vector can be described through different reference frames which will be denoted by the symbol  $\mathcal{F}$ . A frame is completely defined by three mutually perpendicular versors denoting its orientation with respect to an inertial frame. With these concepts in mind, we can now define a *vectorix*  $\hat{\mathcal{F}}_{\mathbf{a}}$  for the frame  $\mathcal{F}_{\mathbf{a}}$  with the following expression [38]

$$\hat{\mathcal{F}}_{\mathbf{a}} \triangleq [\hat{\mathbf{a}}_1, \hat{\mathbf{a}}_2, \hat{\mathbf{a}}_3]^T$$

that is, a *vectorix* simply indicates a frame using the versors it is composed by. It is possible now to give an alternative representation of a vector, by referring it to a generic frame. For example, if we want to describe a vector in the frame  $\mathcal{F}_{\mathbf{a}}$  we can write

$$\mathbf{v} = v_1 \hat{\mathbf{a}}_1 + v_2 \hat{\mathbf{a}}_2 + v_3 \hat{\mathbf{a}}_3$$

This can be synthetically expressed also through the notations

$$\mathbf{v}_a \triangleq [v_1, v_2, v_3]^T$$

where the pedix clarifies in what frame the vector is being decomposed into.

Considering the matrix product, the following equations can be easily derived

$$\mathbf{v} = \mathbf{v}_a^T \hat{\mathcal{F}}_a \equiv \hat{\mathcal{F}}_a^T \mathbf{v}_a \quad (2.1)$$

$$\hat{\mathcal{F}}_a \cdot \hat{\mathcal{F}}_a^T \triangleq \begin{bmatrix} \hat{\mathbf{a}}_1 \cdot \hat{\mathbf{a}}_1 & \hat{\mathbf{a}}_1 \cdot \hat{\mathbf{a}}_2 & \hat{\mathbf{a}}_1 \cdot \hat{\mathbf{a}}_3 \\ \hat{\mathbf{a}}_2 \cdot \hat{\mathbf{a}}_1 & \hat{\mathbf{a}}_2 \cdot \hat{\mathbf{a}}_2 & \hat{\mathbf{a}}_2 \cdot \hat{\mathbf{a}}_3 \\ \hat{\mathbf{a}}_3 \cdot \hat{\mathbf{a}}_1 & \hat{\mathbf{a}}_3 \cdot \hat{\mathbf{a}}_2 & \hat{\mathbf{a}}_3 \cdot \hat{\mathbf{a}}_3 \end{bmatrix} = \begin{bmatrix} 1 & 0 & 0 \\ 0 & 1 & 0 \\ 0 & 0 & 1 \end{bmatrix} \equiv \mathbf{I}_{3 \times 3} \quad (2.2)$$

$$\hat{\mathcal{F}}_a \times \hat{\mathcal{F}}_a^T \triangleq \begin{bmatrix} \hat{\mathbf{a}}_1 \times \hat{\mathbf{a}}_1 & \hat{\mathbf{a}}_1 \times \hat{\mathbf{a}}_2 & \hat{\mathbf{a}}_1 \times \hat{\mathbf{a}}_3 \\ \hat{\mathbf{a}}_2 \times \hat{\mathbf{a}}_1 & \hat{\mathbf{a}}_2 \times \hat{\mathbf{a}}_2 & \hat{\mathbf{a}}_2 \times \hat{\mathbf{a}}_3 \\ \hat{\mathbf{a}}_3 \times \hat{\mathbf{a}}_1 & \hat{\mathbf{a}}_3 \times \hat{\mathbf{a}}_2 & \hat{\mathbf{a}}_3 \times \hat{\mathbf{a}}_3 \end{bmatrix} \equiv \begin{bmatrix} \mathbf{0} & \hat{\mathbf{a}}_1 & -\hat{\mathbf{a}}_2 \\ -\hat{\mathbf{a}}_3 & \mathbf{0} & \hat{\mathbf{a}}_1 \\ \hat{\mathbf{a}}_2 & -\hat{\mathbf{a}}_1 & \mathbf{0} \end{bmatrix} \quad (2.3)$$

In particular, the equations 2.2 and 2.3 prove very useful when dealing with transformation matrices and rotations. In fact, if we have a vector  $\mathbf{v}_a$  described in reference  $\mathcal{F}_a$  and we want to have its representation in a frame  $\mathcal{F}_b$ , it is sufficient to calculate the dot product between the *vetrices*

$$\mathbf{v}_b = \hat{\mathcal{F}}_b \cdot \hat{\mathcal{F}}_a^T \mathbf{v}_a$$

It is possible now to identify the rotation matrix

$$\mathbf{R}_{ba} = \hat{\mathcal{F}}_b \cdot \hat{\mathcal{F}}_a^T$$

as the matrix which allows to obtain the description of a vector initially described in  $\mathcal{F}_a$  to its description in  $\mathcal{F}_b$ , and the matrix  $\mathbf{R}_{ab} = \mathbf{R}_{ba}^{-1}$  which allows to obtain the inverse transformation. It is worth to say that, because the orthonormality property of the versors composing a frame, it is also true that

$$\mathbf{R}_{ba}^{-1} = \mathbf{R}_{ba}^T \Rightarrow \mathbf{R}_{ab} = \mathbf{R}_{ba}^T$$

It is also possible to sum the contribution of several rotation matrices to obtain the

description of a vector in a generic frame  $\mathcal{F}_d$  starting from a frame  $\mathcal{F}_a$  and passing through frames  $\mathcal{F}_b$  and  $\mathcal{F}_c$

$$\mathbf{R}_{da} = \mathbf{R}_{dc}\mathbf{R}_{cb}\mathbf{R}_{ba}$$

The situation becomes more complicated when the reference frame is rotating with respect an inertial one. In fact, in this case if we want to retrieve the time derivative of a vector expressed in a rotating frame we have to consider that also the versors are function of time, so their time derivative is not null. From now on, the generic vector  $\boldsymbol{\omega}^{ba}$  will indicate the angular velocity of the frame  $\mathcal{F}_b$  with respect to  $\mathcal{F}_a$ , while  $\boldsymbol{\omega}_a^{ba}$  will indicate the same relative angular velocity but expressed in  $\mathcal{F}_a$  frame. It is also evident that  $\boldsymbol{\omega}^{ba} = -\boldsymbol{\omega}^{ab}$ . Now, if we consider the time derivative of the versors composing  $\mathcal{F}_b$  with respect to  $\mathcal{F}_a$  frame denoted by the symbol  $(\dot{\phantom{a}})$ , the following relation holds [12]

$$\dot{\hat{\mathbf{b}}}_i = \boldsymbol{\omega}^{ba} \times \hat{\mathbf{b}}_i \quad \forall i = 1, 2, 3$$

which can be represented in a more compact notation as

$$\dot{\hat{\mathcal{F}}}_b = \boldsymbol{\omega}^{ba} \times \hat{\mathcal{F}}_b$$

Developing the cross products it is possible to notice that the following relation holds

$$\dot{\hat{\mathcal{F}}}_b = \boldsymbol{\Omega}^{ba} \hat{\mathcal{F}}_b \Rightarrow \dot{\hat{\mathcal{F}}}_b^T = \hat{\mathcal{F}}_b^T \boldsymbol{\Omega}^{ba}$$

where

$$\boldsymbol{\Omega}^{ba} = \begin{bmatrix} 0 & -\omega_3 & \omega_2 \\ \omega_3 & 0 & -\omega_1 \\ -\omega_2 & \omega_1 & 0 \end{bmatrix}$$

is the skew-symmetric matrix of the cross product and  $\omega_i$  are the components of the relative angular velocity  $\boldsymbol{\omega}^{ba}$ . We can now use this notation to derive the mathematical description of a vector with respect to a rotating frame  $\mathcal{F}_b$ , in fact, the first derivative can be written as follows

$$\dot{\mathbf{v}} = \dot{\hat{\mathcal{F}}}_b^T \mathbf{v}_b + \hat{\mathcal{F}}_b^T \dot{\mathbf{v}}_b = \hat{\mathcal{F}}_b^T (\dot{\mathbf{v}}_b + \boldsymbol{\Omega}^{ba} \mathbf{v}_b) \quad (2.4)$$

and deriving another time

$$\ddot{\mathbf{v}} = \hat{\mathcal{F}}_b^T (\ddot{\mathbf{v}}_b + 2\boldsymbol{\Omega}^{ba}\dot{\mathbf{v}}_b + \dot{\boldsymbol{\Omega}}^{ba}\mathbf{v}_b + \boldsymbol{\Omega}^{ba}\boldsymbol{\Omega}^{ba}\mathbf{v}_b) \quad (2.5)$$

These relations will prove useful when the relative dynamics equations will be derived in Chapter 4, in fact, if the considered vector  $\mathbf{v}$  is the position vector of an object, thus Equations 2.4 and 2.5 represent its velocity and acceleration with respect to a rotating frame.

## 2.2 Reference Frames

After having presented the way it is possible to describe a generic vector, it is of fundamental importance to specify which are the reference frames effectively used to describe the equation of motion, defining of the versors whose they are composed by and their main characteristics.

### 2.2.1 ECI Frame

Earth-Centered-Inertial (ECI) Frame  $\mathcal{F}_I$  is a quasi-inertial frame which is quasi-non-rotating with respect to the fixed stars and has its origin at the center of mass of the Earth. It is often used for describing the motion of a celestial bodies and spacecrafts. It is a righth-handed frame and its axis are usually denoted with  $XYZ$ . Using the notation of the previous section we can define it as

$$\hat{\mathcal{F}}_I \triangleq [\hat{\mathbf{X}}, \hat{\mathbf{Y}}, \hat{\mathbf{Z}}]^T$$

There are different types of ECI frame, in this work the ECIJ2000 frame is used, where the versor  $\hat{\mathbf{X}}$  is pointing towards Earth's mean equinox of 12:00 Terrestrial Time on 1 January 2000,  $\hat{\mathbf{Z}}$  is aligned with the Earth's rotation axis or celestial North Pole, so forming an angle of about  $\epsilon = 23.4^\circ$  with the ecliptic, and  $\hat{\mathbf{Y}}$  completes the right-handed triad. This frame is particularly interesting because classical dynamics equation can be expressed without virtual forces with a good precision considering its very slow rotational movement. A visualization of this frame is presented in figure 2.1.

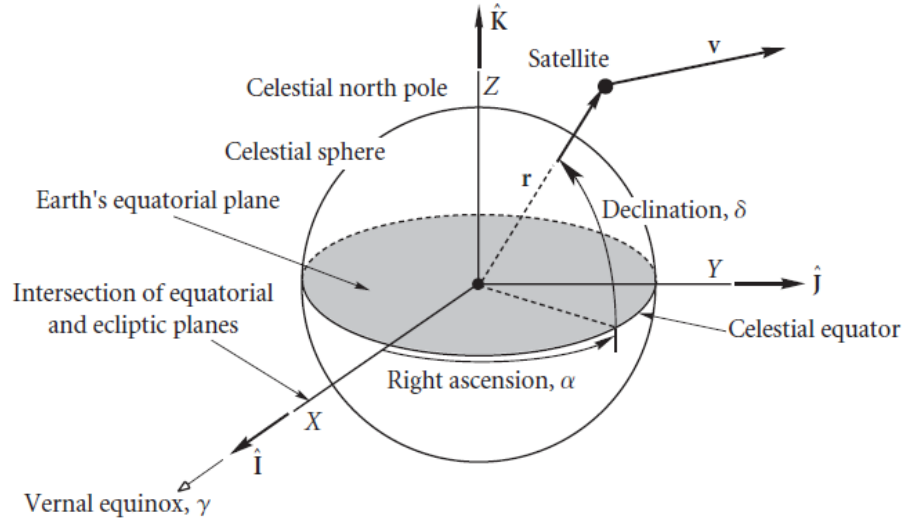


Figure 2.1: ECIJ2000 Frame, [5]

### 2.2.2 LVLH Frame

Local Vertical Local Horizon (LVLH) frame is the main frame used for describing motion in relative dynamics configuration. It was initially developed by [50] in order to describe the linearized relative motion equations for docking and close-proximity maneuvers. It is a right-handed frame and its axis are usually denoted as  $xyz$ . Using the notation of the previous section we can define it as

$$\hat{\mathcal{F}}_L \triangleq [\hat{\mathbf{x}}, \hat{\mathbf{y}}, \hat{\mathbf{z}}]^T$$

It is also referred as an "orbiting frame" because its origin generally coincides with a real satellite or with a virtual orbiting object so following a motion around the principal body. In detail, referring to Figure. 2.2, its  $\hat{\mathbf{x}}$  has the same direction of the current position vector  $\mathbf{r}$  of the satellite with respect to the center  $O$  of ECI frame. The  $\hat{\mathbf{z}}$  points towards the direction of the current angular momentum of the considered point  $\mathbf{h} = \mathbf{r} \times \mathbf{v}$ , where  $\mathbf{v}$  is its velocity vector.  $\hat{\mathbf{y}} = \hat{\mathbf{z}} \times \hat{\mathbf{x}}$  completes the right-handed triad.

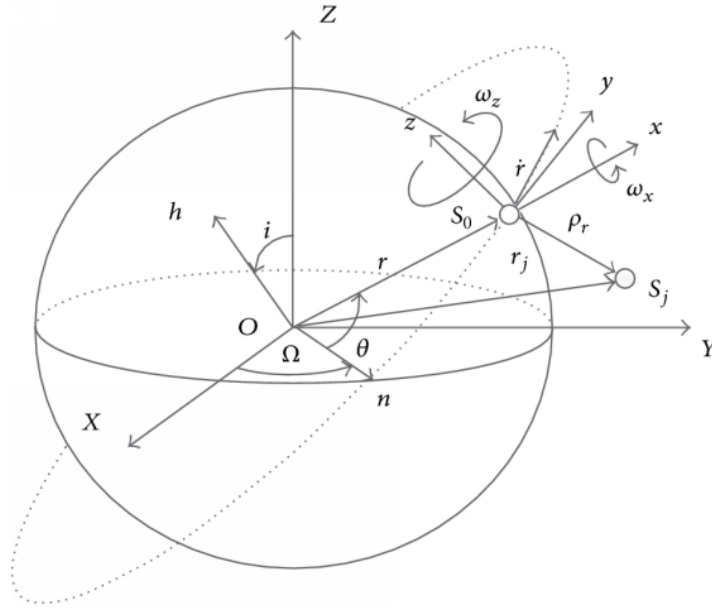


**Figure 2.2:** LVLH Frame, [52]

This reference is very important because it allows to describe in a very convenient way the relative motion between satellites in closed-proximity thus avoiding handling high amplitude vectors that would have been present in case of ECIJ2000 description. There are some disadvantages in using this frame, in fact, in order to describe the dynamics correctly, its angular velocity and acceleration have to be calculated at each instant during the motion, and if the frame undergoes several perturbations, this could be a computationally expensive task. This aspects will be further detailed in Chapter 4.

### 2.2.3 BF frame

The Body frame (BF) is a frame usually centered at the center of mass of the considered satellite and with arbitrary direction depending on the applications. This frame is attached to the body so becoming non-inertial when the satellite is rotating. This frame results particularly useful when considering the perturbation torques both external and internal acting on the satellite. It is right-handed and in this work its axis will be denoted with  $x_b y_b z_b$ . Using the notation of the previous section we can define it as

$$\hat{\mathcal{F}}_{BF} \triangleq [\hat{x}_b, \hat{y}_b, \hat{z}_b]^T$$

For convenience, it has been chosen  $\hat{x}_b$ ,  $\hat{y}_b$  and  $\hat{z}_b$  pointing towards the main directions of inertia, so simplifying the form of the inertial matrix  $\mathbf{J}_b$  which becomes a diagonal matrix.

## 2.3 Description of the Motion

In this section, the state variables used to specify the 6-DoF motion of a rigid body will be detailed. The translational motion description and the rotational one are separated. The notions introduced in this section will be used in Chapter 4 in order to derive the equations of 6-DoF dynamics for a set of satellites.

### 2.3.1 Translational Motion

The translational motion of a point in 3-dimensional space is completely defined by six independent parameters. In this work, two different types of parameters are used:

- **Inertial position and velocity vectors ( $\mathbf{r}_I$  and  $\mathbf{v}_I$ )**

Referring to Figure 2.1, these six parameters (three for the position and three for the velocity) describe, at a given instant, where the satellite is situated and where it will be after an infinitesimal time interval  $dt$  with respect to ECIJ2000 frame. These elements are very useful for using classical dynamics equation.

- **Keplerian elements**

This common representation can be visualized in Figure. 2.3. As the previous elements, they define completely an unperturbed orbit followed by a satellite but they allow a simpler description of an orbiting body. The six elements  $\mathbf{O}$  are usually denoted by the following letters  $\mathbf{O} = (a, e, i, \Omega, \omega, \nu)$  where

- $a$  is the semi-major axis. It represents the mean between the longest  $r_a$  and small  $r_p$  distances of the motion of the satellite about the celestial body,  

$$a = \frac{r_a + r_p}{2}$$
- $e$  is the eccentricity of the orbit. For elliptical motion it is  $0 \leq e < 1$ , where 0 denotes circular orbits and 1 parabolic ones
- $i$  is the inclination of the orbit, the angle between the plane of the orbit and the versor  $\hat{\mathbf{Z}}_I$
- $\Omega$ , also called RAAN, is the angle between the plane of the orbit and the versor  $\hat{\mathbf{X}}_I$
- $\omega$  is the argument of perigee and is the angle in the plane of the orbit between the intersection of the plane of the orbit with the equator and the direction of the perigee with respect to the ECIJ2000 frame (denoted as  $\mathbf{x}_p$  in Figure. 2.3)
- $\nu$  is also called true anomaly and is the angle in the plane of the orbit between

the vector  $\mathbf{x}_p$  and the position of the satellite

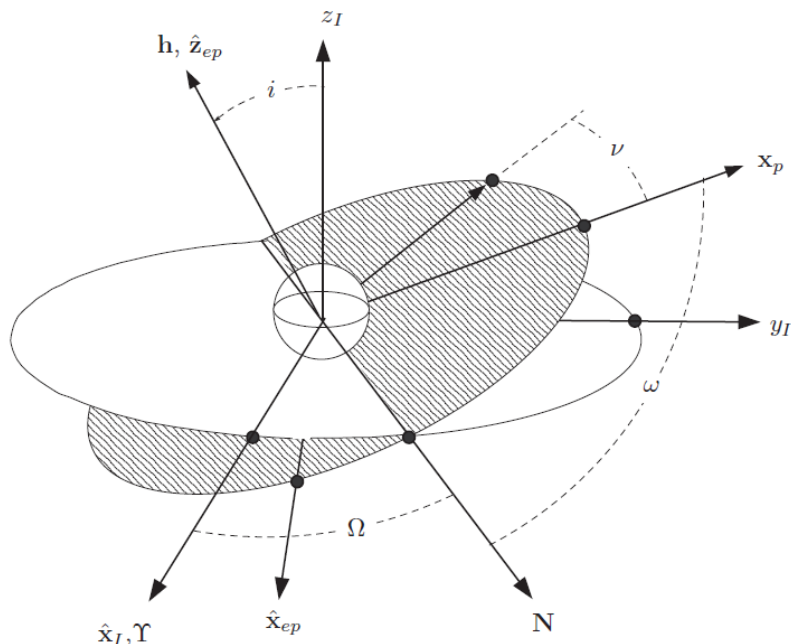


**Figure 2.3:** Keplerian elements, [2]

We can underline the simplicity of the description of the motion of a satellite when only the central gravity force acts on it. In fact, in this situation the true anomaly  $\nu$  is the only parameter which is function of time.

### 2.3.2 Rotational Motion

Rotational motion of a rigid body with respect to an inertial frame, as the translational one, is completely described by a set of six independent parameters. They usually are three angles and the three components of the angular velocity of the body frame with respect to the inertial one. Concerning the angular velocity vector, no additional clarification is required with respect to what has already been stated in the previous sections. Instead, concerning the the other three parameters, a different choice from those stated before has been done in this work. In fact, the description of the attitude of the body through the quaternion representation has been employed. Following the same notation of [16], it is possible to define a

quaternion as a 4-dimensional vector

$$\mathbf{q} = \begin{bmatrix} q_1 \\ q_2 \\ q_3 \\ q_4 \end{bmatrix} = \begin{bmatrix} \mathbf{e} \sin(\frac{\theta}{2}) \\ \cos(\frac{\theta}{2}) \end{bmatrix} = q_1 \hat{\mathbf{i}} + q_2 \hat{\mathbf{j}} + q_3 \hat{\mathbf{k}} + q_4$$

where  $\mathbf{e} \sin(\frac{\theta}{2}) = q_1 \hat{\mathbf{i}} + q_2 \hat{\mathbf{j}} + q_3 \hat{\mathbf{k}}$  is also called the vector part and  $\cos(\frac{\theta}{2}) = q_4$  the scalar one. This comes from the fact that a quaternion simply defines a rotation of intensity given by the value of  $\theta$  in the direction specified by the vector part  $\mathbf{e}$ . For completeness, we report the main results of quaternion algebra:

- **Norm**

The norm of a quaternion is defined as follows

$$\|\mathbf{q}\| = \sqrt{q_1^2 + q_2^2 + q_3^2 + q_4^2}$$

In this work, only unitary quaternions will be considered, i.e. those quaternions which have the property

$$\|\mathbf{q}\| = 1$$

- **Conjugate**

The conjugate of a quaternion is defined as

$$\mathbf{q}^* = \begin{bmatrix} -q_1 \\ -q_2 \\ -q_3 \\ q_4 \end{bmatrix}$$

- **Inverse**

The inverse of a quaternion is defined as

$$\mathbf{q}^{-1} = \frac{\mathbf{q}^*}{\|\mathbf{q}\|^2}$$

- **Multiplication**

The multiplication between quaternions is usually denoted by the symbol  $\otimes$

and it is defined by the following

$$\mathbf{q}_i \otimes \mathbf{q}_j = \begin{bmatrix} s_i \mathbf{v}_j + s_j \mathbf{v}_i + \mathbf{v}_i \times \mathbf{v}_j \\ s_i s_j - \mathbf{v}_i \cdot \mathbf{v}_j \end{bmatrix}$$

where  $s_i$  and  $s_j$  are the scalar parts, while  $\mathbf{v}_i$  and  $\mathbf{v}_j$  are the vector ones.

- **Transformation Matrix**

If the quaternion  $\mathbf{q}$  describes the relative rotation of the frame  $\mathcal{F}_b$  with respect to  $\mathcal{F}_a$ , it is possible to retrieve the rotation matrix from  $\mathcal{F}_a$  to  $\mathcal{F}_b$  as

$$\mathbf{R}_{ab} = \begin{bmatrix} q_1^2 - q_2^2 - q_3^2 + q_4^2 & 2(q_1 q_2 + q_3 q_4) & 2(q_1 q_3 - q_2 q_4) \\ 2(q_1 q_2 - q_3 q_4) & -q_1^2 + q_2^2 - q_3^2 + q_4^2 & 2(q_2 q_3 + q_1 q_4) \\ 2(q_1 q_3 + q_2 q_4) & 2(q_2 q_3 - q_1 q_4) & -q_1^2 - q_2^2 + q_3^2 + q_4^2 \end{bmatrix} \quad (2.6)$$

- **Quaternion rate**

The time derivative of the quaternion is linked to the angular velocity of the body through the kinematics equation given by the following

$$\dot{\mathbf{q}} = \frac{1}{2} W(\boldsymbol{\omega}) \mathbf{q} \quad (2.7)$$

where

$$W(\boldsymbol{\omega}) = \begin{bmatrix} 0 & \omega_3 & -\omega_2 & \omega_1 \\ -\omega_3 & 0 & \omega_1 & \omega_2 \\ \omega_2 & -\omega_1 & 0 & \omega_3 \\ -\omega_1 & -\omega_2 & -\omega_3 & 0 \end{bmatrix} \quad (2.8)$$

The Equation 2.7 will be used in Chapter when the rotational dynamics equations will be derived.

# Chapter 3

## High-Fidelity Orbital Mechanics Propagation Model

Cooperating satellite formations often require high accuracy in relative dynamics management. In many missions involving this type of architecture, the satellites have to work as a large coordinated system in order to take good data minimizing errors due to non-correct pointing of one or more of the satellites. For these reason an accurate modeling of the GN&C system has to be based on a very accurate model of orbit propagation. The model must account for the main perturbations affecting the orbit in which the formation will be flying. For relative dynamics accelerations in the order of  $10^{-5} \frac{m}{s^2}$  have to be properly described because proved to be of significant importance in contributing to the drift of relative orbits. For our purposes a model of orbit propagation accounting for gravity potential, drag, solar pressure and third-body perturbations, has been created and validated with the General Mission Analysis Tool (GMAT) of NASA [17] (see Appendix A). Next pages will describe what force modeling has been chosen for the orbit propagation model in order to better clarify which is the grade of accuracy of the simulations reported in the next chapters.

### 3.1 Force Modeling

For each perturbation, usually there are different kinds of modeling depending mostly on a trade-off between accuracy and computational cost. The choice must be mainly conditioned by the application that it is wanted to accomplish, for example, if I want to propagate the orbit of a satellite in LEO, the accelerations caused by gravity potential (even up to order 4), and drag have to be taken into account, instead

if I want to propagate a GEO orbit the same accelerations can be neglected. In addition, different types of models exist for each of these accelerations [33], e.g. for Drag, there are different types of density modeling that are more or less accurate and that consider more or less factors (heating of the atmosphere by the sun, convection motion of the atmosphere, rotational speed of the atmosphere around the earth etc.). The specification of the model choice for each of the considered perturbations follows in the next subsections.

### 3.1.1 Gravity Potential Perturbation

In Keplerian motion, the Earth is considered as a point whose mass is concentrated in its barycenter. This approximation holds for satellites whose distance from the Earth center is higher of about  $21.9 \times 10^3 \text{ km}$  [33]. For lower orbits, the distribution of the mass of the Earth has to be taken into account. This differential distribution creates a potential field which can be expressed with the following

$$U = \frac{GM_{\oplus}}{r} \sum_{n=0}^{\infty} \sum_{m=0}^n \frac{R_{\oplus}^n}{r^n} P_{nm}(\sin \phi) (C_{nm} \cos(m\lambda) + S_{nm} \sin(m\lambda))$$

where  $GM_{\oplus}$  is the gravitational constant of the Earth,  $R_{\oplus}$  is the reference radius of the Earth,  $r$  is the distance of the satellite from the center of mass of the Earth,  $P_{nm}$  is the Legendre polynomial of degree  $n$  and order  $m$ ,  $\phi$  is the geocentric latitude and  $\lambda$  is the longitude, counted positively towards the East and  $C_{nm}$  and  $S_{nm}$  are the geopotential coefficients which describe the Earth's internal mass distribution. The following expressions hold for these parameters:

$$P_n(u) = \frac{1}{2^n n!} \frac{d^n}{du^n} (u^2 - 1)^n$$

$$x = r \cos \phi \cos \lambda$$

$$y = r \cos \phi \sin \lambda$$

$$z = r \sin \phi$$

$$C_{nm} = \frac{2 - \delta_{0m}}{M_{\oplus}} \frac{(n-m)!}{(n+m)!} \int \frac{\mathbf{s}^n}{R_{\oplus}^n} P_{nm}(\sin \phi') \cos(m\lambda') \rho(\mathbf{s}) ds$$

$$S_{nm} = \frac{2 - \delta_{0m}}{M_{\oplus}} \frac{(n-m)!}{(n+m)!} \int \frac{\mathbf{s}^n}{R_{\oplus}^n} P_{nm}(\sin \phi') \sin(m\lambda') \rho(\mathbf{s}) ds$$

where  $x$ ,  $y$  and  $z$  are the ECI components of the satellite position,  $\rho(\mathbf{s})$  is the mass density at some point  $\mathbf{s}$  inside the Earth and  $\delta_{nm}$  denotes the Kronecker delta, which

is equal to 1 if  $n = m$  and to 0 otherwise. Geopotential coefficients with  $m = 0$  are called zonal coefficients because they describe the distribution of the Earth mass which does not depend on the longitude considering that for  $m = 0$ , all the  $S_{n0}$  vanishes. Usually the  $C_{n0}$  are also denoted using the following notation

$$J_n = -C_{n0}$$

The most important of them is the  $J_2$  coefficient which is cause of the most significant perturbation, after the central one, for a satellite in LEO. This potential generates an acceleration which is given by its gradient, in equations

$$\ddot{\mathbf{r}}_{GP} = \nabla \frac{GM_{\oplus}}{r} \sum_{n=0}^{\infty} \sum_{m=0}^n \frac{R_{\oplus}^n}{r^n} \bar{P}_{nm}(\sin \phi) (\bar{C}_{nm} \cos(m\lambda) + \bar{S}_{nm} \sin(m\lambda))$$

where  $\bar{C}_{nm}$  and  $\bar{S}_{nm}$  are the normalized geopotential coefficients

$$\begin{Bmatrix} \bar{C}_{nm} \\ \bar{S}_{nm} \end{Bmatrix} = \sqrt{\frac{(n+m)!}{(2-\delta_{0m})(2n+1)(n-m)!}} \begin{Bmatrix} C_{nm} \\ S_{nm} \end{Bmatrix} \quad (3.1)$$

Given a position  $\mathbf{r}$  of the satellite in inertial space, Equation 3.1 depends only on the geopotential coefficients. The value of these coefficients depends on the type of gravity model used. It is precisely in the choice of the gravity model used that there may be differences in terms of accuracy of the coefficients and the maximum order that can be considered. The most famous are the EGM96S ad the JGM-3 gravity models. In this work the coefficients calculated by the JGM-3 gravity model (up to order 21 and degree 21) have been considered [4]. The algorithm used for calculating the ECI accelerations can be detailed as follows [33]:

$$\ddot{x}_{GP} = \sum_{n,m} \ddot{x}_{nm} \quad \ddot{y}_{GP} = \sum_{n,m} \ddot{y}_{nm} \quad \ddot{z}_{GP} = \sum_{n,m} \ddot{z}_{nm}$$

where

$$\begin{aligned} \ddot{x}_{nm} &\stackrel{(m=0)}{=} \frac{GM_{\oplus}}{R_{\oplus}^2} \{-C_{n0}V_{n+1,1}\} \\ &\stackrel{(m \geq 0)}{=} \frac{GM_{\oplus}}{R_{\oplus}^2} \frac{1}{2} \{(-C_{nm}V_{n+1,m+1} - S_{nm}W_{n+1,m+1}) \\ &\quad + (n-m+2)(n-m+1)(C_{nm}V_{n+1,m-1} + S_{nm}W_{n+1,m-1})\} \end{aligned}$$

$$\begin{aligned}
\ddot{y}_{nm} &\stackrel{(m=0)}{=} \frac{GM_{\oplus}}{R_{\oplus}^2} \{-C_{n0}W_{n+1,1}\} \\
&\stackrel{(m \geq 0)}{=} \frac{GM_{\oplus}}{R_{\oplus}^2} \frac{1}{2} \{(-C_{nm}W_{n+1,m+1} + S_{nm}V_{n+1,m+1}) \\
&\quad + (n-m+2)(n-m+1)(-C_{nm}W_{n+1,m-1} + S_{nm}V_{n+1,m-1})\} \\
\ddot{z}_{nm} &= \frac{GM_{\oplus}}{R_{\oplus}^2} \{(n-m+1)(-C_{nm}V_{n+1,m} - S_{nm}W_{n+1,m})\}
\end{aligned}$$

where  $V$  and  $W$  obey to the equations

$$\begin{aligned}
V_{mm} &= (2m-1) \left\{ \frac{xR_{\oplus}}{r^2} V_{m-1,m-1} - \frac{yR_{\oplus}}{r^2} W_{m-1,m-1} \right\} \\
W_{mm} &= (2m-1) \left\{ \frac{xR_{\oplus}}{r^2} W_{m-1,m-1} + \frac{yR_{\oplus}}{r^2} V_{m-1,m-1} \right\} \\
V_{nm} &= \left( \frac{2n-1}{n-m} \right) \frac{zR_{\oplus}}{r^2} V_{n-1,m} - \left( \frac{n+m-1}{n-m} \right) \frac{R_{\oplus}^2}{r^2} V_{n-2,m} \\
W_{nm} &= \left( \frac{2n-1}{n-m} \right) \frac{zR_{\oplus}}{r^2} W_{n-1,m} - \left( \frac{n+m-1}{n-m} \right) \frac{R_{\oplus}^2}{r^2} W_{n-2,m}
\end{aligned}$$

starting with  $V_{00} = \frac{R_{\oplus}}{r}$  and  $W_{00} = 0$ .

### 3.1.2 Drag Perturbation

The Drag is the most important non-gravitational perturbation for low altitude satellite. It can be expressed with the following equation

$$\ddot{\mathbf{r}}_D = -\frac{1}{2} \rho \frac{C_d A}{m} v_r^2 \mathbf{e}_v \quad (3.2)$$

where  $\rho$  is the density of the atmosphere at the altitude of the satellite,  $C_d$  is the drag coefficient of the satellite,  $A$  is the reference surface for that coefficient and  $m$  is the mass of the satellite ( $\frac{C_d A}{m}$  is also called the ballistic coefficient),  $v_r$  is the amplitude of the relative velocity between the satellite and the atmosphere and  $\mathbf{e}_v$  is the versor denoting the direction of this relative velocity. So, this acceleration tends to slow the satellite changing its orbital parameter, in particular the drag force tends to reduce the semi-major axis of the orbit and to circularize it. In Equation 3.2 the parameter which is mostly affected by uncertainty is the density  $\rho$ . In fact, because of the complex phenomena which interact with the atmosphere, an accurate description of the variation of the density with altitude, temperature etc. results in

a very hard task. For these reasons, different density models have been developed in the last decades. The most simple is the so-called exponential density model which considers the following law for  $\rho$

$$\rho = \rho_0 e^{-h/H_0}$$

where  $\rho_0 = 2.34 \times 10^{-13} \frac{kg}{m^3}$  and  $H_0 = 68.7km$  is the reference altitude, and  $h$  is the altitude of the satellite. This is a very rough estimation which is usually employed for preliminary calculations. More accurate models are the Jacchia 1971 density model and Harris-Priester density model. In this work the Harris-Priester density model has been used and a little description of it follows.

The Harris-Priester density model foresees the following empirical density law

$$\rho(h) = \rho_m(h) + (\rho_M(h) - \rho_m(h)) \cdot \cos^n \left( \frac{\Psi}{2} \right)$$

where  $h$  is the altitude of the satellite,  $\rho_m(h)$  and  $\rho_M(h)$  are respectively the antapex and apex densities at a given altitude which are computed with an exponential interpolation using tabulated minimum and maximum densities [33] at the altitude  $h_i$  as follows

$$\begin{aligned} \rho_m(h) &= \rho_m(h_i) e^{\frac{h_i-h}{H_m}} \\ \rho_M(h) &= \rho_M(h_i) e^{\frac{h_i-h}{H_M}} \end{aligned} \quad h_i \leq h \leq h_{i+1}$$

and

$$\begin{aligned} H_m(h) &= \frac{h_i - h_{i+1}}{\ln(\rho_m(h_{i+1}) / \rho_m(h_i))} \\ H_M(h) &= \frac{h_i - h_{i+1}}{\ln(\rho_M(h_{i+1}) / \rho_M(h_i))} \end{aligned}$$

Finally, in Equation 3.1.2,  $n$  is a numerical value which equals 2 for low-inclination orbits and 6 for polar orbits, and  $\Psi$  is the angle between the satellite and the apex of diurnal bulge and it is calculated as follows

$$\cos^n \left( \frac{\Psi}{2} \right) = \left( \frac{1 + \cos \Psi}{2} \right)^{\frac{n}{2}} = \left( \frac{1}{2} + \frac{\mathbf{e}_r \cdot \mathbf{e}_b}{2} \right)^{\frac{n}{2}}$$

where  $\mathbf{e}_r$  is the versor denoting the position of the satellite with respect to the Earth

center and  $\mathbf{e}_b$  is the versor giving the direction of the apex of diurnal bulge given by

$$\mathbf{e}_b = \begin{pmatrix} \cos \delta_{\odot} \cos (\alpha_{\odot} + \lambda_l) \\ \cos \delta_{\odot} \sin (\alpha_{\odot} + \lambda_l) \\ \sin \delta_{\odot} \end{pmatrix}$$

where  $\alpha_{\odot}$  and  $\delta_{\odot}$  are the Sun's right ascension and declination and  $\lambda_l \simeq 30^\circ$ .

### 3.1.3 Solar Pressure Perturbation

When a satellite is exposed to the Sun, it experiences an acceleration which is due to the reflection and/or absorption of the incoming radiation. This force depends on many factors and in general it can be expressed as follows

$$\ddot{\mathbf{r}}_{SP} = -P_{\odot} \frac{1\text{AU}^2}{r_{\odot}^2} \frac{A}{m} \cos(\theta) [(1 - \varepsilon)\mathbf{e}_{\odot} + 2\varepsilon \cos(\theta)\mathbf{n}] \quad (3.3)$$

where  $P_{\odot} \simeq 4.56 \times 10^{-6} \frac{N}{m^2}$  is the constant of solar radiation pressure,  $r_{\odot}$  is the distance of the satellite from the Sun,  $AU = 1.495 \times 10^{11} m$  is the astronomical unit,  $A$  is the surface hit by the radiation,  $m$  is the mass of the satellite,  $\varepsilon$  is the coefficient of reflectivity of the surface,  $\mathbf{e}_{\odot}$  is the versor pointing from the satellite to the Sun, and  $\theta$  is the angle between the normal  $\mathbf{n}$  to the illuminated surface and  $\mathbf{e}_{\odot}$ .

The Equation 3.3 requires the knowledge at each time of the orientation of the satellite surface  $\mathbf{n}$  and the surfaces exposed to the radiation. This aspect could result in an excessive computational cost which is not justified by the little improvement in precision of the solar pressure perturbation consequences. For this reason, Equation 3.3 is often simplified with the following

$$\ddot{\mathbf{r}}_{SP} = -P_{\odot} C_R \frac{A}{m} \frac{\mathbf{d}}{d^3} AU^2$$

where  $C_R = 1 + \varepsilon$  and  $\mathbf{d} = \mathbf{r}_{\odot} - \mathbf{r}$  is the distance vector between the geocentric positions of the Sun and the satellite. This equation is a good compromise between accuracy and computational cost, also considering that the geometry of the satellite is not needed anymore, allowing the use of this equation even in a preliminary design phase where the shape of the surfaces has not yet been decided.

One element which has to be taken into account when dealing with solar pressure perturbation is the possibility of alternation between eclipse and sunlight phases.

Even in this case, different possible modelings can be used. In this work the conical shadow model (Figure 3.1) has been employed.

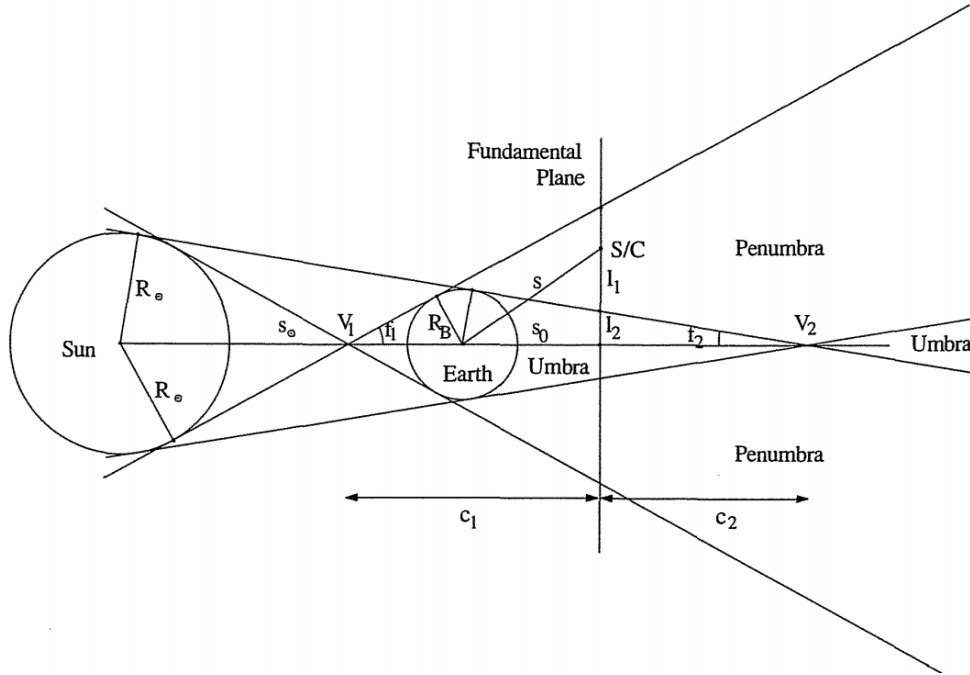


**Figure 3.1:** Conical shadow model, [33]

This model considers a general occultating body (in our case, the Earth has been considered as the only occultating body) which partially or totally absorb the Sun radiation directed to the satellite. Looking at Figure 3.1 it is possible to note two main different regions: the Umbra and Penumbra regions. The Umbra region is that region of the space at which the satellite is totally in eclipse and the acceleration due to solar pressure is null, in the Penumbra region, instead, the satellite receives partial radiation from the Sun. This aspect is included in Equation 3.1.3 by considering a factor denoted by the letter  $\nu$  which equals 0 when the satellite is in Umbra, 1 when it is not in Umbra nor in Penumbra, and  $0 \leq \nu \leq 1$  when the satellite is in Penumbra region. So, the Equation 3.1.3 becomes

$$\ddot{\mathbf{r}}_{SP} = -\nu P_{\odot} C_R \frac{A}{m} \frac{\mathbf{d}}{d^3} \text{AU}^2$$

Considering 3.2, it is possible to calculate the value of  $\nu$ . Figure 3.2 shows the apparent diameters of the Sun and occultating body as seen from the spacecraft.

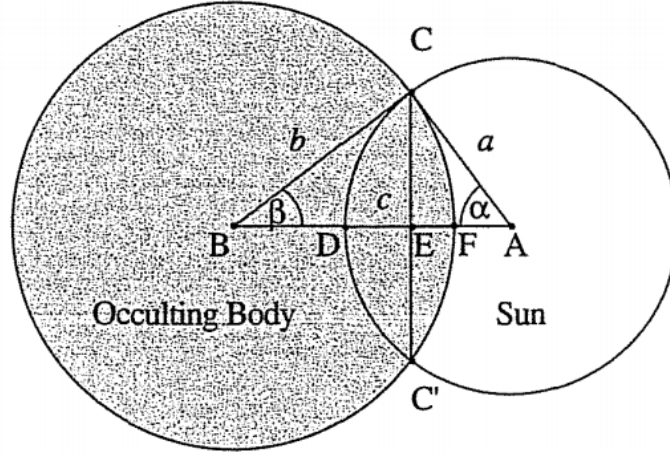


Figure 3.2: Apparent disks for  $\nu$  computation, [33]

Using the same notation of Figure 3.2 the following relations can be easily derived

$$a = \arcsin \left( \frac{R_{\odot}}{|\mathbf{r}_{\odot} - \mathbf{r}|} \right)$$

$$b = \arcsin \left( \frac{R_B}{s} \right)$$

$$c = \arcsin \left( \frac{-\mathbf{s}^T(\mathbf{r}_{\odot} - \mathbf{r})}{|\mathbf{r}_{\odot} - \mathbf{r}|} \right)$$

where  $R_{\odot}$  is the radius of the Sun,  $\mathbf{r}_{\odot}$  is the geocentric position of the Sun,  $\mathbf{r}$  is the geocentric position of the satellite and  $\mathbf{s}$  is the geocentric position of the occultating body. Calling  $\Theta = A_{CFC'} + A_{CDC'}$  the Sun apparent surface which is covered by the occultating body and provided that  $|a - b| \leq c \leq a + b$  in case of partial occultation, it is possible to express it as [33]

$$\Theta = a^2 \arccos \left( \frac{x}{a} \right) + b^2 \arccos \left( \frac{c - x}{b} \right) - cy$$

where

$$x = \frac{c^2 + a^2 - b^2}{2c}$$

$$y = \sqrt{a^2 - x^2}$$

Finally,  $\nu$  is given by

$$\nu = 1 - \frac{\Theta}{\pi a^2}$$

If the equation  $|a - b| < c < a + b$  does not hold no occultation occurs ( $a + b \leq c$ )

or the occultation is total ( $c < b - a$  with  $a < b$ ) or partial but maximum ( $c < a - b$  with  $a > b$ ).

### 3.1.4 Third-body Perturbation

Celestial bodies which are very massive and/or in proximity of the satellite cause an attraction force which is not negligible for relative dynamics precise modeling. In this study the perturbations on the satellites of the formation of the Sun and the Moon have been considered. Considering the average distances between operational Earth orbits and Moon and Sun, these bodies can be considered as point-mass perturbing bodies. So, the following equations for the acceleration holds

$$\ddot{\mathbf{r}}_{TB} = GM \left( \frac{\mathbf{s} - \mathbf{r}}{|\mathbf{s} - \mathbf{r}|^3} - \frac{\mathbf{s}}{|\mathbf{s}|^3} \right)$$

where  $GM$  is the celestial body gravitational constant,  $\mathbf{r}$  is the geocentric position vector of the satellite and  $\mathbf{s}$  is the geocentric position vector of the perturbing body. The precision of this equation is mostly affected by the knowledge of  $\mathbf{s}$  which is given by the ephemerides calculation of the considered body.

### 3.1.5 Propagation of the Orbit

After having defined all the modelings for different acting forces, it is possible to integrate the equation of translational motion of the satellite in inertial frame through the following

$$\ddot{\mathbf{r}} = \ddot{\mathbf{r}}_{GP} + \ddot{\mathbf{r}}_D + \ddot{\mathbf{r}}_{SP} + \ddot{\mathbf{r}}_{TB, Moon} + \ddot{\mathbf{r}}_{TB, Sun} \quad (3.4)$$

This integration could be computationally expensive, considering also that stringent tolerances have to be applied for a good convergence, but this equation proves very stable for all possible orbits (for example circular ones) for which an osculating Keplerian elements integration would have very large errors.

# Chapter 4

## Relative motion

This chapter aims at reporting the main equations which describe the relative motion between two different satellites. This approach will be extended to any number of satellites, giving the opportunity of describing the dynamics of entire formations and/or constellation of satellites. As already discussed in Chapter 2, relative motion is usually described in LVLH frame. Many works in literature focused on deriving the equation of motion of the LVLH frame. In particular, since LVLH frame is a non-inertial frame, the efforts have been focused on deriving its angular velocity  $\mathbf{\Omega}$  and acceleration  $\dot{\mathbf{\Omega}}$  vectors which are essential for the description of the relative motion. Deriving these quantities starting from the definition of the versors composing the LVLH is as difficult as inefficient (this aspect will be described in the next sections). For the reasons above, analytical solutions to this problem has been found by [14] considering a LVLH affected only by  $J_2$  perturbation and by [19] for a LVLH affected by  $J_2$  and Drag perturbations. In this work the solution considering only  $J_2$  perturbation has been used and it proved sufficiently accurate for the reasons this frame is usually implied for.

Figure 4.1 shows the main elements involved in the description of the relative motion. In particular, the motion involves two satellite, a chief and a deputy. The chief is the satellite the dynamics is described with respect to. Its center of mass is the origin of LVLH frame and it can be a real satellite or a virtual one, in the latter case it is not forced to undergo all the perturbations the deputy is subjected to. In fact, it is used as a local observer whose main purpose is to be able to describe the motion considering relative distances and velocities, which are the controlled quantities in formation flying.

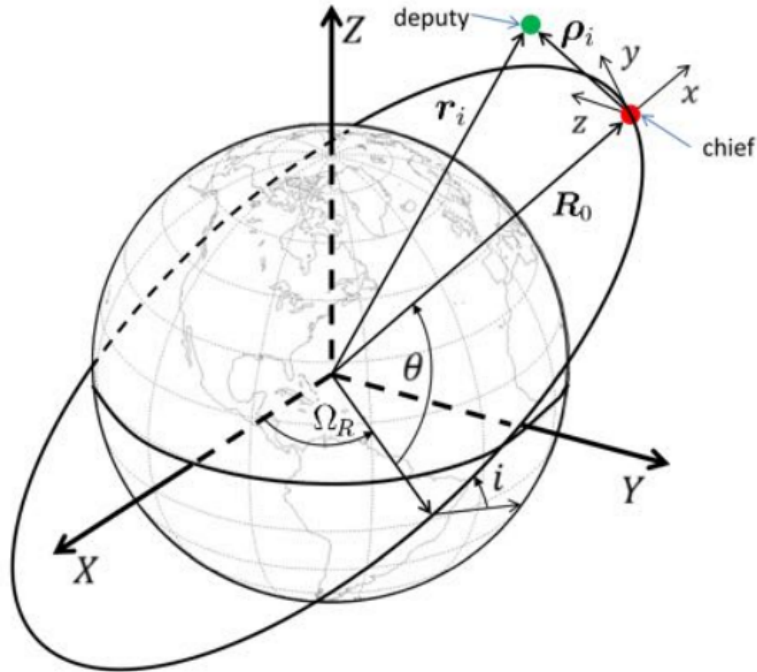


Figure 4.1: Chief and deputy LVLH frame description, [7]

The deputy is a real satellite whose motion has to be described relatively to the chief. Using the notation present in Figure 4.1, the following equation can be easily derived

$$\mathbf{r}_i = \boldsymbol{\rho}_i + \mathbf{R}_0 \quad (4.1)$$

where  $\mathbf{R}_0$  is the ECI position vector of the chief spacecraft,  $\boldsymbol{\rho}_i$  is the relative position vector of the deputy spacecraft with respect to the chief and  $\mathbf{r}_i$  is the ECI position vector of the deputy. It is convenient to solve Equation 4.1 for obtaining the expression of the relative position  $\boldsymbol{\rho}_i$  which is the quantity relative motion equations are interested in. So, the next equation is obvious

$$\boldsymbol{\rho}_i = \mathbf{r}_i - \mathbf{R}_0 \quad (4.2)$$

In the following sections translational and rotational dynamics equations will be derived.

## 4.1 Relative Translational Dynamics Modeling

There are two possible ways to obtain the relative quantities of a spacecraft relative to another. In fact, it is always possible to integrate Equation 3.4 both for chief and the deputy spacecrafts, and then using the following equations in order to find relative position, velocity and acceleration seen by LVLH frame in LVLH components [16]

$$\boldsymbol{\rho}_i = \mathbf{R}_{LI}(\mathbf{r}_d - \mathbf{r}_c)$$

$$\dot{\boldsymbol{\rho}}_i = \mathbf{R}_{LI}(\dot{\mathbf{r}}_d - \dot{\mathbf{r}}_c - \boldsymbol{\Omega} \times (\mathbf{r}_d - \mathbf{r}_c))$$

$$\ddot{\boldsymbol{\rho}}_i = \mathbf{R}_{LI}(\ddot{\mathbf{r}}_d - \ddot{\mathbf{r}}_c - \dot{\boldsymbol{\Omega}} \times (\mathbf{r}_d - \mathbf{r}_c) - \boldsymbol{\Omega} \times \boldsymbol{\Omega} \times (\mathbf{r}_d - \mathbf{r}_c) - 2\boldsymbol{\Omega} \times (\dot{\mathbf{r}}_d - \dot{\mathbf{r}}_c))$$

where  $\mathbf{r}_d$  and  $\mathbf{r}_c$  are the inertial position vectors of the deputy and the chief in ECI components and  $\mathbf{R}_{LI}$  is the transformation matrix from ECI to LVLH frame. Particular attention has to be paid for the quantities  $\ddot{\mathbf{r}}_c$  and  $\ddot{\mathbf{r}}_d$ , in fact they represent the inertial acceleration of the chief and deputy respectively. Regarding  $\ddot{\mathbf{r}}_d$ , all perturbation of Equation 3.4 can be considered without any particular problem, instead, regarding  $\ddot{\mathbf{r}}_c$  which is also the center of LVLH frame, the same perturbations which are taken into account in the derivation of the angular velocity and acceleration ( $\boldsymbol{\Omega}$  and  $\dot{\boldsymbol{\Omega}}$ ) have to be used for the integration, if not, the model is inconsistent.

Another possibility is to integrate directly the relative dynamics equations in LVLH frame. Considering Equations 2.4 and 2.5 introduced in Chapter 2, deriving two times the left side of Equation 4.2 in LVLH frame, it is possible to obtain

$$\dot{\boldsymbol{\rho}}_i = \hat{\mathcal{F}}_L^T \boldsymbol{\rho}_{i,L} + \hat{\mathcal{F}}_L^T \dot{\boldsymbol{\rho}}_{i,L} = \hat{\mathcal{F}}_L^T \dot{\boldsymbol{\rho}}_{i,L} + \hat{\mathcal{F}}_L^T \boldsymbol{\Omega} \times \boldsymbol{\rho}_{i,L} \quad (4.3)$$

$$\begin{aligned} \ddot{\boldsymbol{\rho}}_i &= \hat{\mathcal{F}}_L^T \dot{\boldsymbol{\rho}}_{i,L} + \hat{\mathcal{F}}_L^T \ddot{\boldsymbol{\rho}}_{i,L} + \dot{\hat{\mathcal{F}}}_L^T \boldsymbol{\Omega} \times \boldsymbol{\rho}_{i,L} + \hat{\mathcal{F}}_L^T \dot{\boldsymbol{\Omega}} \times \boldsymbol{\rho}_{i,L} + \hat{\mathcal{F}}_L^T \boldsymbol{\Omega} \times \dot{\boldsymbol{\rho}}_{i,L} \\ &= \hat{\mathcal{F}}_L^T \ddot{\boldsymbol{\rho}}_{i,L} + \hat{\mathcal{F}}_L^T \dot{\boldsymbol{\Omega}} \times \boldsymbol{\rho}_{i,L} + \dot{\hat{\mathcal{F}}}_L^T \boldsymbol{\Omega} \times \boldsymbol{\rho}_{i,L} + 2\hat{\mathcal{F}}_L^T \boldsymbol{\Omega} \times \dot{\boldsymbol{\rho}}_{i,L} \end{aligned} \quad (4.4)$$

Where in particular  $\hat{\mathcal{F}}_L^T \boldsymbol{\Omega}$  and  $\dot{\hat{\mathcal{F}}}_L^T \dot{\boldsymbol{\Omega}}$  are the angular velocity and acceleration of LVLH frame with respect to ECI written in LVLH components. Considering now the right side of Equation 4.2 and deriving it two times and expressing the components

of the accelerations in LVLH frame the relative dynamics for translational motion are obtained

$$\begin{aligned} \hat{\mathcal{F}}_L^T \ddot{\boldsymbol{\rho}}_{i,L} = & \hat{\mathcal{F}}_L^T (\hat{\mathcal{F}}_I^T (\ddot{\mathbf{r}}_{i,I} - \ddot{\mathbf{R}}_{0,I})) - \hat{\mathcal{F}}_L^T \boldsymbol{\Omega} \times \hat{\mathcal{F}}_L^T \boldsymbol{\Omega} \times \boldsymbol{\rho}_{i,L} \\ & - \hat{\mathcal{F}}_L^T \dot{\boldsymbol{\Omega}} \times \boldsymbol{\rho}_{i,L} - 2\hat{\mathcal{F}}_L^T \boldsymbol{\Omega} \times \dot{\boldsymbol{\rho}}_{i,L} \end{aligned} \quad (4.5)$$

Where  $\hat{\mathcal{F}}_I^T (\ddot{\mathbf{r}}_{i,I} - \ddot{\mathbf{R}}_{0,I})$  represent the difference between inertial accelerations of the deputy and the chief expressed with components in inertial frame. After deriving rigorously the equations exemplifying the management of different frames, in the next chapters the notation  $\hat{\mathcal{F}}_b^T \mathbf{v}_b$  will be abandoned in favor of the simpler  $\mathbf{v}_b$ , so denoting a vector expressed in  $\mathcal{F}_b$  frame. Adopting the new notation, Equation 4.5 becomes

$$\ddot{\boldsymbol{\rho}}_{i,L} = \mathbf{R}_{LI} (\ddot{\mathbf{r}}_{i,I} - \ddot{\mathbf{R}}_{0,I}) - \boldsymbol{\Omega}_L \times \boldsymbol{\Omega}_L \times \boldsymbol{\rho}_{i,L} - \dot{\boldsymbol{\Omega}}_L \times \boldsymbol{\rho}_{i,L} - 2\boldsymbol{\Omega}_L \times \dot{\boldsymbol{\rho}}_{i,L} \quad (4.6)$$

This second approach results in a more practical way of describing the relative motion, in fact, it is possible to impose relative initial and final condition in a simpler way, this makes the control algorithm simpler and more evident having in mind that relative position and velocity vectors are the controlled quantities. This aspect will be better exemplified in the last section of this chapter.

## 4.2 Rotational Dynamics Modeling

Concerning rotational motion, it is also possible to describe the relative attitude between the deputy and chief spacecrafts, in particular, in [46], the dynamics equation for the relative angular accelerations between the body-frames of two different spacecrafts is found. This approach can prove very useful in many applications, especially for those applications which need to know relative position between any two points of two spacecrafts which are not the center of mass. In fact, assuming the approximations of rigid bodies, thanks to relative rotational dynamics it is possible to calculate the velocity and acceleration of any point of the spacecraft by knowing the position vector with respect to the center of mass. Examples of this kind of applications are tethered systems [28] [31] [30], [27], in which the links between tethers do not necessarily pass through the center of mass or systems which present instruments for relative dynamics metrology that have to be positioned in the external surfaces of the spacecraft [45] [53] and whose position has to be known in order to improve the precision of the calculations they perform. In other kind of application, like in case of Earth system monitoring [11] or Interferometry [13], it can be useful

to derive the equations of absolute rotational dynamics, i.e. it is convenient to have the relative attitude between the body-frame and the inertial frame. In this work, this second way of describing rotational dynamics has been pursued

Having in mind Equation 2.8 which describes the kinematic relation between the quaternion and angular velocity of the frame, the equation for angular acceleration is needed to complete the dynamics. Applying the same notation of [16], it is possible to write for each spacecraft the following equation in case of absence of external torques

$$\dot{\mathbf{H}}_G = \frac{d}{dt}(\mathbf{J}_G\boldsymbol{\omega} + \sum_i \mathbf{h}_i) = 0 \quad (4.7)$$

where  $\mathbf{H}_G$  is the angular momentum of the body with respect to its center of mass which can be written as the sum between the angular momentum of the body  $\mathbf{J}_G\boldsymbol{\omega}$ , where  $\mathbf{J}_G$  is the moment of inertia matrix with respect to the considered frame whose origin coincides with the center of mass of the body and  $\boldsymbol{\omega}$  is the angular velocity of the body-frame wrt inertial frame, and the internal angular momentum  $\mathbf{h}_i$  (reaction wheels etc..). Perturbations and internal torques act on the spacecraft conditioning its rotational dynamics, so adding this contribution to the Equation 4.7, the following holds

$$\dot{\mathbf{H}}_G = \frac{d}{dt}(\mathbf{J}_G\boldsymbol{\omega} + \sum_i \mathbf{h}_i) = \sum_j \boldsymbol{\tau}_j^{pert} + \sum_k \boldsymbol{\tau}_k^{int} \quad (4.8)$$

where  $\boldsymbol{\tau}_j^{pert}$  denotes the j-th perturbation torque,  $\boldsymbol{\tau}_k^{int}$  denotes the k-th unwanted internal torque.

It is now possible to apply the derivative of the left side of the Equation 4.8, assuming that the body is not flexible ( $\frac{d}{dt}\mathbf{J}_G = 0$ )

$$\mathbf{J}_G\dot{\boldsymbol{\omega}} + \sum_i \dot{\mathbf{h}}_i = \sum_j \boldsymbol{\tau}_j^{pert} + \sum_k \boldsymbol{\tau}_k^{int} \quad (4.9)$$

It is convenient to solve the Equation 4.9 for the angular acceleration  $\dot{\boldsymbol{\omega}}$ . If the Equation 4.9 is referred to a moving frame, when deriving, the angular velocity of the frame has to be considered. Considering a generic frame  $\mathcal{F}_b$  and adopting the notation of the previous section, the following holds

$$\dot{\boldsymbol{\omega}}_b = \mathbf{J}_{G,b}^{-1} \left( \sum_j \boldsymbol{\tau}_{j,b}^{pert} + \sum_k \boldsymbol{\tau}_{k,b}^{int} - \sum_i \dot{\mathbf{h}}_{i,b} - \boldsymbol{\omega}_b \times (\mathbf{J}_{G,b}\boldsymbol{\omega}_b + \sum_i \mathbf{h}_{i,b}) \right) \quad (4.10)$$

In this work Equation 4.10 has been written for the body-frame  $\mathcal{F}_{BF}$  so becoming

$$\begin{aligned} \dot{\boldsymbol{\omega}}_{BF} = & \mathbf{J}_{G,BF}^{-1} \left( \sum_j \boldsymbol{\tau}_{j,BF}^{pert} + \sum_k \boldsymbol{\tau}_{k,BF}^{int} \right. \\ & \left. - \sum_i \dot{\mathbf{h}}_{i,BF} - \boldsymbol{\omega}_{BF} \times (\mathbf{J}_{G,BF} \boldsymbol{\omega}_{BF} + \sum_i \mathbf{h}_{i,BF}) \right) \end{aligned} \quad (4.11)$$

Where  $\mathbf{J}_{G,BF}$  denotes the inertia matrix passing through the center of mass and referred to the body-frame axis. The integration of Equation 4.11 calculates directly the body-frame components of the angular acceleration of the body-frame wrt the inertial frame  $\mathcal{F}_I$ . Recalling Equation 2.7 and writing it for body-frame components

$$\dot{\mathbf{q}}_{BF} = \frac{1}{2} W(\boldsymbol{\omega}_{BF}) \mathbf{q}_{BF} \quad (4.12)$$

where the notation  $\mathbf{q}_{BF}$  underlines that the quaternion components are expressed in body-frame. Equations 4.12 and 4.11 will be used in the next section for deriving the general non-linear dynamics system describing the relative motion of all the formation.

### 4.3 Non-Linear Complete State Space Representation

Now that both the translational motion equations and rotational ones have been reported, it is possible to use the results of Chapter 3 and 4 for writing the non-linear system whose integration returns relative position and velocities wrt LVLH frame and attitude and angular velocities of the body-frame wrt Inertial frame for each spacecraft of the formation. This system will be extensively used in next chapters when dealing with the control of the system.

In a free-flying architecture, each spacecraft is dynamically independent from the others, so applying Equations 4.6 and 4.11 to the single spacecraft and defining the state vector in the following way

$$\mathbf{X}_i = \begin{pmatrix} \boldsymbol{\rho}_{i,L} \\ \dot{\boldsymbol{\rho}}_{i,L} \\ \mathbf{q}_{BF} \\ \boldsymbol{\omega}_{BF} \end{pmatrix}$$

it is possible to obtain non-linear dynamical system for each spacecraft

$$\dot{\mathbf{X}}_i = f(\ddot{\mathbf{r}}_i, \ddot{\mathbf{R}}_0, \boldsymbol{\Omega}, \dot{\boldsymbol{\Omega}}, \mathbf{X}_i) \quad (4.13)$$

where the dependence on the inertial accelerations of the spacecraft and LVLH frame, and its angular velocity and acceleration has been highlighted. The pedex  $i$  indicates that all quantities in  $f$  are referred to the  $i$ -th spacecraft. It is possible to expand 4.13 as

$$f = \left( \begin{array}{c} \mathbf{R}_{LI}(\ddot{\mathbf{r}}_{i,I} - \ddot{\mathbf{R}}_{0,I}) - \boldsymbol{\Omega}_L \times \boldsymbol{\Omega}_L \times \boldsymbol{\rho}_L - \dot{\boldsymbol{\Omega}}_L \times \boldsymbol{\rho}_L - 2\boldsymbol{\Omega}_L \times \dot{\boldsymbol{\rho}}_L \\ \frac{d}{dt} \boldsymbol{\rho}_L \\ \frac{1}{2} W(\boldsymbol{\omega}_{BF}) \mathbf{q}_{BF} \\ \mathbf{J}_{G,BF}^{-1} (\sum_j \boldsymbol{\tau}_{j,BF}^{pert} + \sum_k \boldsymbol{\tau}_{k,BF}^{int} - \sum_i \dot{\mathbf{h}}_{i,BF} \\ - \boldsymbol{\omega}_{BF} \times (\mathbf{J}_{G,BF} \boldsymbol{\omega}_{BF} + \sum_i \mathbf{h}_{i,BF})) \end{array} \right) \quad (4.14)$$

In order to be able to integrate Equation 4.14, the quantities  $\ddot{\mathbf{r}}_{i,I}$  and  $\ddot{\mathbf{R}}_{0,I}$  are needed. Both of them can be derived by Equation 3.4, concerning  $\ddot{\mathbf{R}}_{0,I}$  a brief discussion has been done at the beginning of the chapter, while concerning  $\ddot{\mathbf{r}}_{i,I}$  the following holds

$$\ddot{\mathbf{r}}_{i,I} = \ddot{\mathbf{r}}_{GP,i} + \ddot{\mathbf{r}}_{D,i} + \ddot{\mathbf{r}}_{SP,i} + \ddot{\mathbf{r}}_{TB,Moon,i} + \ddot{\mathbf{r}}_{TB,Sun,i}$$

The perturbations are function of the absolute inertial position  $\mathbf{r}_{i,I}$  and velocity  $\dot{\mathbf{r}}_{i,I}$  that are not available a priori from the state vector  $\mathbf{X}_i$ , but they can easily be computed as follows

$$\mathbf{r}_{i,I} = \mathbf{R}_{IL} \boldsymbol{\rho}_{i,L} + \mathbf{R}_{0,I}$$

$$\dot{\mathbf{r}}_{i,I} = \mathbf{R}_{IL} \dot{\boldsymbol{\rho}}_{i,L} + \boldsymbol{\Omega}_I \times (\mathbf{R}_{IL} \boldsymbol{\rho}_{i,L}) + \dot{\mathbf{R}}_{0,I}$$

where  $\mathbf{R}_{IL}$  is the transformation matrix from LVLH to inertial frame, and  $\boldsymbol{\Omega}_I$  is the angular velocity of the LVLH wrt Inertial frame in inertial components (i.e.  $\boldsymbol{\Omega}_I = \mathbf{R}_{IL} \boldsymbol{\Omega}$ ). Now it is possible to write the complete system which considers the entire formation dynamics wrt LVLH frame. If  $N$  denotes the number of satellites composing the formation, the system can be written as

$$\begin{pmatrix} \dot{\mathbf{R}}_0 \\ \ddot{\mathbf{R}}_0 \\ \dot{\mathbf{X}}_1 \\ \vdots \\ \dot{\mathbf{X}}_N \end{pmatrix} = \begin{pmatrix} \frac{d}{dt}\mathbf{R}_0 \\ \sum_j \mathbf{a}_{j,I} \\ f(\ddot{\mathbf{r}}_1, \ddot{\mathbf{R}}_0, \boldsymbol{\Omega}, \dot{\boldsymbol{\Omega}}, \mathbf{X}_1) \\ \vdots \\ f(\ddot{\mathbf{r}}_N, \ddot{\mathbf{R}}_0, \boldsymbol{\Omega}, \dot{\boldsymbol{\Omega}}, \mathbf{X}_N) \end{pmatrix} \quad (4.15)$$

where  $\sum_j \mathbf{a}_{j,I}$  indicates the sum in inertial frame of the accelerations acting on the chief spacecraft.

Given a set of initial conditions, in particular, the initial position and velocity vectors of the LVLH frame, and the initial relative position and velocity vectors expressed in LVLH components of all the spacecrafts of the formation, it is possible to integrate Equation 4.15 to obtain the relative dynamics at each instant of the integration interval. It is good to remark that Equation 4.15 does not consider the control laws which will be presented in Chapter 6, so it describes just the free-flying motion.

# Chapter 5

## Configurations and Stability

In Chapter 1 a few examples of applications have been presented highlighting the great versatility of this kind of system. Depending on the application the formation is designed to have a particular relative configuration of the followers so that mission requirements can be met in the best possible way. Considering that the spacecrafts are subject to the perturbations, the most important presented in Chapter 3, they tend to drift apart from their assigned position so decomposing the desired structure of the entire formation. It is possible to correct periodically this drift by using some active control techniques, some of them analysed in Chapter 6, but this requires the use of energy coming from stored propellant. As mentioned in the introduction, the satellites are equipped with a limited amount of propellant, which implies a tendency to reduce these corrections to a minimum in order to extend the duration of the mission. The capability of the formation to maintain its initial relative positions without external control actions is called *Stability*. In this chapter, passive techniques which have the purpose of improving the stability of the formation are analysed. In particular, the Initial Relative Conditions (IRC) of the followers with respect to the chief represent the most important aspect to consider when designing a long-lasting mission. These conditions can be divided into Initial Relative Positions (IRP) and Initial Relative Velocities (IRV). IRP are usually fixed by external constraints, the main one is the kind of data the mission is designed to take, for example LISA mission (Chapter 1) requires a triangular shape in order to measure gravitational waves. IRP define the configuration of the formation, and they often represent the principal quantities control algorithms aim at keeping constant. While IRV are usually chosen to improve the stability. The objectives of this chapter are to present some of the most used configurations for remote sensing and the problems on the stability of the formation related to non-correct initial conditions. Then, the method of the *Energy Matching* which describes how to derive correct IRC is

reported. Finally, some results quantifying how this method improved the stability of the presented configurations are showed and discussed.

## 5.1 Clohessy-Wiltshire IRC

The most important relative dynamics equations derivation can be attributed to Clohessy-Wiltshire (CW equations) [50]. They obtained the equations in a simple case, i.e. they derived relative motion equations of a target (a follower in our case) moving in a circular orbit wrt a chaser (LVLH frame or chief in our case) following an elliptical or circular orbit. The equations, usually written for the uncontrolled propagation (appropriate for a stability analysis), are the following:

$$\begin{aligned}
 \ddot{x} &= 3n^2x + 2n\dot{y} \\
 \ddot{y} &= -2n\dot{x} \\
 \ddot{z} &= -n^2z \\
 n &= \sqrt{\frac{\mu}{a^3}}
 \end{aligned} \tag{5.1}$$

where  $x$ ,  $y$ ,  $z$  are the relative LVLH position components of the target wrt to the chaser, and  $n$  is the orbital rate of the target body. These equations prove very interesting mostly because a close solution of them exist. So, it is possible to express the position vector and velocity vector of the target as functions of time and initial position and velocity. By introducing the state transition matrices  $\Phi_{\rho\rho}(t)$ ,  $\Phi_{\rho\dot{\rho}}(t)$ ,  $\Phi_{\dot{\rho}\rho}(t)$ ,  $\Phi_{\dot{\rho}\dot{\rho}}(t)$  which describe the influences of the initial position and velocity on the next state, it is possible to report the solution of Equation 5.1

$$\begin{aligned}
 \boldsymbol{\rho}(t) &= \Phi_{\rho\rho}(t) \boldsymbol{\rho}_0 + \Phi_{\rho\dot{\rho}}(t) \dot{\boldsymbol{\rho}}_0 \\
 \dot{\boldsymbol{\rho}}(t) &= \Phi_{\dot{\rho}\rho}(t) \boldsymbol{\rho}_0 + \Phi_{\dot{\rho}\dot{\rho}}(t) \dot{\boldsymbol{\rho}}_0
 \end{aligned} \tag{5.2}$$

$$\Phi_{\rho\rho}(t) = \begin{bmatrix} 4 - 3 \cos nt & 0 & 0 \\ 6(\sin nt - nt) & 1 & 0 \\ 0 & 0 & \cos nt \end{bmatrix}$$

$$\Phi_{\rho\dot{\rho}}(t) = \begin{bmatrix} \frac{1}{n} \sin nt & \frac{2}{n}(1 - \cos nt) & 0 \\ \frac{2}{n}(\cos nt - 1) & \frac{1}{n}(4 \sin nt - 3nt) & 0 \\ 0 & 0 & \frac{1}{n} \sin nt \end{bmatrix}$$

$$\Phi_{\dot{\rho}\rho}(t) = \begin{bmatrix} 3n \sin nt & 0 & 0 \\ 6n(\cos nt - 1) & 0 & 0 \\ 0 & 0 & -n \sin nt \end{bmatrix}$$

$$\Phi_{\dot{\rho}\dot{\rho}}(t) = \begin{bmatrix} \cos nt & 2 \sin nt & 0 \\ -2 \sin nt & 4 \cos nt - 3 & 0 \\ 0 & 0 & \cos nt \end{bmatrix}$$

where  $\boldsymbol{\rho}_0$  and  $\dot{\boldsymbol{\rho}}_0$  are the initial position and velocity of the target wrt to the chaser (the pedex  $L$  indicating that the vectors are referred to LVLH frame has been omitted to lighten the notation). CW equations were firstly applied to rendez-vous problems for which they proved as a sufficient precise solutions where dealing with relative motion with spacecrafts in close-proximity. The linearizations used by this derivation become relevant when the distance between target and chaser increases or when the circularity assumption on the target's orbit is not satisfied. The literature is full of works trying to improve Equations 5.2 deriving the relative dynamics for arbitrary near-circular orbits subject to  $J_2$  perturbing potential [11] or the state transition matrix of relative motion for the perturbed non-circular reference orbit [48]. Further details on the variety of the works accomplished in this domain can be found in [18].

In the context of this work, Equations 5.2 are not appropriate to describe the evolution of relative positions and velocities but they can prove very useful to find initial relative parameters to give to the followers in order to create a desired configuration. In fact, it is possible to re-write the components of equations 5.2 in terms of differential Keplerian elements as follows [37]

$$\begin{aligned} x_i(t) &= -a \cdot \delta e_i \cos(nt - \alpha_i) \\ y_i(t) &= 2a \cdot \delta e_i \sin(nt - \alpha_i) + a \cdot \delta \theta_i \\ z_i(t) &= a \cdot \delta i_i \sin(nt - \beta_i) \end{aligned} \tag{5.3}$$

in particular, Equations 5.3 describe respectively the relative radial, relative along-

track and relative across-track evolution of the  $i$ -th follower wrt chief spacecraft (or the LVLH frame) given the differential orbit inclination  $\delta i_i$ , eccentricity  $\delta e_i$  and argument of latitude  $\delta \theta_i$ . In addition,  $a$  is the semi-major axis of the chief and  $\alpha_i$  and  $\beta_i$  define respectively the initial phase angles in  $xy$  and  $z$  planes.

From Equations 5.3 it is clearer that in the context of CW assumptions the relative radial and along-track motion is decoupled from the across-track motion. A very important remark is that in  $xy$  plane the relative motion describe an ellipse centered at  $[x_i, y_i] = [0, \delta \theta_i]$  while in the  $z$  one the motion is simply harmonic. It is simple to obtain the components of relative velocity vector  $\dot{\boldsymbol{\rho}}_i$  by deriving Equations 5.3

$$\begin{aligned}\dot{x}_i(t) &= a \cdot \delta e_i n \sin(nt - \alpha_i) \\ \dot{y}_i(t) &= 2a \cdot \delta e_i n \cos(nt - \alpha_i) \\ \dot{z}_i(t) &= a \cdot \delta i_i n \cos(nt - \beta_i)\end{aligned}\tag{5.4}$$

As stated before, Equations 5.3 and 5.4 are not accurate to describe relative motions in general case, it will be necessary to integrate the system 4.15, but it is possible to use them in order to set the parameters  $\delta e_i$ ,  $\alpha_i$ ,  $\delta \theta_i$ ,  $\delta i_i$  and  $\beta_i$  to correctly initialize position and velocities of a formation given a desired configuration. It is sufficient to evaluate the equations at  $t = 0$  to obtain the IRC for the  $i$ -th spacecraft

$$\begin{aligned}x_i(0) &= -a \cdot \delta e_i \cos(-\alpha_i) \\ y_i(0) &= 2a \cdot \delta e_i \sin(-\alpha_i) + a \cdot \delta \theta_i \\ z_i(0) &= a \cdot \delta i_i \sin(-\beta_i) \\ \dot{x}_i(0) &= a \cdot \delta e_i n \sin(-\alpha_i) \\ \dot{y}_i(0) &= 2a \cdot \delta e_i n \cos(-\alpha_i) \\ \dot{z}_i(0) &= a \cdot \delta i_i n \cos(-\beta_i)\end{aligned}\tag{5.5}$$

In the following section Equations 5.5 will be used to initialize some configurations which are mostly used for remote sensing, then the stability of these configurations will be tested using the propagation model presented in Chapter 3.

## 5.2 Remote Sensing Configurations

Formation Flying is a particularly interesting system for remote sensing purposes. The literature presents many studies on this subject [37] [21], in particular, applications of the system working as Synthetic Aperture Radar (SAR) have been studied in the last years. Such a system aims at creating a high-resolution image by using the motion of platform on which the equipment is mounted on. The working principle

consists in sending multiple radar pulses in the direction of the target from an initial location, and then in recapturing the echo of the pulses at a different locations in space; signal processing is needed to combine recordings from these multiple antenna positions to create the final image. As the name SAR suggests, this process simulates data taking of a large antenna whose aperture is from hundreds or thousands of meters.

The system just described can be implemented in monostatic, bistatic or multistatic approaches. Monostatic consists in a single platform which works both as transmitter and receiver, sending and collecting the pulses it has previously generated (as described above).

Bistatic and multistatic approaches are those of interest for Formation Flying because more than one platform is involved in the process. In fact, in the first case, the transmitter and receiver antennas are mounted on different platforms, the transmitter has the purpose of illuminating the scene and the receiver collects the echoes in order to create the image (Figure 5.1).

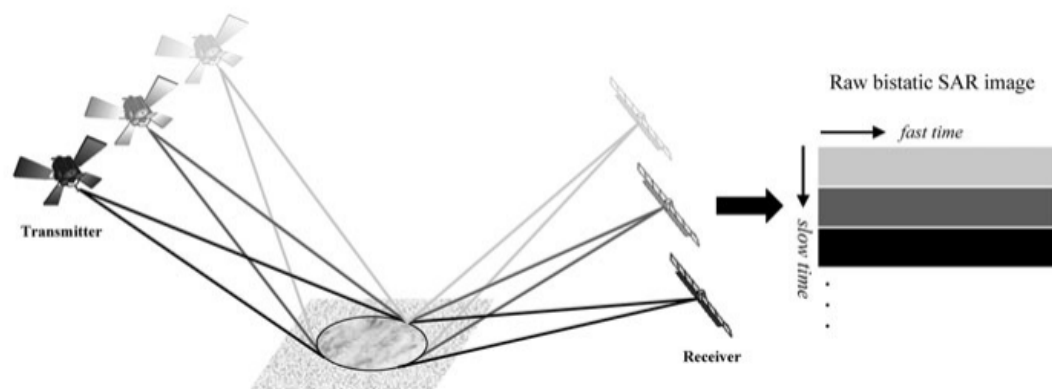


**Figure 5.1:** Bistatic radar working principle, [37]

Multistatic radars extend this concept by using multiple receivers and/or transmitters in order to take more captures making more reliable the target characterization. They can be used in several different configurations. Most used are the *Fully-active* configuration, in which all spacecrafts act as a monostatic radar by sending and receiving the pulses themselves have generated or the *Semi-active* configuration in which one transmitter illuminates the scene and multiple receivers collect the echoes (Figure 5.2).

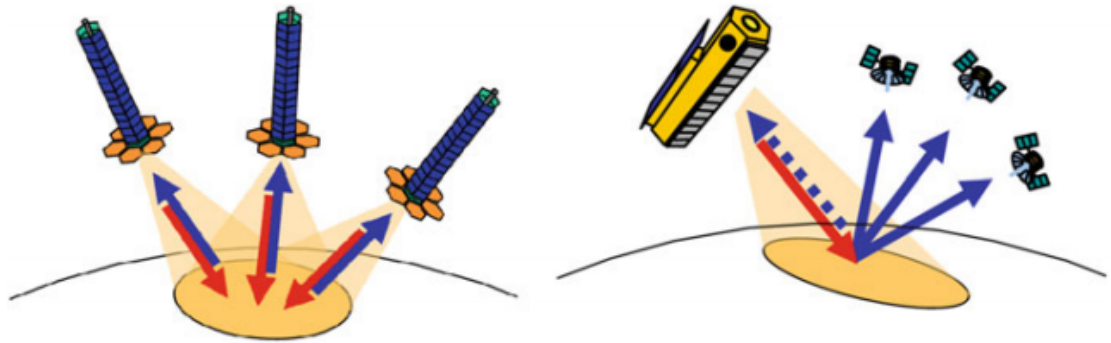


**Figure 5.2:** Multistatic radar working principle. *Left:* Fully-active configuration. *Right:* Semi-active configurations, [37]

From Figures 5.1 and 5.2, it is evident that a fine control of relative position between spacecrafts is required to improve data quality.

In particular, one of the most important quantity to control in such a system to improve performances is the *Baseline* between the spacecrafts of the formation. Considering two spacecrafts of the formation it is possible to define the baseline as the distance between satellites-target conjunctions as showed in Figure 5.3.

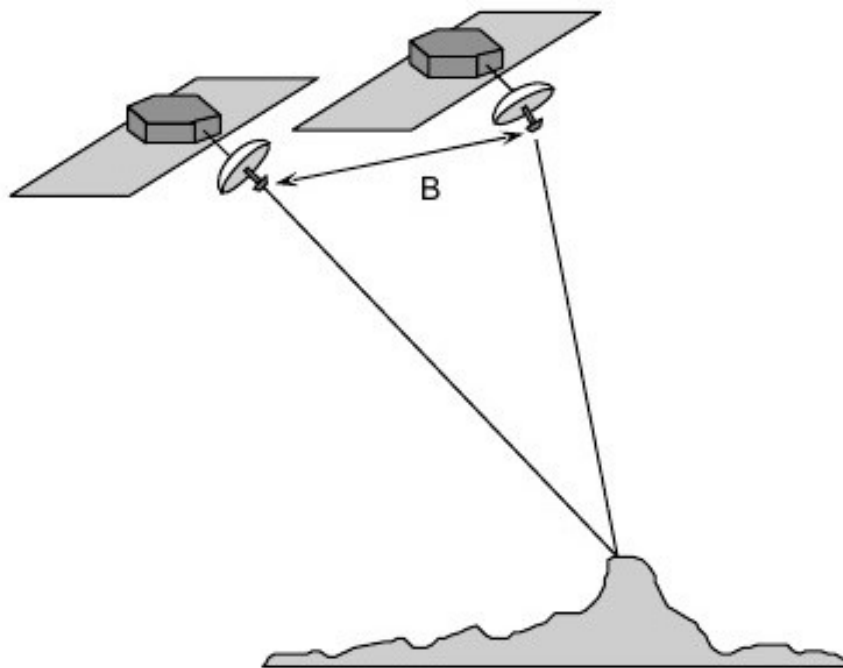


**Figure 5.3:** Representation of radar *Baseline*, [23]

*Baseline* is of relevant importance for the resulting interferometric ground patterns

created by the antennas which ultimately imply the type of measurements and the trend of the Signal to Noise Ratio (SNR) as function of the terrain characteristics. After having introduced the working principles of remote sensing systems involving Formation Flying and the quantities which the data taken depend on, it is possible to analyze the configurations more used in this domain so that practical examples can help in the understanding of the much more general logical process with which it is wanted to carry out the design of the GN&C system and of the problems associated with it.

### 5.2.1 Interferometric Cartwheel (IC) Configuration

Interferometric Cartwheel is a well-known configuration in which the satellites of the formation move in the same orbital plane. Considering the parameters introduced in CW initial conditions Equation 5.5, the last statement implies  $\delta i_i = 0$  ( so that separation in cross-track plane is equal to 0). In addition, the relative eccentricities of the followers wrt the chief is equal for all the spacecrafts ( $\delta e_i = \delta e$ ) ensuring the same amplitude of the motion in the  $xy$  plane elliptic motion. Finally, in order to have an interferometric baseline it is necessary to decide the initial phasing of each spacecraft ( $\alpha_i$ ). This can be done according to different criteria but usually an equal spacing between the followers is the one that guarantees a lower risk of collision. In this configuration it is not necessary to give an initial differential argument of latitude  $\delta \theta_i$  because the phasing above mentioned guarantees in principle the non-intersection of trajectories. It is then possible to summarize the parameters setting through the following equations:

$$\begin{aligned}
 \delta i_i &= 0 \\
 \delta e_i &= \delta e & i = 1, 2, \dots, N \\
 \alpha_i &= \alpha_1 + \frac{2\pi}{N}(i - 1) \\
 \delta \theta_i &= 0
 \end{aligned} \tag{5.6}$$

where  $N$  is the number of the followers spacecrafts (considering that a chief spacecraft could be place at the center of the formation) and  $\alpha_1$  is an arbitrary start phase angle of the first follower. It is possible to visualize a 3D representation of the Interferometric Cartwheel configuration composed by 11 satellites in Figure 5.4 presenting the leader at the center of the formation.

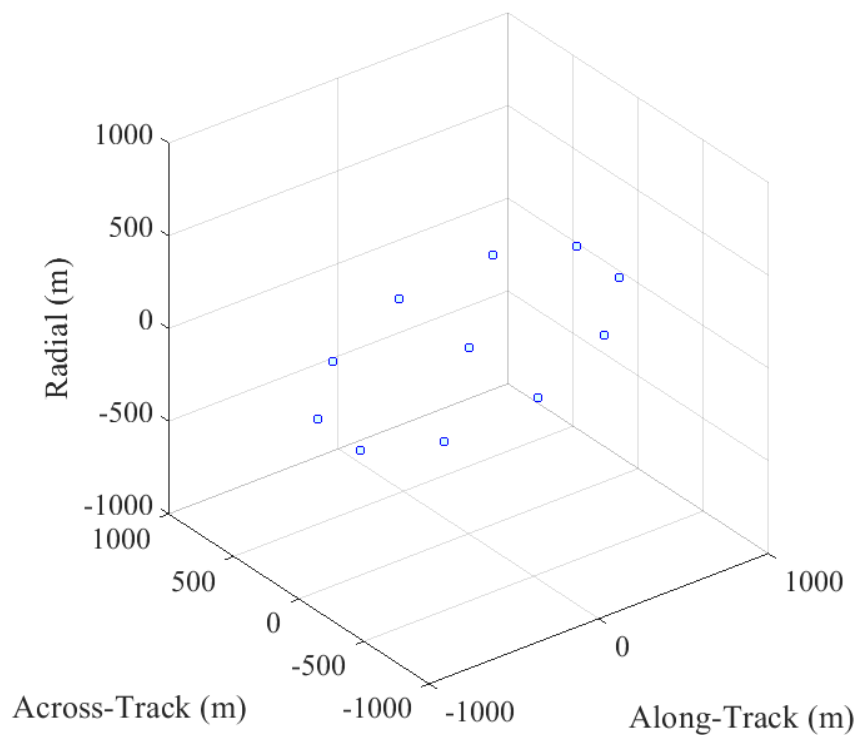


**Figure 5.4:** 3D representation of IC configuration

Regarding its time-evolution, in Figure 5.5 (where  $\Delta r_r$ ,  $\Delta r_t$ ,  $\Delta r_t$  are the radial, along-track and across-track relative positions) it is visible as the initial conditions given by Equation 5.6 have the effect of maintaining the motion in  $xy$  plane in theoretical cases if the CW assumptions are respected. The advantages of this configuration comprise a good stability of the maximum baseline along the orbit with a small variation and a little across-track drift which usually is the drift which implies a greater amount of fuel consumption to be corrected wrt along-track and radial drifts.

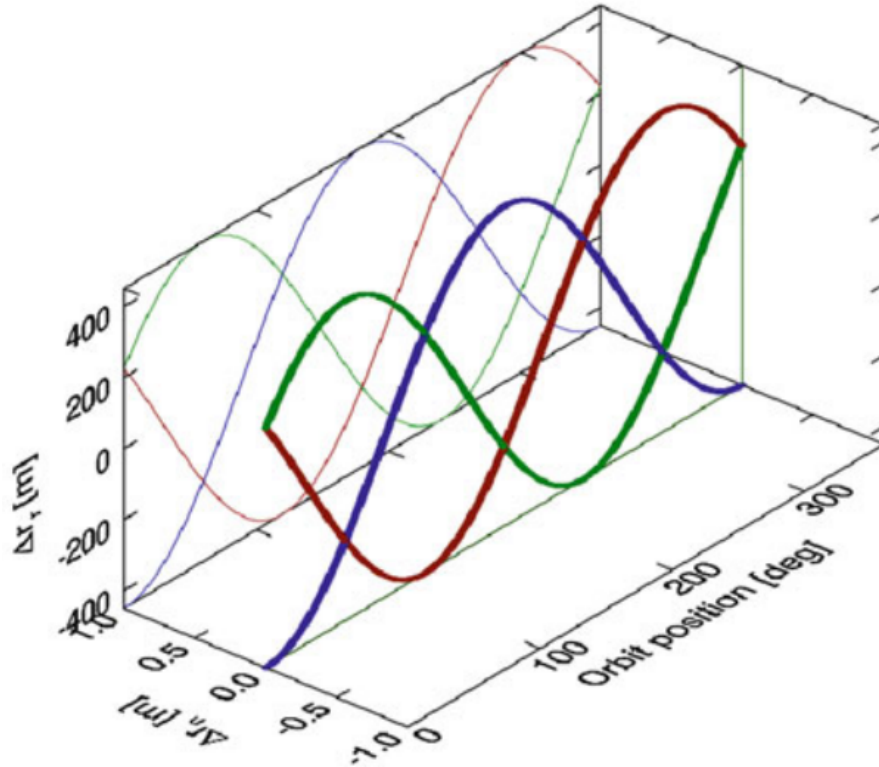


Figure 5.5: Time-evolution of IC configuration, [37]

### 5.2.2 Cross-Track Pendulum (CTP) Configuration

Cross-Track Pendulum is one of the most used configuration for remote sensing applications. It can be said that it represents the opposite case to the IC configuration. In fact, in this case the satellites present a separation in across-track direction through a differential inclination equal for all the spacecrafts ( $\delta i_i = \delta i$ ) with respect to that of the chief. Regarding instead the eccentricity, this configuration foresees  $\delta e_i = 0$  cancelling in this way a difference in radial direction (the motion results therefore confined to the plane  $yz$ ). In this case, however, it is necessary to give a separation in along-track directions through a difference in argument of latitude  $\delta \theta_i$  in order to avoid collisions. Finally, in order to obtain a baseline in cross-track direction it is necessary to give a difference in  $\beta_i$ . Analogously to the previous case, the choice of equispaced phasing is normally used to minimize the risk of collision. Finally, this configuration follows the following:

$$\begin{aligned}
\delta i_i &= \delta i \\
\delta e_i &= 0 \\
\beta_i &= \beta_1 + \frac{2\pi}{N}(i-1) \\
\delta \theta_i &\neq 0
\end{aligned}
\quad i = 1, 2, \dots, N \tag{5.7}$$

Where  $\beta_1$  is an arbitrary start phase angle and the choice of  $\delta \theta_i$  depends on the application. In Figure 5.6 it is possible to see a 3D visualization of the initial CTP configuration composed by 11 spacecraft with the leader placed at the center.

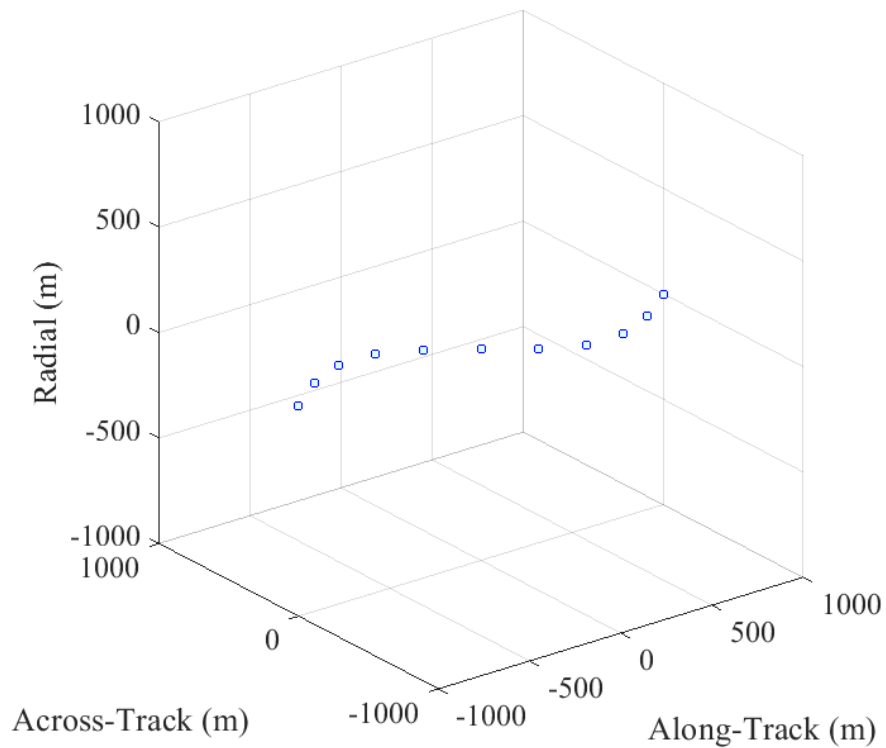


**Figure 5.6:** 3D representation of CTP configuration

Instead, the time-evolution for a 3 satellites case is reported in Figure 5.7 where it is visible the only  $yz$  plane motion and the baselines created in radial direction. The main advantage of CTP is the possibility to have constant along-track baselines, while one of the major disadvantage is that the difference in inclination leads to a differential precession of the RAAN, thus implying a relatively significant drift in across-track direction after a few orbits.

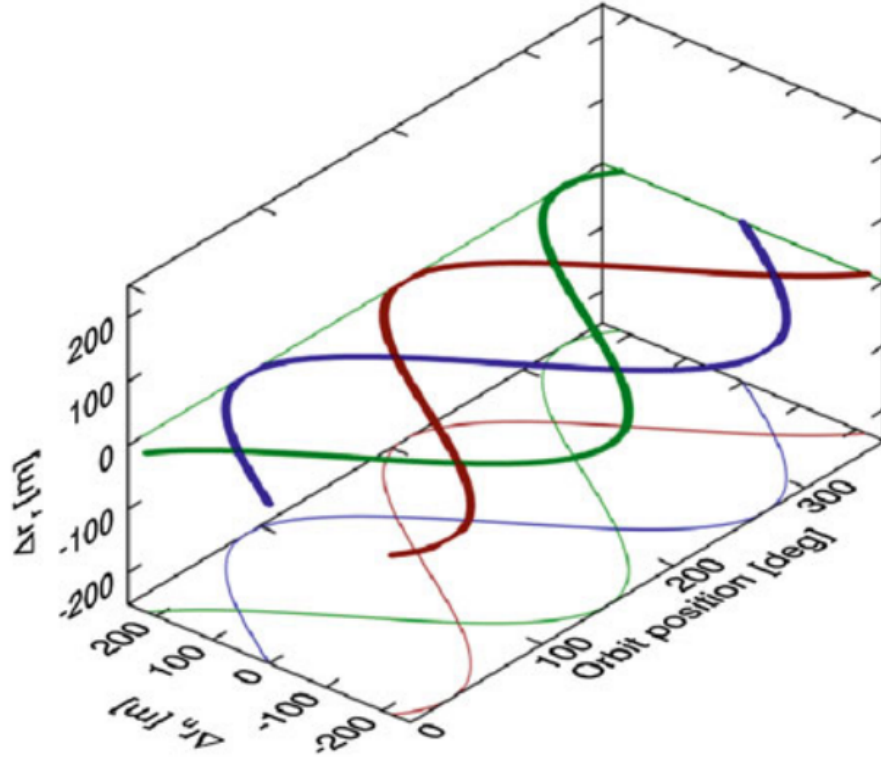


Figure 5.7: Time-evolution of CTP configuration, [37]

### 5.2.3 Cartwheel-Pendulum (CP) Configuration

IC and CTP can be combined in order to create the Cartwheel-Pendulum configuration. It is usually used in a 3 or 4 spacecrafts configuration depending on the presence or not of a leader spacecraft. In this case, CP foresees 2 spacecrafts in a CTP configuration and 1 spacecraft in an IC configuration. Denoting with subscripts 1,2 the quantities of the CP configuration spacecrafts and with 3 the IC one, the parameters to introduce in Equations 5.2 can be summarized as follows

$$\begin{aligned}
 \delta i_{1,2} &= \delta i \neq 0 & \delta i_3 &= 0 \\
 \delta e_{1,2} &= 0 & \delta e_3 &= \delta e \neq 0 \\
 \beta_2 &= \beta_1 + \pi \\
 \alpha_3 &= \alpha \\
 \delta \theta_1 &\neq \delta \theta_2 \neq 0 & \delta \theta_3 &= 0
 \end{aligned} \tag{5.8}$$

where  $\beta_1$  and  $\alpha$  are arbitrary initial phase angles,  $\delta \theta_1 \neq \delta \theta_2 \neq 0$  is needed for the same reasons presented in CTP tractation and  $\delta \theta_3 = 0$  because it is preferable for minimisation risk of collision that spacecraft 3 follows an elliptic motion with the leader placed at the center.

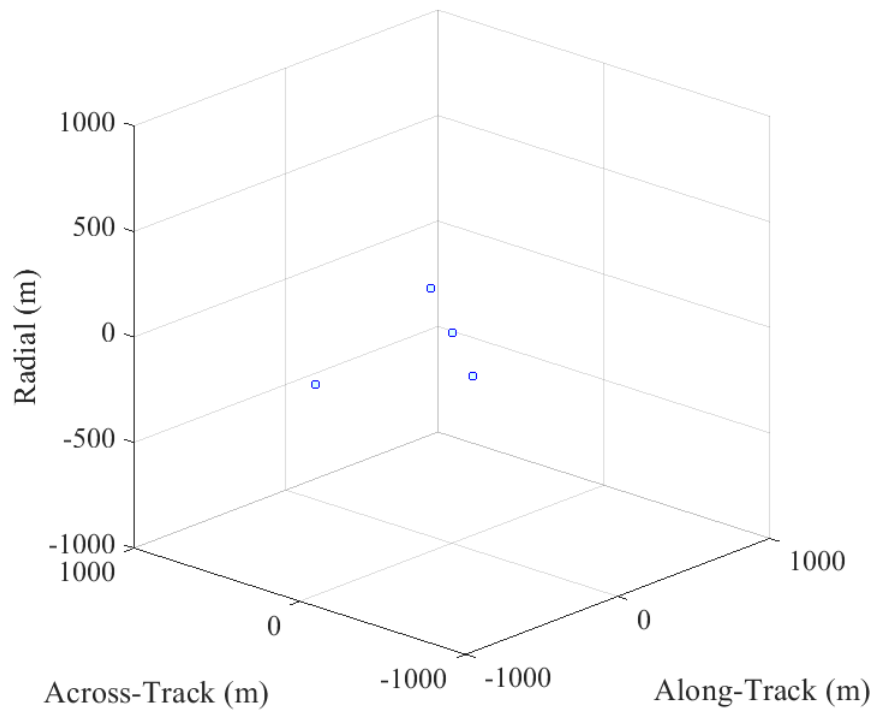


**Figure 5.8:** 3D representation of CP configuration

This configuration simply acquires the disadvantages and advantages of the configurations from which it derives. As previously done, in Figures 5.8 and 5.9 it is possible to visualize a 3D representation of the CP and its orbital propagation in order to better understand the evolution of the baselines created by this configuration. In particular in Figure 5.8 the most distant satellite is the satellite that follows the IC configuration and the others are the two CTP satellites, with the leader at the center. Instead, Figure 5.9 does not present the leader spacecraft at the center.

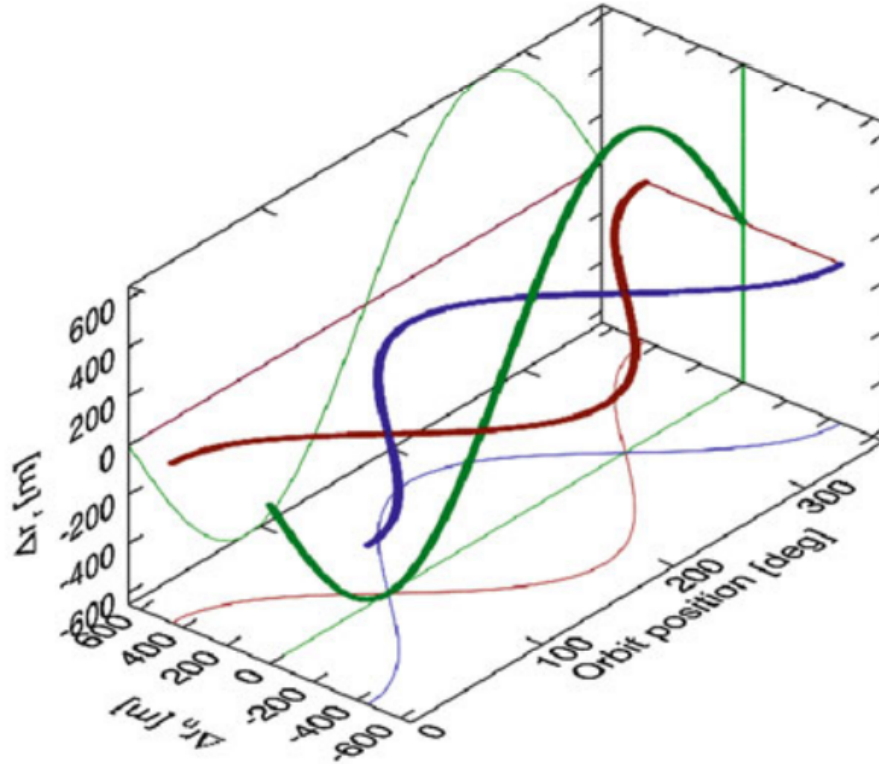


Figure 5.9: Time-evolution of CP configuration, [37]

### 5.2.4 Helix Configuration

In the most general case, Equations 5.2 create an Helix wrt the leader. In simple case, the satellite have the same differential eccentricities and inclination which guarantees separation wrt all planes making this configuration particularly safe with no need for differential argument of latitude, and equispaced phasing in  $xy$  plane at  $z$  direction. In addition, the cross-track and along-track baselines can be easily changed with a relatively low fuel consumption allowing for a multi-objectives mission. The equations of the parameters for composing the Helix configuration are:

$$\begin{aligned}
 \delta i_i &= \delta i \\
 \delta e_i &= \delta e \\
 \alpha_i &= \alpha_1 + \frac{2\pi}{N}(i-1) & i = 1, 2, \dots, N \\
 \alpha_i &= \beta_i \\
 \delta \theta_i &= 0
 \end{aligned} \tag{5.9}$$

Where  $\alpha_1$  is the arbitrary start phase angle. In Figure 5.10 is possible to visualize a 11 spacecrafts Helix configuration.

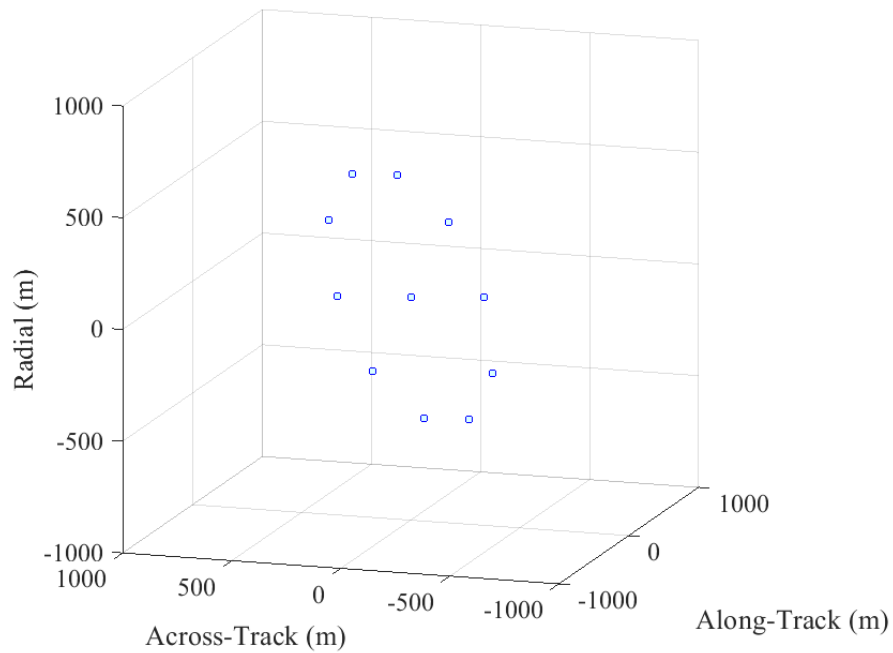


**Figure 5.10:** 3D representation of Helix configuration

Concerning the time-evolution of the configuration, Figure 5.11 presents the most simple Helix case with only two spacecrafts, used in TanDEM-X mission [13]. This configuration allows for a cross-track baseline that never nullifies (except in case of only two spacecrafts where it nullifies in two different instants during the orbit) which is also the cause of unwanted differential RAAN precession.

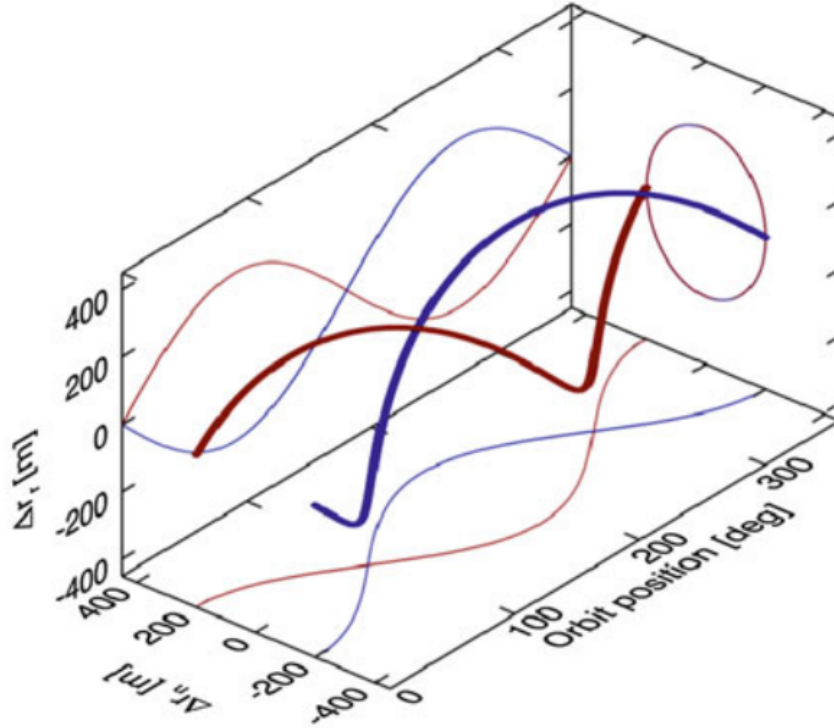


Figure 5.11: Time-evolution of Helix configuration, [37]

### 5.2.5 Stability of the CW Initial Conditions

In this section the stability of the presented configurations initialized with Equations 5.2 is analysed. In particular, each configuration is propagated with the model presented in Chapter 3 in order to monitor the evolution of relative distances in the three directions. In the ideal case, the drift with respect to the leader of each spacecraft should be small over the course of hundreds of orbits so that corrections are kept to a minimum. In the following simulations, the initial leader orbital elements are those presented in Table 5.1.

|          |                         |
|----------|-------------------------|
| $a$      | $6.94761 \times 10^6 m$ |
| $e$      | 0.01                    |
| $i$      | $97^\circ$              |
| $\Omega$ | $270^\circ$             |
| $\omega$ | $70^\circ$              |
| $\nu$    | $0^\circ$               |

Table 5.1: Initial Orbital Parameter of the Leader spacecraft

### 5.2.6 IC free-flying CW Initial Conditions stability

In Figure 5.12 it is possible to visualize relative propagation of Interferometric Cartwheel configuration present in Figure 5.4 initialized with CW initial conditions and parameters as in Table 5.2. After 80 orbits, relative radial and across-track drift is limited, approximately in the worst case, radial drift is of  $2.5 \text{ m/orbit}$  while across-track one is only  $3.8 \times 10^{-2} \text{ m/orbit}$ . On the other hand, as far as along-track stability is concerned, the initial conditions used result in an exaggerated drift (about  $100 \text{ m/orbit}$ ) that would require frequent corrections in order to restore the initial configuration, greatly decreasing the maximum possible mission duration.

|                    |              |
|--------------------|--------------|
| $a \cdot \delta e$ | 100 <i>m</i> |
| $\alpha_1$         | 9°           |
| $N$                | 10           |

**Table 5.2:** IC parameters for simulation.

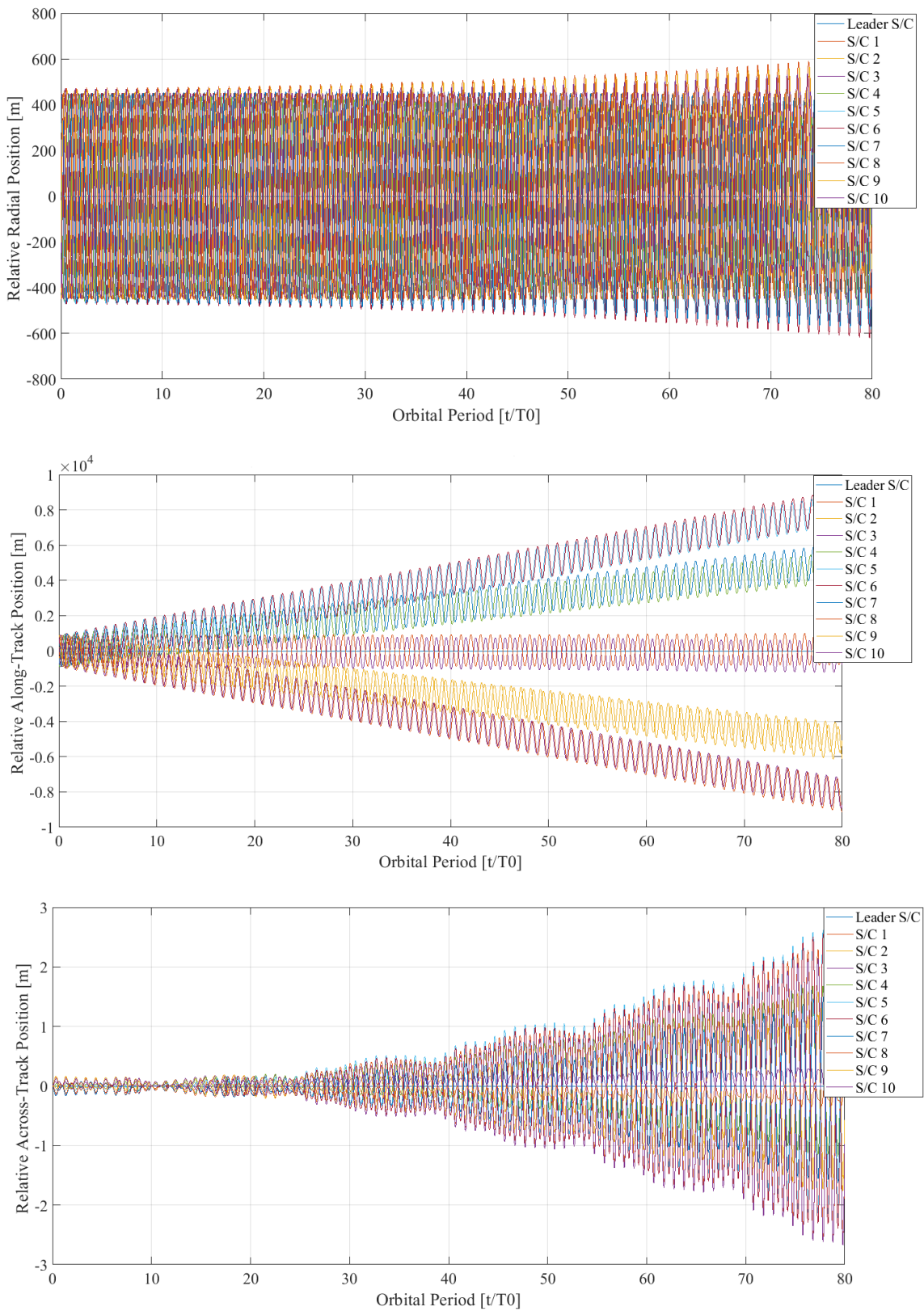


Figure 5.12: IC relative dynamics propagation, CW Initial Conditions

### 5.2.7 CTP free-flying CW Initial Conditions stability

Cross-Track Pendulum configuration presented in Figure 5.6 has a very similar behaviour wrt the IC one. Figure 5.13 reports the results of relative positions for a 80 orbits simulation using parameters of the configuration as in Table 5.3. Also in this case, radial and across-track drifts are quite limited, about  $0.38 m/orbit$  for radial drift and  $1.25 m/orbit$  for across-track one. Along-track drift has the opposite direction wrt IC configuration, in fact, spacecrafts trajectories tend to converge towards the chief spacecraft, this behaviour is not acceptable because, if not corrected, could lead the spacecrafts to multiple collisions after only 40 orbits. It is possible to affirm that, in terms of fuel consumption, CTP configuration initialized through Equations 5.2, is more sustainable than IC one, but not still feasible for long-duration missions.

|                         |       |
|-------------------------|-------|
| $a \cdot \delta i$      | 250 m |
| $\beta_1$               | 9°    |
| $N$                     | 10    |
| $a \cdot \delta \theta$ | 200 m |

**Table 5.3:** CTP parameters for simulation.

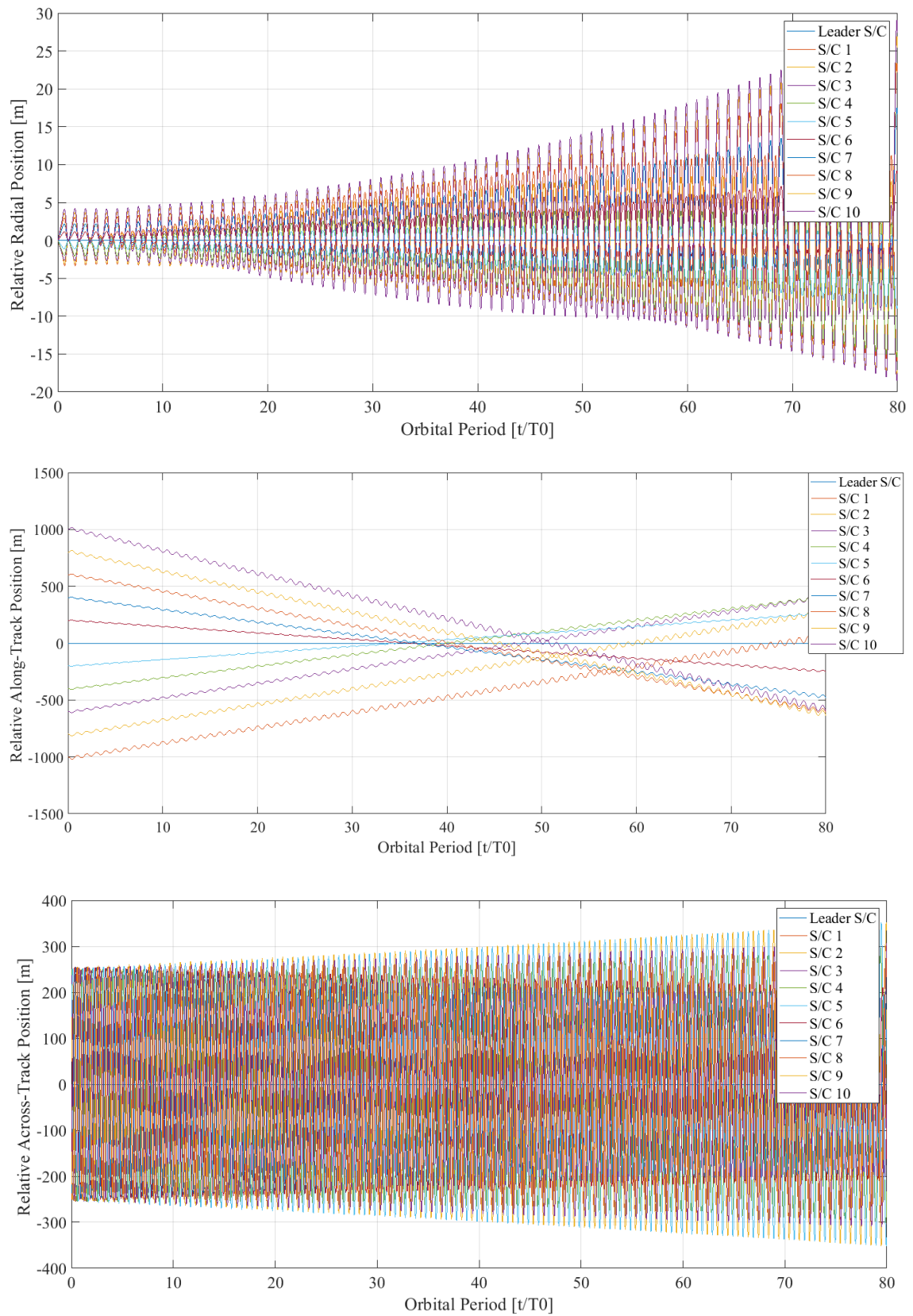


**Figure 5.13:** CTP relative dynamics propagation, CW Initial Conditions

### 5.2.8 CP free-flying CW Initial Conditions stability

Figure 5.14 presents the simulation for Cartwheel-Pendulum configuration showed in Figure 5.8. The parameters for the simulation are reported in Table 5.4. In this case, the two spacecrafts in CTP configuration present no significant radial and across-track drifts, as showed in the previous section, In the same way, the satellite moving predominantly in the  $xy$  plane, exhibits a very small drifts relatively to the same directions. Instead, similarly to the previous configurations, the behaviour in along-track direction is not acceptable. In particular the third satellite drifts with a rate of about  $18 m/orbit$ , which is not adapt for a long-duration mission.

|                           |             |
|---------------------------|-------------|
| $a \cdot \delta i_1$      | 450 m       |
| $a \cdot \delta i_2$      | 450 m       |
| $a \cdot \delta e_3$      | 650 m       |
| $\beta_1$                 | $90^\circ$  |
| $\beta_2$                 | $270^\circ$ |
| $\alpha_3$                | $90^\circ$  |
| $a \cdot \delta \theta_1$ | 350 m       |
| $a \cdot \delta \theta_2$ | -350 m      |

**Table 5.4:** CP parameters for simulation.

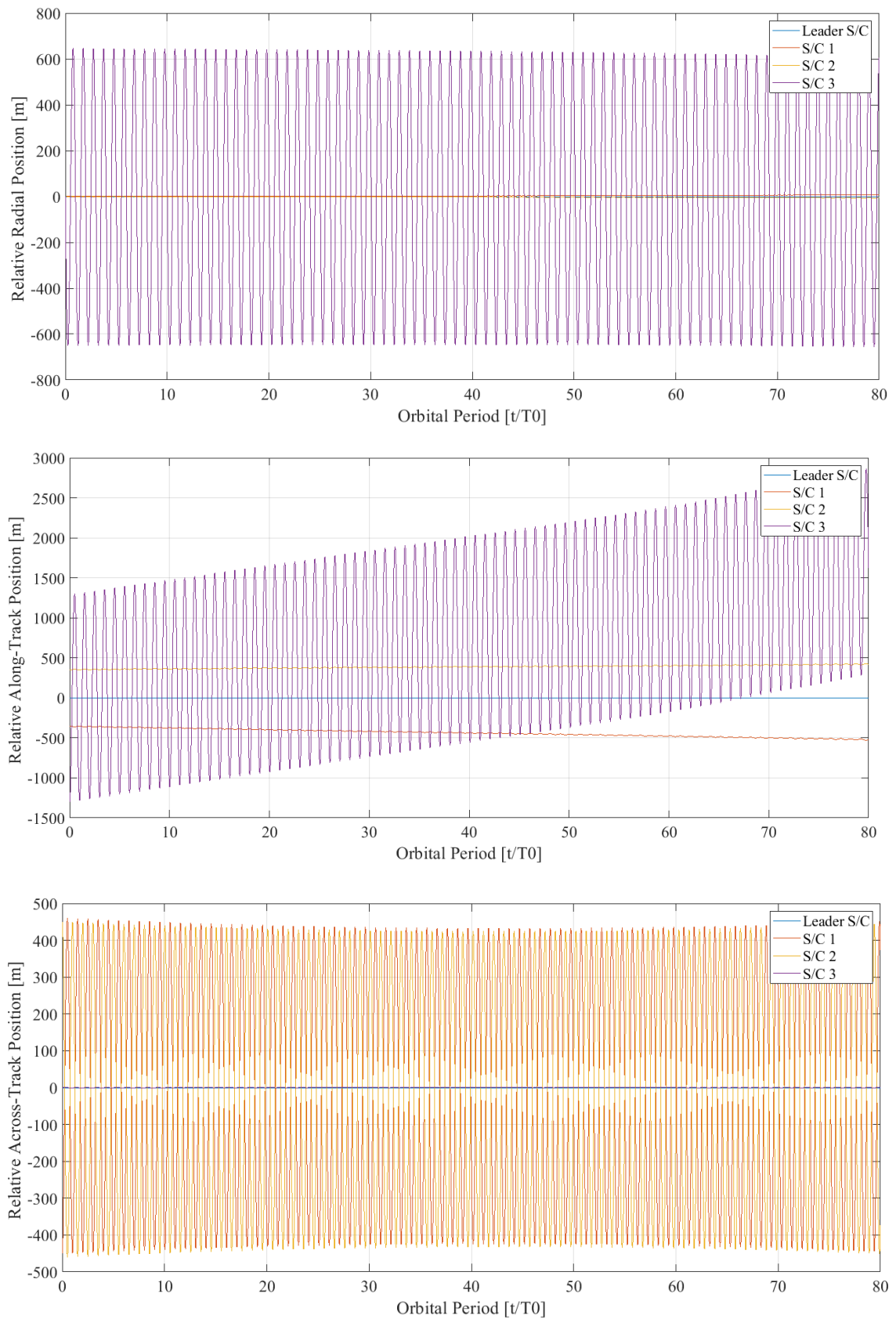


**Figure 5.14:** CP relative dynamics propagation, CW Initial Conditions

### 5.2.9 Helix free-flying CW Initial Conditions stability

Finally, the free-flying Helix configuration propagation is presented in Figure 5.15. The configuration is that reported in Figure 5.10 but with seven spacecrafts in total. The parameters of the configuration are reported in Table 5.5

|                    |              |
|--------------------|--------------|
| $a \cdot \delta i$ | 450 <i>m</i> |
| $a \cdot \delta e$ | 650 <i>m</i> |
| $\alpha_1$         | 9°           |

**Table 5.5:** Helix parameters for simulation.

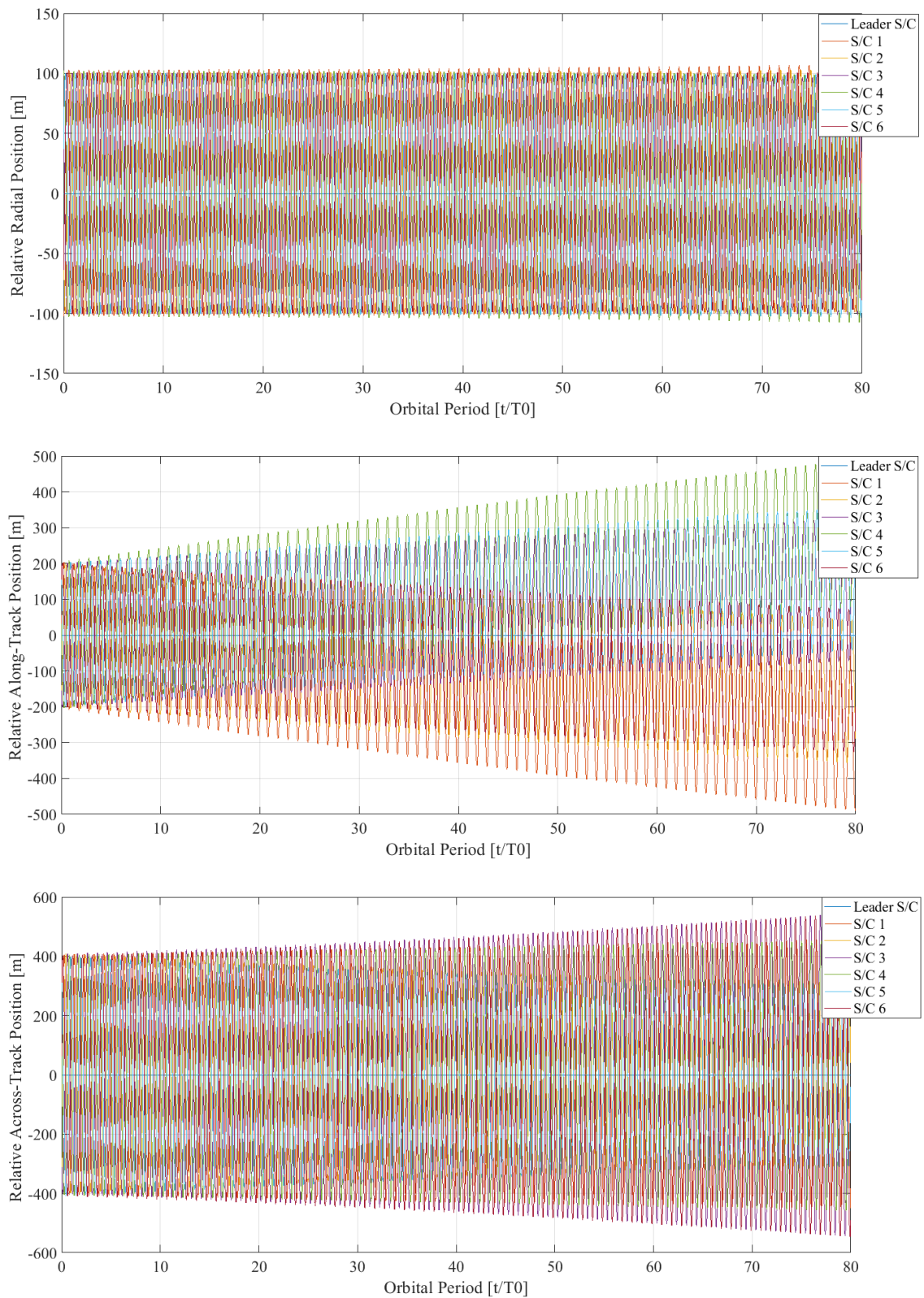


**Figure 5.15:** Helix relative dynamics propagation, CW Initial Conditions

### 5.3 Energy Matching (EM) Initial Conditions Method

As it has been shown in previous sections the CW initial conditions are not suitable for long-duration missions. In particular, the along-track drift proved to be the main problem for the stability of the analysed configurations, even reaching the order of hundreds meters per orbit. For the reasons above, it is clear that an alternative initialization is needed.

In order to find the solution to this problem it is necessary to find the cause of these large drifts. Firstly, it is evident that the linearization and assumptions done by CW initial conditions are the primary source of instability. The great advantage of this methodology is its simpleness in the physical interpretation thus resulting in an easy task of finding parameters which return a given configuration. In order to maintain this useful aspect, the Energy Matching (EM) Initial Conditions Method analyses Equations 5.2 and finds Initial Relative Velocities for the followers which minimize the drifts by imposing no difference in energy between the spacecrafts of the formation.

In order to simplify the logical process that EM method follows to find these IRVs, it is possible to approach the problem by considering the simple Keplerian dynamics. In fact, in such dynamics, it is possible to state that the period of the  $i$ -th satellite depends only on the gravitational constant and the semi-major axis of the orbit through the following relation

$$T_i = 2\pi \sqrt{\frac{a_i^3}{\mu}}$$

So, it is evident, that in Keplerian dynamics a differential semi-major axis would cause a differential period thus resulting in relative drift between the spacecrafts of the formation. The semi-major axis also defines the energy of the orbit from which the name of the method derives. In fact, if the energy (represented by  $a$ ) is matched (or balanced), the relative drift will be reduced. Of course, the only equality of  $a$  is not sufficient to stabilize a formation which is subject to many conservative and non-conservative perturbing forces, but, if through the same procedure, the main perturbations are taken into account when calculating the energy of the spacecrafts, good results can be achieved. With these notions in mind, following sections will show how EM considering  $J_2$  potential field will allow to find IRVs which make the formation stable for several orbits [8].

#### 5.3.1 Linear Energy Matching

For the clarity of the discussion, it is convenient to recall in this sections the Equations 5.2

$$\begin{bmatrix} x(t) \\ y(t) \\ z(t) \\ \dot{x}(t) \\ \dot{y}(t) \\ \dot{z}(t) \end{bmatrix} = \Phi(t) \begin{bmatrix} x(0) \\ y(0) \\ z(0) \\ \dot{x}(0) \\ \dot{y}(0) \\ \dot{z}(0) \end{bmatrix}$$

where  $\Phi(t)$  equals

$$\begin{bmatrix} 4 - 3 \cos nt & 0 & 0 & \sin nt/n & 2(1 - \cos nt)/n & 0 \\ 6 \sin nt - 6nt & 1 & 0 & 2(-1 + \cos nt)/n & 4 \sin nt/n - 3t & 0 \\ 0 & 0 & \cos nt & 0 & 0 & \sin nt/n \\ 3n \sin nt & 0 & 0 & \cos nt & 2 \sin nt & 0 \\ 6n(-1 + \cos nt) & 0 & 0 & -2 \sin nt & -3 + 4 \cos nt & 0 \\ 0 & 0 & -n \sin nt & 0 & 0 & \cos n \end{bmatrix}$$

The majority of coefficients in CW equations are sinusoidal, but there are some terms which are linear in time (all the terms which are multiplied for  $t$ ). These terms are those which contribute more to the drift presented in the last sections. In fact, it can be noticed how these terms are present in the second line of the matrix, i.e. in the line describing the evolution of the relative along-track direction.

For these considerations, it is possible to initialize relative velocities in order to nullify these terms, thus results in the following equation

$$\dot{y}_{LEM}(0) = -2nx(0) \quad (5.10)$$

where the subscript LEM stays for Linear Energy Matching. Equation 5.10 is sufficient to eliminate the time-linear coefficients, but, for defining completely the IRV, also  $\dot{x}(0)$  and  $\dot{z}(0)$  have to be initialized. If no particular initial velocities are required, a good choice in order to minimize propellant is to set them to 0. So, the final conditions are

$$\dot{x}_{LEM}(0) = 0 \quad \dot{y}_{LEM}(0) = -2nx(0) \quad \dot{z}_{LEM}(0) = 0 \quad (5.11)$$

Otherwise, if a particular configuration wants to be created,  $\dot{x}(0)$  and  $\dot{z}(0)$  can be initialized as done in previous sections.

This is a first step towards a greater stability but it is not sufficient. In fact, the equations used consider Keplerian dynamics and their efficiency drastically reduces when the satellites so initialized are subject to non-Keplerian dynamics.

### 5.3.2 Non-Linear Energy Matching

It is possible to impose Energy Matching using non-linear energy equation for Keplerian dynamics. If  $\mathbf{V}_{NEM}$  is the absolute velocity vector of the general follower which has to be retrieved, and  $\mathbf{V}$  is the absolute velocity of the leader spacecraft, non-linear energy matching condition holds

$$\frac{\|\mathbf{V}\|^2}{2} - \frac{\mu}{r} = \frac{\|\mathbf{V}_{NEM}\|^2}{2} - \frac{\mu}{r_{NEM}} \quad (5.12)$$

where  $r$  and  $r_{NEM}$  are the norm of the inertial positions of leader and follower respectively. Equation 5.12 can be solved for  $\|\mathbf{V}_{NEM}\|$ , thus obtaining

$$\|\mathbf{V}_{NEM}\| = \sqrt{\|\mathbf{V}\|^2 + 2\left(\frac{\mu}{r_{NEM}} - \frac{\mu}{r}\right)} \quad (5.13)$$

In Keplerian dynamics, it is possible to express the vectors  $\mathbf{V}_{NEM}$  and  $\mathbf{V}$  in LVLH components as follows

$$\begin{aligned} \mathbf{V} &= v_x \hat{\mathbf{x}} + \frac{h}{r} \hat{\mathbf{y}} \\ \mathbf{V}_{NEM} &= (v_x + \dot{x}_{NEM} - y_{NEM}\omega_z) \hat{\mathbf{x}} + \left(\frac{h}{r} + \dot{y}_{NEM} + x_{NEM}\omega_z\right) \hat{\mathbf{y}} + \dot{z}_{NEM} \hat{\mathbf{z}} \end{aligned}$$

where  $\hat{\mathbf{x}}$ ,  $\hat{\mathbf{y}}$ ,  $\hat{\mathbf{z}}$  are the LVLH versors, while  $v_x$ ,  $h$  and  $\omega_z = n$  are respectively the radial velocity, the angular momentum of the leader and the component in  $\hat{\mathbf{z}}$  of the LVLH frame angular velocity. Equation 5.12 adds a condition on the module of the velocity vector of the follower, so if its direction is the same of Linear Energy Matching, it is possible to calculate the vector  $\mathbf{V}_{NEM}$  through the following

$$\mathbf{V}_{NEM} = \frac{\|\mathbf{V}_{NEM}\|}{\|\mathbf{V}_{LEM}\|} \mathbf{V}_{LEM} = \frac{\sqrt{\|\mathbf{V}\|^2 + 2\left(\frac{\mu}{r_{NEM}} - \frac{\mu}{r}\right)}}{\|\mathbf{V}_{LEM}\|} \mathbf{V}_{LEM}$$

writing  $\mathbf{V}_{LEM}$  in LVLH frame as done for  $\mathbf{V}_{NEM}$  as follows

$$\mathbf{V}_{LEM} = (v_x + \dot{x}_{LEM} - y_{LEM}\omega_z) \hat{\mathbf{x}} + \left(\frac{h}{r} + \dot{y}_{LEM} + x_{LEM}\omega_z\right) \hat{\mathbf{y}} + \dot{z}_{LEM} \hat{\mathbf{z}}$$

and substituting it in Equation 5.3.2, imposing the same initial relative position ( $\boldsymbol{\rho}_{NEM} = \boldsymbol{\rho}_{LEM} = \boldsymbol{\rho}(0) = [x(0), y(0), z(0)]^T$ ) and evaluating for  $t = 0$ , the initial

relative velocity which considers non-linear energy matching is found

$$\begin{aligned}
 \dot{x}_{NEM}(0) &= \frac{\|\mathbf{V}_{NEM}\|}{\|\mathbf{V}_{LEM}\|} \dot{x}_{LEM}(0) + \left( \frac{\|\mathbf{V}_{NEM}\|}{\|\mathbf{V}_{LEM}\|} - 1 \right) (v_x - y(0)\omega_z) \\
 \dot{y}_{NEM}(0) &= \frac{\|\mathbf{V}_{NEM}\|}{\|\mathbf{V}_{LEM}\|} \dot{y}_{LEM}(0) + \left( \frac{\|\mathbf{V}_{NEM}\|}{\|\mathbf{V}_{LEM}\|} - 1 \right) \left( \frac{h}{r_0} + x(0)\omega_z \right) \\
 \dot{z}_{NEM}(0) &= \frac{\|\mathbf{V}_{NEM}\|}{\|\mathbf{V}_{LEM}\|} \dot{z}_{LEM}(0)
 \end{aligned} \tag{5.14}$$

It is possible to substitute Equations 5.11, in order to obtain the final version

$$\begin{aligned}
 \dot{x}_{NEM}(0) &= \left( \frac{\|\mathbf{V}_{NEM}\|}{\|\mathbf{V}_{LEM}\|} - 1 \right) (v_x - y(0)\omega_z) \\
 \dot{y}_{NEM}(0) &= \frac{\|\mathbf{V}_{NEM}\|}{\|\mathbf{V}_{LEM}\|} (-2\omega_z x(0)) + \left( \frac{\|\mathbf{V}_{NEM}\|}{\|\mathbf{V}_{LEM}\|} - 1 \right) \left( \frac{h}{r_0} + x(0)\omega_z \right) \\
 \dot{z}_{NEM}(0) &= 0
 \end{aligned} \tag{5.15}$$

where  $r_0$  represents the initial distance of the leader from the center of the Earth and  $\|\mathbf{V}_{NEM}\|$  can be calculated through Equation 5.13.

The derived equations present minimal drift in all directions when the relative motion includes arbitrary eccentricity of both the leader and the followers. Instead, when the followers are initialized with Equations 5.15 and then propagated in a non-Keplerian dynamics the stability of the formation is still compromised. In fact, the perturbations act modifying the energy of the orbit followed by the followers thus resulting in a modification of Equation 5.12 and consequently all the procedure above presented is not valid anymore. [8] proposes an alternative method for initializing any leader-follower pair such that the motion is stable in an environment where the non-perfect sphericity of the earth ( $J_2$ ) is considered. Since  $J_2$  is the most important perturbation in low orbit, these initial conditions are very efficient in case of formations working in LEO and are able to maintain a good level of stability even if the dynamics with which the formation is propagated includes perturbations of minor importance (Drag, Solar Pressure, etc... Chapter 3).

### 5.3.3 Energy Matching including $J_2$ perturbation

Before explaining the procedure to impose Energy Matching including  $J_2$ , it can be useful to make some clarifications. In general, through the CW equations, the only fixed initial relative velocity is the along-track component  $\dot{y}_{LEM}(0) = -2\omega_z x(0)$ , the radial and across-track components, observing the Equations 5.2 have not to satisfy particular conditions in order to eliminate some particular drift. As they are free, they can be set to zero, as done in Equation 5.11 for fuel saving in deployment phase, or they can be set in order that other conditions are satisfied. In particular, [8] set them in order to reduce risk of collision (condition on  $\dot{x}_{LEM}(0)$ ) and to reduce across-track drift due to differential RAAN (condition on  $\dot{z}_{LEM}(0)$ ). In this case their values are

$$\dot{x}_{LEM}(0) = \frac{1}{2}\omega_z y(0) \quad (5.16)$$

$$\dot{z}_{LEM}(0) = -\omega_z z(0) \tan \theta_0 \quad (5.17)$$

where  $\theta_0$  is the initial argument of latitude of the leader spacecraft. It is possible to express Equations 5.16, 5.10 and 5.17 in matrix form

$$\begin{bmatrix} \dot{x}_{LEM}(0) \\ \dot{y}_{LEM}(0) \\ \dot{z}_{LEM}(0) \end{bmatrix} = \mathbf{R}_{\omega_z} \begin{bmatrix} x(0) \\ y(0) \\ z(0) \end{bmatrix} = \begin{bmatrix} 0 & \frac{1}{2}\omega_z & 0 \\ -2\omega_z & 0 & 0 \\ 0 & 0 & -\omega_z \tan \theta_0 \end{bmatrix} \begin{bmatrix} x(0) \\ y(0) \\ z(0) \end{bmatrix} \quad (5.18)$$

For simplicity of equations, in this work, Equation 5.18 will be used as the starting point for the development of the Non-Linear EM with  $J_2$  method, but, in general, the steps that will be presented can be performed perfectly in the same way in the case where it is possible to express the initial relative velocities as linear functions in the relative initial positions, i.e. in the following way

$$\begin{bmatrix} \dot{x}_{LEM}(0) \\ \dot{y}_{LEM}(0) \\ \dot{z}_{LEM}(0) \end{bmatrix} = \begin{bmatrix} a_1 & a_2 & a_3 \\ -2\omega_z & 0 & 0 \\ b_1 & b_2 & b_3 \end{bmatrix} \begin{bmatrix} x(0) \\ y(0) \\ z(0) \end{bmatrix} \quad (5.19)$$

where  $a_1, a_2, a_3, b_1, b_2, b_3$  are arbitrary constants chosen following different criteria. After detailing this aspect, it is possible to derive EM in case of presence of  $J_2$  perturbation.

As explained in Chapter 3, after the central body perturbation the main effect on

an orbiting satellite of the gravity potential is that due to first zonal coefficient  $J_2$ . Thanks to conservative property of the force field generated by gravity potential, it is possible to write the gravity potential and its gradient truncated to consider up to  $J_2$  term as follows [14]

$$U_{J_2} = -\frac{\mu}{r} - \frac{k_{J_2}}{r^3} \left( \frac{1}{3} - \sin^2 i \sin^2 \theta \right) \quad (5.20)$$

$$\nabla U_{J_2} = \frac{\mu}{r^2} \hat{\mathbf{x}} + \frac{k_{J_2}}{r^4} (1 - 3 \sin^2 i \sin^2 \theta) \hat{\mathbf{x}} + \frac{k_{J_2} \sin^2 i \sin 2\theta}{r^4} \hat{\mathbf{y}} + \frac{k_{J_2} \sin 2i \sin \theta}{r^4} \hat{\mathbf{z}}$$

where  $k_{J_2} = \frac{3}{2} J_2 \mu R_e^2$  and  $R_e$  is the reference Earth radius,  $i$  and  $\theta$  are the inclination and argument of latitude of the considered spacecraft.  $U_{J_2}$  represents the energy of a satellite subject to  $J_2$  potential field. It can be noticed that  $\nabla U_{J_2}$  is not aligned with the radial given by the versor  $\hat{\mathbf{x}}$  of the LVLH. This aspect is important because, Equation 5.18 is written in a frame which is aligned with the force acting on the LVLH frame, and in order to exploit it properly, a frame aligned with  $\nabla U_{J_2}$  has to be considered. If we consider a frame in which its versor  $\hat{\mathbf{x}}'$  is aligned with  $\nabla U_{J_2}$  and  $\hat{\mathbf{y}}'$  remains in the orbital plane, it is possible to transform a generic vector described in the LVLH frame into this new frame by two rotations, a counterclockwise rotation about the  $\hat{\mathbf{z}}$  axis by the angle  $\alpha$ , resulting in the intermediate frame of versors  $\hat{\hat{\mathbf{x}}}, \hat{\hat{\mathbf{y}}}, \hat{\hat{\mathbf{z}}}$ , and a second rotation  $\beta$  about the  $\hat{\hat{\mathbf{y}}}$  axis. In equations, the rotation matrix which allows to describe a general vector in LVLH into  $[\hat{\mathbf{x}}', \hat{\mathbf{y}}', \hat{\mathbf{z}}']$  ( $U_{J_2}$  frame) can be written as

$$\mathbf{R}_{U_{J_2}, L} = \begin{bmatrix} c_\alpha c_\beta & s_\alpha c_\beta & s_\beta \\ -s_\alpha & c_\alpha & 0 \\ -c_\alpha s_\beta & -s_\alpha s_\beta & c_\beta \end{bmatrix} \quad (5.21)$$

where  $s_x = \sin(x)$  and  $c_x = \cos(x)$ , and  $\alpha$  and  $\beta$  are given by the following

$$\alpha = \arctan \left( \frac{\nabla U_{J_2} \cdot \hat{\mathbf{y}}}{\nabla U_{J_2} \cdot \hat{\mathbf{x}}} \right)$$

$$\beta = \arctan \left( \frac{\nabla U_{J_2} \cdot \hat{\mathbf{z}}}{\sqrt{(\nabla U_{J_2} \cdot \hat{\mathbf{x}})^2 + (\nabla U_{J_2} \cdot \hat{\mathbf{y}})^2}} \right)$$

It is now possible to impose relation 5.18 in the  $U_{J_2}$  frame and then to retrieve the components in LVLH frame through 5.21, thus obtaining

$$\begin{aligned}
\begin{bmatrix} \dot{x}'_{LEMJ_2}(0) \\ \dot{y}'_{LEMJ_2}(0) \\ \dot{z}'_{LEMJ_2}(0) \end{bmatrix} &= \begin{bmatrix} 0 & \frac{1}{2}\omega_z & 0 \\ -2\omega_z & 0 & 0 \\ 0 & 0 & -\omega_z \tan \theta_0 \end{bmatrix} \begin{bmatrix} x'(0) \\ y'(0) \\ z'(0) \end{bmatrix} \\
&= \begin{bmatrix} 0 & \frac{1}{2}\omega_z & 0 \\ -2\omega_z & 0 & 0 \\ 0 & 0 & -\omega_z \tan \theta_0 \end{bmatrix} \mathbf{R}_{U_{J_2},L} \begin{bmatrix} x(0) \\ y(0) \\ z(0) \end{bmatrix} \\
&= \begin{bmatrix} -\frac{1}{2}\omega_z s_\alpha & \frac{1}{2}\omega_z c_\alpha & 0 \\ -2\omega_z c_\alpha c_\beta & -2\omega_z s_\alpha c_\beta & -2\omega_z s_\beta \\ \omega_z c_\alpha s_\beta \tan \theta_0 & \omega_z s_\alpha s_\beta \tan \theta_0 & -\omega_z c_\beta \tan \theta_0 \end{bmatrix} \begin{bmatrix} x(0) \\ y(0) \\ z(0) \end{bmatrix}
\end{aligned} \tag{5.22}$$

where in this case  $\omega_z \neq n$  but  $\omega_z = \sqrt{\frac{\|\nabla U_{J_2}\|}{r}}$  because the LVLH is also subject to  $J_2$  perturbation [14]. Initial vector of velocity  $[\dot{x}'_{LEMJ_2}(0), \dot{y}'_{LEMJ_2}(0), \dot{z}'_{LEMJ_2}(0)]^T$  can be also rotated in LVLH frame in order to obtain IRV in LVLH frame

$$\begin{aligned}
\begin{bmatrix} \dot{x}_{LEMJ_2}(0) \\ \dot{y}_{LEMJ_2}(0) \\ \dot{z}_{LEMJ_2}(0) \end{bmatrix} &= \mathbf{R}_{L,U_{J_2}} \begin{bmatrix} \dot{x}'_{LEMJ_2}(0) \\ \dot{y}'_{LEMJ_2}(0) \\ \dot{z}'_{LEMJ_2}(0) \end{bmatrix} \\
&= \mathbf{R}_{U_{J_2},L}^T \begin{bmatrix} \dot{x}'_{LEMJ_2}(0) \\ \dot{y}'_{LEMJ_2}(0) \\ \dot{z}'_{LEMJ_2}(0) \end{bmatrix} \\
&= \mathbf{R}_{U_{J_2},L}^T \mathbf{R}_{\omega_z} \mathbf{R}_{U_{J_2},L} \begin{bmatrix} x(0) \\ y(0) \\ z(0) \end{bmatrix}
\end{aligned} \tag{5.23}$$

where  $\mathbf{R}_{U_{J_2},L}^T \mathbf{R}_{\omega_z} \mathbf{R}_{U_{J_2},L}$  equals

$$\omega_z \begin{bmatrix} \frac{3}{2}c_\alpha s_\alpha c_\beta - c_\alpha^2 s_\beta^2 t_{\theta_0} & \frac{1}{2}c_\alpha^2 c_\beta + 2s_\alpha^2 c_\beta - c_\alpha s_\alpha s_\beta^2 t_{\theta_0} & 2s_\alpha s_\beta + c_\alpha c_\beta s_\beta t_{\theta_0} \\ -2c_\alpha^2 c_\beta - \frac{1}{2}s_\alpha^2 c_\beta - c_\alpha s_\alpha s_\beta^2 t_{\theta_0} & -\frac{3}{2}c_\alpha s_\alpha c_\beta - s_\alpha^2 s_\beta^2 t_{\theta_0} & -2c_\alpha s_\beta + s_\alpha c_\beta s_\beta t_{\theta_0} \\ -\frac{1}{2}s_\alpha s_\beta + c_\alpha c_\beta s_\beta t_{\theta_0} & \frac{1}{2}c_\alpha s_\beta + s_\alpha c_\beta s_\beta t_{\theta_0} & -c_\beta^2 t_{\theta_0} \end{bmatrix}$$

and  $t_x = \tan(x)$ . Equation 5.23 simply considers the linearized conditions but in the  $U_{J_2}$  frame the Energy Matching condition still needs to be imposed.

If we now consider the energy of a generic follower as described by relative quantities instead of absolute ones as done in Equation 5.20 which will be used for the leader

spacecraft (or LVLH frame) the following holds

$$U_{EMJ_2} = -\frac{\mu}{r_{EMJ_2}} - \frac{k_{J_2}}{r_{EMJ_2}^3} \left( \frac{1}{3} - \frac{(r+x) \sin i \sin \theta + y \sin i \cos \theta + z \cos i}{r_{EMJ_2}^2} \right)$$

it is possible to write the Energy Matching considering  $J_2$  perturbation as

$$\|\mathbf{V}_{EMJ_2}\| = \sqrt{\|\mathbf{V}\|^2 + 2(U_{EMJ_2} - U)}$$

where  $U$  is the energy of the leader spacecraft and expressed by Equation 5.20. It is possible to follow the same passages done in the previous section but considering that the velocity of the follower as described in a LVLH frame subject to  $J_2$  ([14]) can be written as

$$\begin{aligned} \mathbf{V}_{EMJ_2} = & (v_x + \dot{x}_{EMJ_2} - y_{EMJ_2}\omega_z) \hat{\mathbf{x}} \\ & + \left( \frac{h}{r} + \dot{y}_{EMJ_2} + x_{EMJ_2}\omega_z - z_{EMJ_2}\omega_x \right) \hat{\mathbf{y}} + (\dot{z}_{EMJ_2} + y_{EMJ_2}\omega_x) \hat{\mathbf{z}} \end{aligned}$$

in this case  $\omega_x \neq 0$  because of the  $J_2$  perturbation [14]. The components  $\dot{x}_{EMJ_2}, \dot{y}_{EMJ_2}, \dot{z}_{EMJ_2}$  can be found by imposing that Equation 5.23 satisfy

$$\mathbf{V}_{EMJ_2} = \frac{\|\mathbf{V}_{EMJ_2}\|}{\|\mathbf{V}_{LEMJ_2}\|} \mathbf{V}_{LEMJ_2} = \frac{\sqrt{\|\mathbf{V}\|^2 + 2(U_{EMJ_2} - U)}}{\|\mathbf{V}_{LEMJ_2}\|} \mathbf{V}_{LEMJ_2} \quad (5.24)$$

Developing both sides of Equation 5.24, using Equation 5.23 and evaluating it at  $t = 0$ , the initial relative velocity conditions described in the LVLH frame subject to  $J_2$  perturbation can be found

$$\begin{aligned}
\dot{x}_{EMJ_2}(0) &= \frac{\|\mathbf{V}_{EMJ_2}\|}{\|\mathbf{V}_{LEMJ_2}\|} \left[ \left( \frac{3}{2}c_\alpha s_\alpha c_\beta - c_\alpha^2 s_\beta^2 t_{\theta_0} \right) x(0) \right. \\
&\quad \left. + \left( \frac{1}{2}c_\alpha^2 c_\beta + 2s_\alpha^2 c_\beta - c_\alpha s_\alpha s_\beta^2 t_{\theta_0} \right) y(0) + (2s_\alpha s_\beta + c_\alpha c_\beta s_\beta t_{\theta_0}) z(0) \right] \omega_z \\
&\quad + \left( \frac{\|\mathbf{V}_{EMJ_2}\|}{\|\mathbf{V}_{LEMJ_2}\|} - 1 \right) (v_x - y(0)\omega_z) \\
\dot{y}_{EMJ_2}(0) &= \frac{\|\mathbf{V}_{EMJ_2}\|}{\|\mathbf{V}_{LEMJ_2}\|} \left[ \left( -2c_\alpha^2 c_\beta - \frac{1}{2}s_\alpha^2 c_\beta - c_\alpha s_\alpha s_\beta^2 t_{\theta_0} \right) x(0) \right. \\
&\quad \left. + \left( -\frac{3}{2}c_\alpha s_\alpha c_\beta - s_\alpha^2 s_\beta^2 t_{\theta_0} \right) y(0) + (-2c_\alpha s_\beta + s_\alpha c_\beta s_\beta t_{\theta_0}) z(0) \right] \omega_z \\
&\quad + \left( \frac{\|\mathbf{V}_{EMJ_2}\|}{\|\mathbf{V}_{LEMJ_2}\|} - 1 \right) \left( \frac{h}{r} + x(0)\omega_z - z(0)\omega_x \right) \\
\dot{z}_{EMJ_2}(0) &= \frac{\|\mathbf{V}_{EMJ_2}\|}{\|\mathbf{V}_{LEMJ_2}\|} \left[ \left( -\frac{1}{2}s_\alpha s_\beta + c_\alpha c_\beta s_\beta t_{\theta_0} \right) x(0) \right. \\
&\quad \left. + \left( \frac{1}{2}c_\alpha s_\beta + s_\alpha c_\beta s_\beta t_{\theta_0} \right) y(0) + (-c_\beta^2 t_{\theta_0}) z(0) \right] \omega_z \\
&\quad + \left( \frac{\|\mathbf{V}_{EMJ_2}\|}{\|\mathbf{V}_{LEMJ_2}\|} - 1 \right) y(0)\omega_x
\end{aligned} \tag{5.25}$$

Equation 5.25 defines the Initial Relative Velocity of a generic follower in LVLH components which minimize relative drifts in all directions when  $J_2$  perturbation is considered. In the next section, the stability of the presented configurations initialized with Equation 5.25 will be analysed and compared with results obtained in Section. 5.2.5.

### 5.3.4 Stability of the EM including $J_2$ Initial Conditions

The aim of this section is to show the efficacy of Equations 5.25 wrt the initialization of the formation through CW Equations To do so properly, exactly the same parameters of the simulations showed in Section. 5.2.5 have been used, in particular the leader initial orbital elements are those presented in Table 5.1, and Initial Relative Positions of the followers in the different configurations are the same reported in Figures 5.2, 5.3, 5.4, 5.5. Figures 5.16, 5.17, 5.18 and 5.19 report the results of the simulations for all the analysed configurations. It is evident that EM Initial Conditions improve the stability of the formations, the envelopes remain nearly the same after 80 orbits. The only case in which relative drift is more evident, regards

across-track direction of IC configuration, but it remains very limited showing a relative drift of about  $0.03 \text{ m/orbit}$ .

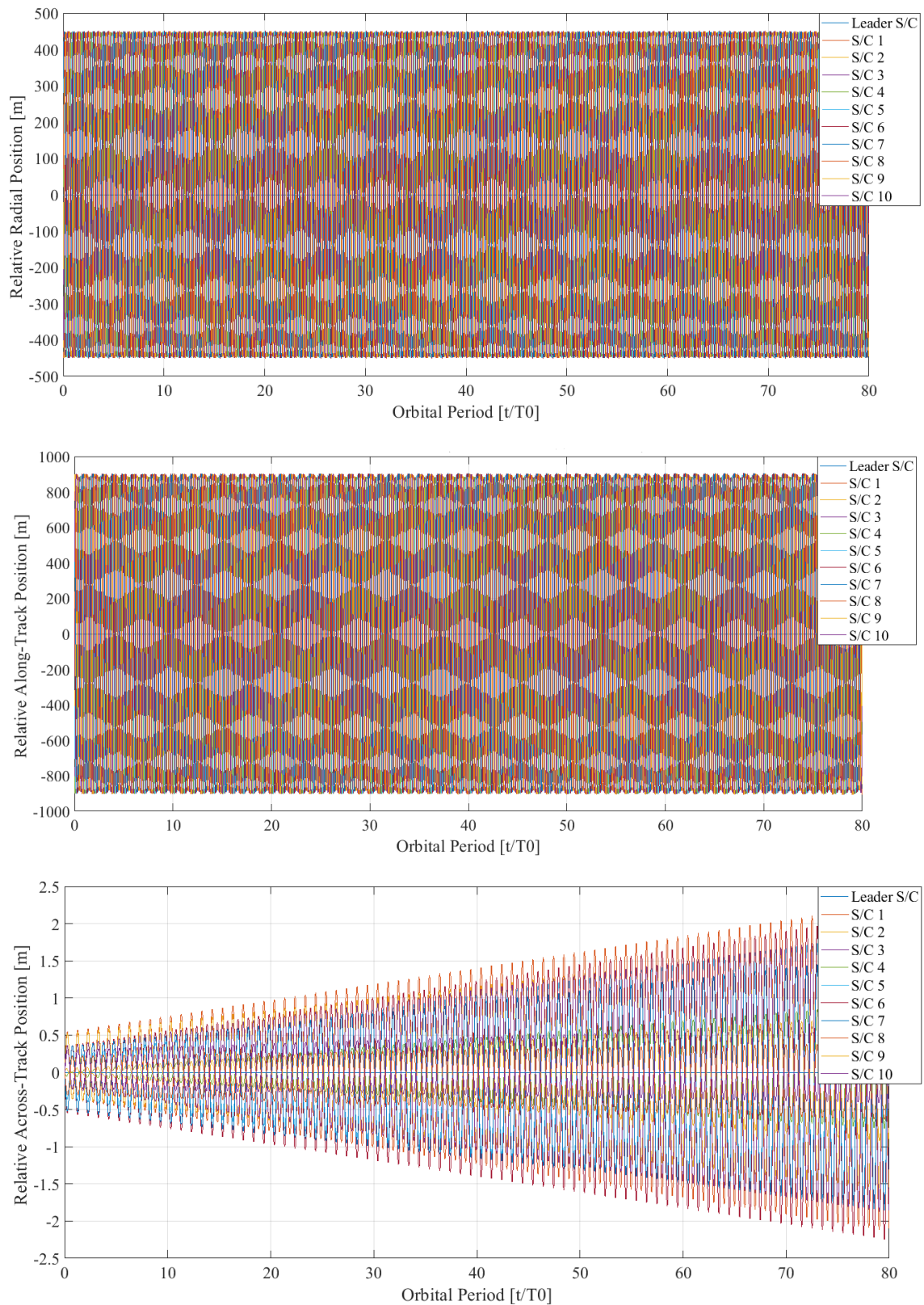


**Figure 5.16:** IC relative dynamics propagation, EM  $J_2$  Initial Conditions

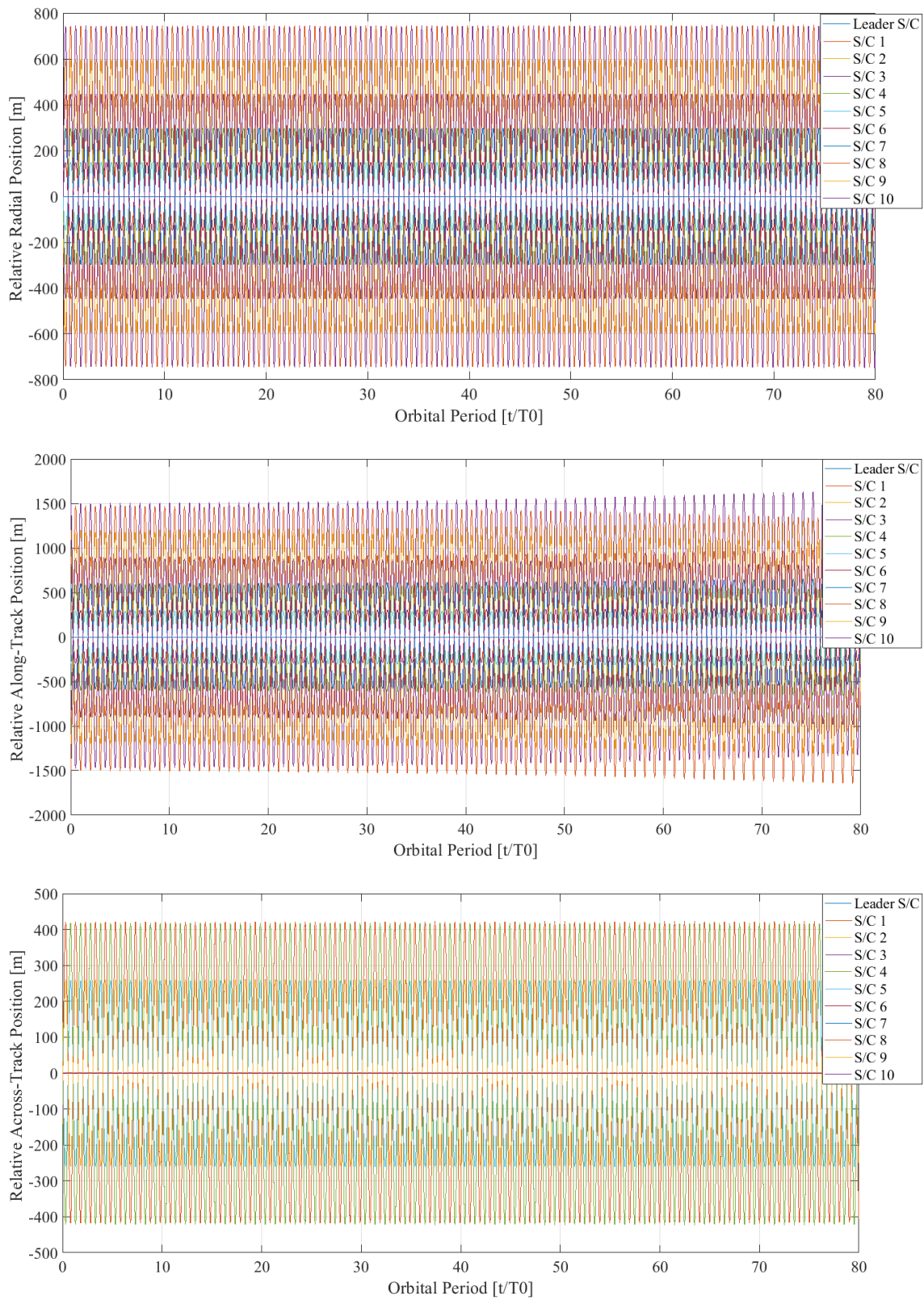


**Figure 5.17:** CT relative dynamics propagation, EM  $J_2$  Initial Conditions

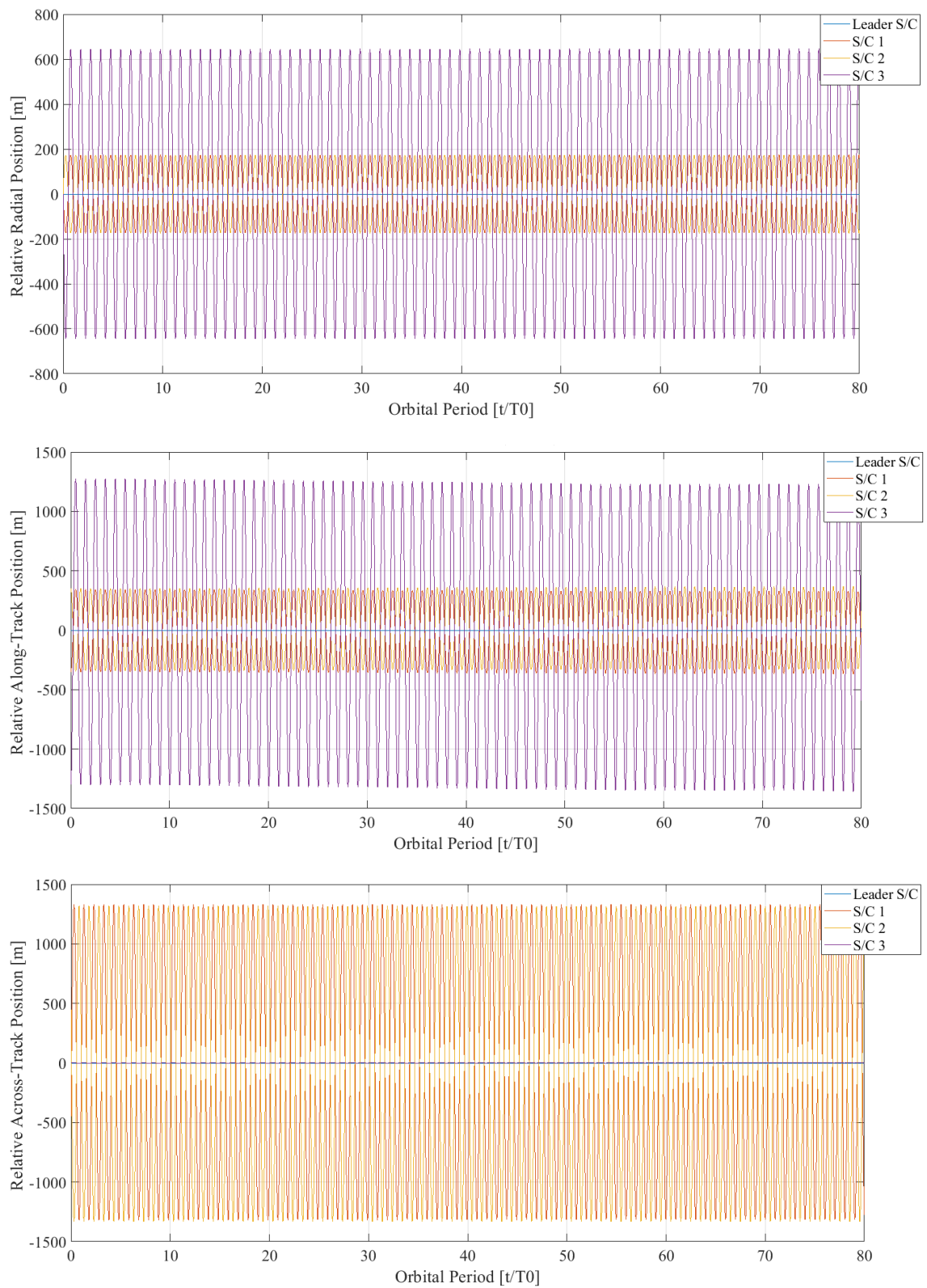


**Figure 5.18:** CP relative dynamics propagation, EM  $J_2$  Initial Conditions

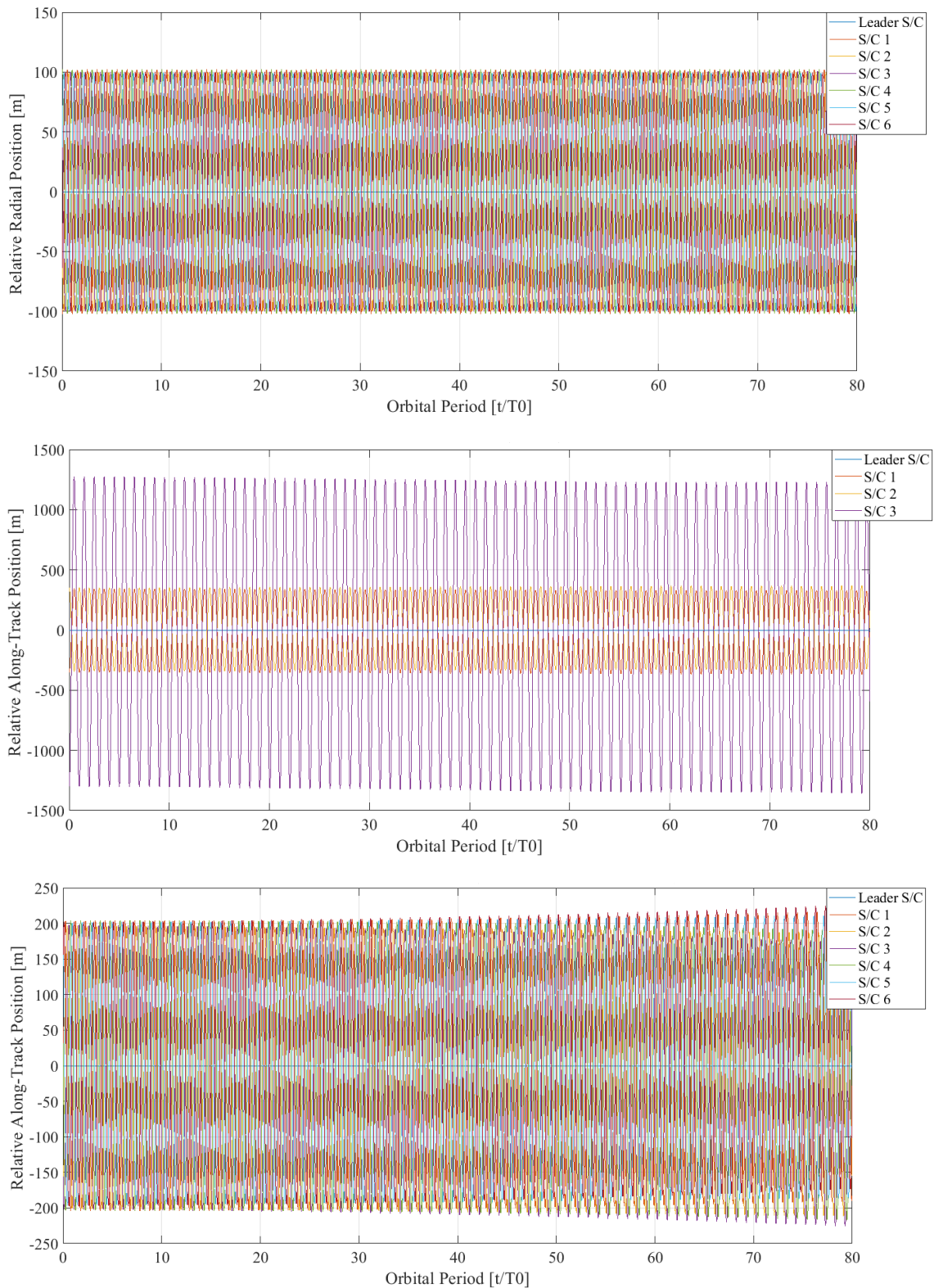


**Figure 5.19:** Helix relative dynamics propagation, EM  $J_2$  Initial Conditions

It has to be underlined that, even if the stability has been improved, Equations 5.25 tend to give higher Initial Relative Velocities, thus resulting in larger oscillations in

relative positions and consequently higher risk of collision. For this reason, when controlling the formation (Chapter 6), Collision Avoidance strategies have to be used for the safety of the mission.

After hundreds orbits, minor perturbations start to destabilize the formation (i.e. differential Drag), and Formation Control becomes necessary to maintain high system performances.

# Chapter 6

## Formation Control and Reconfigurability

After having analysed the stability of different configurations, it has been underlined that, even if the IRC are properly chosen, relative drifts can be limited but never nullified. For these reasons, control algorithms strategies have to be implemented. This chapter aims at presenting only some of the possible control strategies which can be realized. The synthesis of control laws is a very current branch of research, there are a large number of possible methods that allow to find more or less satisfactory results. Clearly, the methodology adopted depends on several factors including available computational resources, control accuracy requirements, instrumentation available for the implementation and for the measurement of state variables, physical constraints related to the system being analyzed, etc... In [20] some techniques used for the control of formations are reported. In the context of this work, in particular two different methodologies for the synthesis of control are reported.

The first one is a classical *Proportional Derivative (PD)* controller, it is a technique as simple as effective. In our case, it has been implemented for controlling the 6-DoF dynamics of the entire formation. The downside of this technique is that intrinsically it does not optimize the fuel quantity, a very important aspect according to the considerations made in the Chapter. 1. Therefore, a second method of synthesizing the 6-DoF dynamics control law was investigated.

*Optimal Control* technique finds a control solution that minimizes a desired cost-function. In addition, in order to have the same computational efficiency of the PD case, it has been used in the perspective of convex optimization which has the advantage to find the optimal solution in a very short time by convexifying all equations of the problem. This technique is widely used in missions that involve the autonomous synthesis of control laws because it allows to obtain very advantageous results, more-

over thanks to the speed of the algorithm it is possible to find the control law of hundreds of satellites in a reasonable amount of time (very suitable for formations) [25][24][39]. The performances of this algorithm are tested considering two different approaches, de-centralized and centralized (Chapter. 1), in order to better appreciate the advantages and disadvantages of having computational resources distributed among the followers or concentrated in a single spacecrafts. In the next sections all the considerations above reported will be extensively detailed.

## 6.1 Proportional Derivative (PD) Control Method

The basic idea behind PD control method is the following:

The purpose is to control precise physical quantities belonging to a system subject to a dynamics, making sure that after a certain time interval they are equal to some reference values. In order to make this happen, a control action must be performed until there is a difference between the instantaneous values of these quantities and the reference values.

Most simple law it is possible to think of is the proportional control law which foresees a control action which is proportional wrt the difference between the reference and the measured value of the variable to control. The synthesis of the constant of proportionality can be done following different criteria, this aspect won't be deepened because out of the scope of this work. If higher accuracy is required, a simple proportional control is not sufficient anymore. For improving the quality of the law, other measurements (or estimations of them) are necessary. In the context of this work, it is assumed that also the measurement of the derivative of the variable to control is available. So doing, a proportional-derivative control law can be implemented. According to classical assumption that translational motion is decoupled by rotational one, two different control laws, but with the same mathematical structure, have been implemented resulting in a complete 6-DoF dynamics control. Concerning the translational motion, the control force for the  $i$ -th spacecraft  $\mathbf{F}_i$  can be expressed as

$$\mathbf{F}_i = k_p(\boldsymbol{\rho}_{i,ref} - \boldsymbol{\rho}_i) + k_v(\dot{\boldsymbol{\rho}}_{i,ref} - \dot{\boldsymbol{\rho}}_i) \quad (6.1)$$

where  $k_p$  and  $k_v$  are the gains of the control law. Their values change the time response of the controlled system, they have a great impact on accuracy and stability of the control law and if not properly chosen they can give rise to instabilities which have to be absolutely avoided.  $\boldsymbol{\rho}_{i,ref}$  and  $\dot{\boldsymbol{\rho}}_{i,ref}$  are respectively the reference relative

position and velocity which the spacecraft should have after the end of the control action. It is evident as the elements multiplying the gains give the direction to the control force and a contribution to the amplitude of the control force which depends on how much the spacecraft is distant from its reference. Considering that, as widely explained in Chapter. 4, the relative dynamics has been directly propagated, in the simulations the vectors of Equation 6.1 have been decomposed in LVLH frame. It is possible to further improve Equation 6.1 considering that the main purpose is to control a formation which has a given configuration. In fact, in case metrology instrumentation could return relative positions of the spacecraft it is mounted on with respect to all the spacecrafts of the formation, the difference between these measurements and reference relative distances (calculated considering that a desired configuration wants to be reached) can give rise to additional proportional control terms. In equation this can be written as

$$\mathbf{F}_i = k_p(\boldsymbol{\rho}_{i,ref} - \boldsymbol{\rho}_i) + k_v(\dot{\boldsymbol{\rho}}_{i,ref} - \dot{\boldsymbol{\rho}}_i) + \sum_{i,j;j \neq i}^N k_{f,ij}(\mathbf{d}_{ij,ref} - \mathbf{d}_{ij}) \quad (6.2)$$

where  $N$  is the total number of satellites,  $\mathbf{d}_{ij,ref} = \boldsymbol{\rho}_{i,ref} - \boldsymbol{\rho}_{j,ref}$  is the distance reference vector between the  $i$ -th and  $j$ -th spacecrafts and it is given by the final configuration that wants to be reached, and  $\mathbf{d}_{ij} = \boldsymbol{\rho}_i - \boldsymbol{\rho}_j$  is the actual distance vector given by relative metrology measurements.

Considering now the rotational motion, the same reasoning can be pursued. In fact, if quaternions and angular velocities are measured, it is possible to create a control torque which is proportional wrt the differences between attitude and angular velocity of reference and their actual values. The problem is mathematically the same of that solved by Equation 6.2, so the instantaneous control torque for the  $i$ -th spacecraft can be calculated as follows

$$\boldsymbol{\tau}_i = k_q(\mathbf{q}_{i,ref} \otimes \mathbf{q}_i^{-1}) + k_\omega(\boldsymbol{\omega}_{i,ref} - \boldsymbol{\omega}_i) + \sum_{i,j;j \neq i}^N k_{\tau,ij}(\tilde{\mathbf{q}}_{ij,ref} - \tilde{\mathbf{q}}_{ij}) \quad (6.3)$$

where the  $\otimes$  indicates quaternion multiplication as defined in Chapter. 2, while  $\tilde{\mathbf{q}}_{ij,ref} = \mathbf{q}_{i,ref} \otimes \mathbf{q}_{j,ref}^{-1}$  and  $\tilde{\mathbf{q}}_{ij} = \mathbf{q}_i \otimes \mathbf{q}_j^{-1}$  are respectively relative reference and actual attitudes of the  $i$ -th spacecraft wrt  $j$ -th one. It has to be remarked that the multiplication between quaternions returns another four components quaternion whose dimensions are inconsistent with those of the control torque, for these reasons only the first three components of the derived quaternion have been extracted in Equation 6.3 (there is not a loss of information because the choice of unitary quaternion has been made). In this work, Equation 6.3 has been decomposed in

$i$ -th spacecraft body-frame  $\mathcal{F}_{i,BF}$  to be in line with the fact that the integration of rotational dynamics was done in the same frame. This method proves to be very simple and computationally cheap. Control forces and torques are quickly computed making PD adapt to be implemented for autonomous formations.

This control law presents some disadvantages. The choice of the different gains is not an easy task. There is not a perfect set of parameters, so some iterations have to be made before finding the most adapt ones. Another disadvantage involves the rapidity of convergence, in particular when the algorithm is about to converge, the errors are very small, so decreasing the velocity of the convergence. In addition, as previously underlined, one of the main problem of this method is that it does not take into account the minimization of the fuel consumption. For this reason, the results of PD controller have been used rather as reference results for comparison with methods more appropriate to the type of applications studied.

As last remark, Equations 6.2 and 6.3 tend to return very high control forces and torques because of the great number of terms they depend on. Physical constraints on actuation impose limits to the maximum and minimum values attainable, so the saturation phases have been considered by adding the following constraints to the algorithm

$$\begin{bmatrix} F_{ix} \\ F_{iy} \\ F_{iz} \end{bmatrix} \leq \begin{bmatrix} F_{ix,max} \\ F_{iy,max} \\ F_{iz,max} \end{bmatrix} \quad \begin{bmatrix} \tau_{ix} \\ \tau_{iy} \\ \tau_{iz} \end{bmatrix} \leq \begin{bmatrix} \tau_{ix,max} \\ \tau_{iy,max} \\ \tau_{iz,max} \end{bmatrix}$$

## 6.2 Optimal Control Method

After discussing the constraints to which Flying Formations are subject to (Chapter. 1), it is possible to affirm that the main goals of a control algorithm should be: the minimization of fuel consumption to re-configure the system and low computational cost for calculating the control inputs. Concerning the first affirmation, optimal control is the most adapt method, in fact, as the name suggests, it tries to find a solution which minimizes (or maximizes) a given cost function. Regarding the second, the question is more complicated. In fact, computational cost does not depend only on the intrinsic characteristics of the method but also on the way it is implemented (i.e. centralized or de-centralized architecture)

In order to reduce to a minimum the computational effort, a wide branch of research has developed methods to reduce a general non-linear optimization problem in a convex one. Convex optimization problems have the great advantage that they are solvable in very short amount of time, making them very suitable for autonomous real-time applications involving a considerable number of variables. Further details

about convex programming will be furnished in the next subsections. The discussion is organized as follows: firstly, the general problem will be presented, then the convex version of the problem follows and finally its final implementation in a SCP (Sequential Convex Programming) and in a Closed Loop with Sequential Convex Programming (CL-SCP) algorithm will be derived.

### 6.2.1 Definition of the General Optimal Control Problem

The goal is to solve an optimization problem in order to find optimal control forces and torques which are able to minimize energy actuation consumption for the 6DoF dynamics. For reasons which will be better explained later, two different optimization problems, one for translational dynamics and one for rotational are written. In addition, to avoid being too repetitive, the discussion will be carried out considering a de-centralized architecture, in which all satellites are equipped with sufficient computational resources to be able to independently calculate their optimal trajectory, the particularization for the centralized case is reported in Appendix D.

Calling  $\mathbf{x}(t) = [\boldsymbol{\rho}^T(t), \dot{\boldsymbol{\rho}}^T(t)]^T = [x(t), y(t), z(t), \dot{x}(t), \dot{y}(t), \dot{z}(t)]^T$  the translational state vector and  $\mathbf{u}(t) = [u_x(t), u_y(t), u_z(t)]^T$  the control input, the general non-linear optimization problem can be written for the  $i$ -th spacecraft as in Problem 1.

---

#### Problem 1 *Translational case, Non-linear Optimal Control*

$$\min_{\mathbf{u}_i(t)} \int_0^{t_f} \|\mathbf{u}_i(t)\|_2 dt$$

subject to

$$\begin{aligned} \dot{\mathbf{x}}_i(t) &= f(\mathbf{x}_i(t), \mathbf{u}_i(t)) & \forall t \in [0, t_f] \\ \|\mathbf{u}_i(t)\|_2 &\leq U_{\max} & \forall t \in [0, t_f] \\ \|C[\mathbf{x}_i(t) - \mathbf{x}_j(t)]\|_2 &\geq R_{\text{col}} & \forall t \in [0, t_f] \quad j = 1, \dots, N \quad j \neq i \\ \mathbf{x}_i(0) &= \mathbf{x}_{i,0} \\ \mathbf{x}_i(t_f) &= \mathbf{x}_{i,f} \end{aligned}$$


---

where  $t_f$  represents the final time at which the reconfiguration ends,  $f$  represents the controlled dynamics where the dependence on the state of LVLH frame (or chief) has been omitted,  $U_{\max}$  is the maximum available thrust (considering that spacecrafts are equipped with single thrust [44]),  $N$  is the total number of spacecrafts,  $R_{\text{col}}$  is the minimum distance required for collision avoidance,  $\mathbf{x}_{i,0}$  and  $\mathbf{x}_{i,f}$  are respectively

the initial and final state vector conditions, while  $C = [\mathbf{I}_{3 \times 3}, \mathbf{0}_{3 \times 3}]$  just extracts the relative positions from the state vector.

Analogously, it is possible to express the optimization problem in case of rotational motion. If  $\mathbf{x}(t) = [\mathbf{q}^T(t), \dot{\boldsymbol{\omega}}^T(t)]^T = [q_1(t), q_2(t), q_3(t), q_4(t), \omega_x(t), \omega_y(t), \omega_z(t)]^T$  is the state vector and  $\mathbf{g}(t) = [g_x(t), g_y(t), g_z(t)]^T$  is the control input, for  $i$ -th spacecraft, it is possible to derive Problem 2.

---

**Problem 2** *Rotational case, Non-linear Optimal Control*

$$\min_{\mathbf{g}_i(t)} \int_0^{t_f} \|\mathbf{g}_i(t)\|_2 dt$$

subject to

$$\begin{aligned} \dot{\mathbf{x}}_i(t) &= f(\boldsymbol{\rho}_i, \dot{\boldsymbol{\rho}}_i, \mathbf{x}_i(t), \mathbf{g}_i(t)) & \forall t \in [0, t_f] \\ \|\mathbf{g}_i(t)\|_2 &\leq \tau_{\max} & \forall t \in [0, t_f] \\ \mathbf{x}_i(0) &= \mathbf{x}_{i,0} \\ \mathbf{x}_i(t_f) &= \mathbf{x}_{i,f} \end{aligned}$$

---

where  $\tau_{\max}$  is the saturation of the actuator and the dependence of the rotational dynamics on relative positions and velocities has been highlighted (external torques depend on accelerations and accelerations depend on absolute position and velocity of the vector).

Problems 1 and 2 try to minimize the integral over an interval of time of the norm of the control inputs. This is in line with the fact that fuel consumption is related to this quantity, so the objective functions considered represent indirectly the cost of fuel consumption. The presented problems are non-linear and constrained optimization problems. They are difficult to solve, also by indirect methods which can take a very long run time. A solution often adopted is that one to make to re-enter the problem in the so-called convex optimization problems for which convex programming succeeds to guarantee times of resolution much lower.

## 6.2.2 Convexification of the Optimal Control Problem

Convex programming requires that the problem being treated be expressed as

$$\begin{aligned} &\text{minimize} && J(\mathbf{Z}) \\ &\text{subject to} && g_j(\mathbf{Z}) \leq 0, \quad j = 1, \dots, l \\ &&& \mathbf{a}_i^T \mathbf{Z} - \mathbf{b}_i = 0, \quad i = 1, \dots, m \end{aligned} \tag{6.4}$$

where the vector  $\mathbf{Z}$  is the variable to be optimized,  $g_j$  are convex functions while the equality constraints  $\mathbf{a}_i^T \mathbf{Z} - \mathbf{b}_i = 0$  are expressed as affine functions. In order to reduce Problems 1 and 2 to the problem given by (6.4), it is necessary to linearize the dynamics and discretize the continuous problem in order to identify a single vector to optimize.

### Linearization of the Dynamics

It is possible to approximate the non-linear dynamics of the system by using a reference trajectory through Taylor expansion. If only the first term of this expansion is considered the resulting approximation function is linear. Considering the Problem 1, if we call  $\bar{\mathbf{x}}_i(t)$  the reference trajectory and  $\bar{\mathbf{u}}_i(t)$  the reference control law (for Problem 2 the considerations are exactly the same), the linearized dynamics can be written as

$$\dot{\mathbf{x}}_i(t) = A_i(t)\mathbf{x}_i(t) + B_i(t)\mathbf{u}_i(t) + c_i(t) \quad (6.5)$$

where  $A_i(t) = \left. \frac{\partial f}{\partial \mathbf{x}_i} \right|_{\bar{\mathbf{x}}_i(t), \bar{\mathbf{u}}_i(t)}$ ,  $B_i(t) = \left. \frac{\partial f}{\partial \mathbf{u}_i} \right|_{\bar{\mathbf{x}}_i(t), \hat{\mathbf{u}}_i(t)}$  and  $c(t) = f(\bar{\mathbf{x}}_i(t), \bar{\mathbf{u}}_i(t)) - A_i(t)\bar{\mathbf{x}}_i(t) - B_i(t)\bar{\mathbf{u}}_i(t)$ . The main problem is that Equation 6.5 requires reference trajectories and the more distant this reference will be from the real value of the trajectory the coarser the approximation will be resulting in a lower accuracy in reaching the final state. This problem will be solved by adopting the sequential convex programming explained in the next sections. In the context of this work, the linearizations presented require the calculation of the Jacobian of the function  $f$ . This is a complex task, especially in the case where the model takes into account all the perturbations presented in Chapter 3. For such motivations, in this work, the Jacobians have been numerically estimated through the finite difference method.

*Remark:*

Concerning  $B$  matrix it is possible to do some remarks. In fact, in simple case the translational dynamics can be written as the sum between the uncontrolled dynamics and the effect of the control. Using Equation 4.6 this means

$$\ddot{\boldsymbol{\rho}}_L = \mathbf{R}_{LI}(\ddot{\mathbf{r}}_I - \ddot{\mathbf{R}}_{0,I}) - \boldsymbol{\Omega}_L \times \boldsymbol{\Omega}_L \times \boldsymbol{\rho}_L - \dot{\boldsymbol{\Omega}}_L \times \boldsymbol{\rho}_L - 2\boldsymbol{\Omega}_L \times \dot{\boldsymbol{\rho}}_L + \frac{\mathbf{F}_{c,L}}{m}$$

where  $\mathbf{F}_{c,L}$  is the control force expressed in LVLH frame and  $m$  is the mass of the considered spacecraft. Depending on the definition of control input  $\mathbf{u}$  of the optimization control  $B$  matrix could take simple form. For example if  $\mathbf{u} = \frac{\mathbf{F}_{c,L}}{m}$

it is easy to find that  $B = [\mathbf{0}_{3 \times 3}, \mathbf{I}_{3 \times 3}]$ . Instead, if  $\mathbf{u} = \mathbf{F}_{c,L}$ , and the constant mass assumption has been done  $B = [\mathbf{0}_{3 \times 3}, \frac{1}{m} \mathbf{I}_{3 \times 3}]$  also constant in time. In general case, in which  $\mathbf{u} = \mathbf{F}_{c,L}$  but the mass is not constant, the solution holds  $B = [\mathbf{0}_{3 \times 3}, \frac{1}{m(t)} \mathbf{I}_{3 \times 3}]$  and a model for the dynamics of the mass of the spacecraft  $\dot{m}(t)$  has to be taken into account.

### Discretization

The optimization time interval  $[0, t_f]$  is discretized in  $K$  points.  $t_k$  is the time in the  $k$ -th point and,  $\Delta t_k = t_{k+1} - t_k$  is the  $k$ -th interval of time. In this work, an equispaced discretization has been used so  $\Delta t_k = \Delta t \quad \forall k = 0, 1, \dots, K-1$  thus resulting also in  $t_f = K\Delta t$ . We can now apply this discretization to Problem 1 starting from the cost-function. The integral becomes a sum over the time-interval

$$\sum_{k=0}^{K-1} \|\mathbf{u}_i^k\|_2$$

where  $\mathbf{u}_i^k = \mathbf{u}_i(t_k)$ , while the dynamics can be written as follows

$$\dot{\mathbf{x}}_i^{k+1} = A_i^k \mathbf{x}_i^k + B_i^k \mathbf{u}_i^k + c_i^k \quad k = 0, 1, \dots, K-1 \quad (6.6)$$

where  $\mathbf{x}_i^k = \mathbf{x}_i(t_k)$  and

$$A_i^k = e^{A_i(t_k)\Delta t} \quad B_i^k = \int_0^{\Delta t} e^{A_i(t_k)\tilde{t}} B(\tilde{t}) d\tilde{t} \quad c_i^k = \int_0^{\Delta t} e^{A_i(t_k)\tilde{t}} c(\tilde{t}) d\tilde{t}$$

The other conditions do not need any other clarification and it is possible to write directly the problems 1 and 2 in discretized form

---

### Problem 3 *Translational case, Discretized Optimal Control*

$$\min_{\mathbf{u}_i} \sum_{k=0}^{K-1} \|\mathbf{u}_i^k\|_2$$

subject to

$$\begin{aligned} \dot{\mathbf{x}}_i^{k+1} &= A_i^k \mathbf{x}_i^k + B_i^k \mathbf{u}_i^k + c_i^k & k &= 0, 1, \dots, K-1 \\ \|\mathbf{u}_i^k\|_2 &\leq U_{\max} & k &= 0, 1, \dots, K-1 \\ \|C [\mathbf{x}_i^k - \mathbf{x}_j^k]\|_2 &\geq R_{\text{col}} & k &= 0, 1, \dots, K \quad j = 1, \dots, N \quad j \neq i \\ \mathbf{x}_i^0 &= \mathbf{x}_{i,0} \\ \mathbf{x}_i^K &= \mathbf{x}_{i,f} \end{aligned}$$

---



---

**Problem 4** *Rotational case, Discretized and Convex Optimal Control*

$$\min_{\mathbf{g}_i} \sum_{k=0}^{K-1} \|\mathbf{g}_i^k\|_2$$

subject to

$$\begin{aligned} \dot{\mathbf{x}}_i^{k+1} &= A_i^k \mathbf{x}_i^k + B_i^k \mathbf{g}_i^k + c_i^k & k = 0, 1, \dots, K-1 \\ \|\mathbf{g}_i^k\|_2 &\leq \tau_{\max} & k = 0, 1, \dots, K-1 \\ \mathbf{x}_i^0 &= \mathbf{x}_{i,0} \\ \mathbf{x}_i^K &= \mathbf{x}_{i,f} \end{aligned}$$


---

*Remark:*

Concerning rotational case, the derivation of matrices  $A_i^k$  and  $B_i^k$  is slight different from previous case. In fact, as highlighted before, i-th spacecraft rotational dynamics depends also on  $\boldsymbol{\rho}_i$  and  $\dot{\boldsymbol{\rho}}_i$ , thus resulting in the need of translational reference trajectories ( $\bar{\boldsymbol{\rho}}_i(t)$  and  $\bar{\dot{\boldsymbol{\rho}}}_i(t)$ ) for the computation of the first-order Taylor expansion, so that  $A_i(t) = \left. \frac{\partial f}{\partial \mathbf{x}_i} \right|_{\bar{\mathbf{x}}_i(t), \bar{\mathbf{u}}_i(t), \bar{\boldsymbol{\rho}}_i(t), \bar{\dot{\boldsymbol{\rho}}}_i(t)}$ ,  $B_i(t) = \left. \frac{\partial f}{\partial \mathbf{u}_i} \right|_{\bar{\mathbf{x}}_i(t), \bar{\mathbf{u}}_i(t), \bar{\boldsymbol{\rho}}_i(t), \bar{\dot{\boldsymbol{\rho}}}_i(t)}$  and  $c(t) = f(\bar{\mathbf{x}}_i(t), \bar{\mathbf{u}}_i(t), \bar{\boldsymbol{\rho}}_i(t), \bar{\dot{\boldsymbol{\rho}}}_i(t)) - A_i(t)\bar{\mathbf{x}}_i(t) - B_i(t)\bar{\mathbf{u}}_i(t)$ . The discretization process does not change wrt the translational case.

It is now more evident the reasons why the choice of writing two different problems, one for translational motion and one for rotational, has been taken. In general, a single problem involving all variables for 6DoF dynamics could be derived, thus resulting in a very huge problem increasing the difficulty of finding the solution. By splitting this single problem into two sub-problems allows to control only one type of motion without solving the other. For example, if the formation pointing has to be corrected without controlling translational motion, it is possible to solve problems 2 or 4 by linearizing the dynamics about the free-flying translational motion (from Equations 4.15). This results in a lower computational effort. In addition, especially if SCP strategy is not adopted, if a 6DoF control is needed, it is possible to solve Problem 3 and then using the controlled trajectories so obtained as reference trajectories for Problem 4. Being these trajectories closer to reality, the linearization error decreases.

Problem 4 is a convex problem. In fact if we define the optimization variable for the i-th spacecraft as  $\mathbf{Z}_i$  as  $\mathbf{Z}_i = [(\mathbf{x}_i^0)^T, \dots, (\mathbf{x}_i^K)^T, (\mathbf{g}_i^0)^T, \dots, (\mathbf{g}_i^{K-1})^T]^T$ , all the constraints and cost-function can be re-written with the formalism of Equation 6.4.

Concerning Problem 3, the Collision Avoidance constraint makes the problem still non-convex. In addition, it requires the knowledge of the position of all the spacecrafts for all instants  $\mathbf{x}_i^k$  which is a complicated aspect. If a centralized strategy is adopted, the task is simpler because the chief can calculate all the trajectories and then send them to each spacecraft considering the CA constraint. Instead, if a de-centralized strategy is adopted, each spacecraft should calculate its optimal trajectory without CA constraint, send this to the chief and then receive all other trajectories in order to add CA constraint and re-calculate the optimal trajectory. These aspects will be considered in the following subsection where the CA constraints is convexified.

### Convexification of Collision Avoidance Constraint

The convexification of CA constraint follows the procedure adopted by [44]. It is possible to show that a sufficient condition for the non-convex CA constraint  $\|C[\mathbf{x}_i^k - \mathbf{x}_j^k]\|_2 \geq R_{\text{col}} \quad k = 0, 1, \dots, K \quad j = 1, \dots, N \quad j \neq i$  is the following

$$(\bar{\mathbf{x}}_i^k - \bar{\mathbf{x}}_j^k)^T C^T C (\mathbf{x}_i^k - \mathbf{x}_j^k) \geq R_{\text{col}} \|C(\bar{\mathbf{x}}_i^k - \bar{\mathbf{x}}_j^k)\|_2 \quad (6.7)$$

where  $\bar{\mathbf{x}}_i$  is an initial guess trajectory for the  $i$ -th spacecraft. The idea behind Equation 6.7 can be better understood with Figure 6.1. Figure 6.1 (*Left*) shows the constraint before convexification, it is clear that a prohibited spherical volume prevents the two spacecrafts from collision, while Figure 6.1 (*Right*) shows the convexified constraint by changing the prohibited spherical volume into a larger one which encompasses the old prohibited volume.

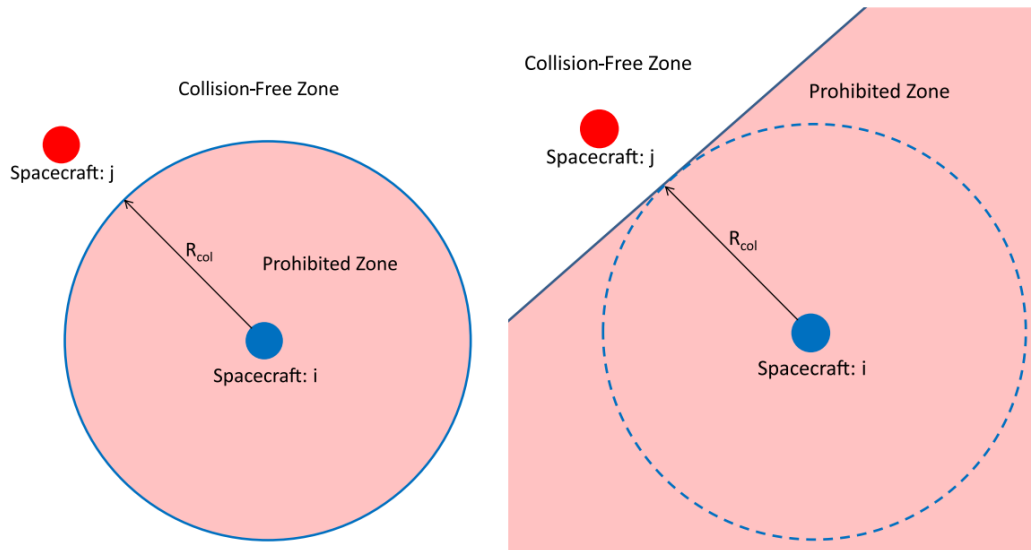


**Figure 6.1:** *Left* Non-convex CA constraint, *Right* Convex CA constraint, [44]

A proof that Equation 6.7 is a sufficient condition of the CA constraint can be quickly derived.

*Proof:*

$$\begin{aligned}
(\bar{\mathbf{x}}_i^k - \bar{\mathbf{x}}_j^k)^T C^T C (\mathbf{x}_i^k - \mathbf{x}_j^k) &\geq R_{\text{col}} \|C (\bar{\mathbf{x}}_i^k - \bar{\mathbf{x}}_j^k)\|_2 \\
\|C (\bar{\mathbf{x}}_i^k - \bar{\mathbf{x}}_j^k)\|_2 \|C (\mathbf{x}_i^k - \mathbf{x}_j^k)\|_2 \cos \phi &\geq R_{\text{col}} \|C (\bar{\mathbf{x}}_i^k - \bar{\mathbf{x}}_j^k)\|_2 \\
\|C (\mathbf{x}_i^k - \mathbf{x}_j^k)\|_2 \cos \phi &\geq R_{\text{col}} \\
\|C (\mathbf{x}_i^k - \mathbf{x}_j^k)\|_2 &\geq \|C (\bar{\mathbf{x}}_i^k - \bar{\mathbf{x}}_j^k)\|_2 \cos \phi \geq R_{\text{col}}
\end{aligned}$$

*Remark:*

Equation 6.7 implies that the spacecraft performing the optimization should know trajectories of all the satellites. This is not verified in case of de-centralized strategy where each satellite optimizes its own trajectory. For this reason the constraint just presented needs to be changed so that we can have a CA requirement in this strategy as well. This problem can be solved by changing Equation 6.7 in

$$(\bar{\mathbf{x}}_i^k - \bar{\mathbf{x}}_j^k)^T C^T C (\mathbf{x}_i^k - \bar{\mathbf{x}}_j^k) \geq R_{\text{col}} \|C (\bar{\mathbf{x}}_i^k - \bar{\mathbf{x}}_j^k)\|_2 \quad (6.8)$$

which implies that also the trajectory of the j-th spacecraft is estimated. This problem is not present in centralized strategy where the optimization involves all the spacecrafts.

This procedure allows to make Problem 3 solvable through convex programming. However, two negative aspects are still present. The first is that this methodology makes the solution of the problem a potentially sub-optimal solution, in fact, by increasing the volume of forbidden space, solutions that could present a lower cost-function are discarded. The second is that guess trajectories are necessary. These trajectories can be obtained in different ways. The choice that has been made in this work, consists, in the case of de-centralized architecture, in solving the optimization problem at least two times. The first solution does not consider the CA constraint and the second uses the trajectories found in the first one as guess trajectories in order to include the CA convex constraint. In the case of centralized architecture, the procedure is the same, but in this case there is no need for the frequent passage of information between satellites, only after all optimal trajectories have been calculated, the satellites receive the control inputs. Problem 3 can be finally written as Problem 5 including Equation. 6.8

**Problem 5** *Translational case, De-centralized Convex Optimal Control*

$$\min_{\mathbf{u}_i} \sum_{k=0}^{K-1} \|\mathbf{u}_i^k\|_2$$

subject to

$$\begin{aligned} \dot{\mathbf{x}}_i^{k+1} &= A_i^k \mathbf{x}_i^k + B_i^k \mathbf{u}_i^k + c_i^k & k = 0, 1, \dots, K-1 \\ \|\mathbf{u}_i^k\|_2 &\leq U_{\max} & k = 0, 1, \dots, K-1 \\ (\bar{\mathbf{x}}_i^k - \bar{\mathbf{x}}_j^k)^T C^T C (\mathbf{x}_i^k - \bar{\mathbf{x}}_j^k) &\geq R_{\text{col}} \|C (\bar{\mathbf{x}}_i^k - \bar{\mathbf{x}}_j^k)\|_2 & k = 0, 1, \dots, K \quad j = 1, \dots, N \quad j \neq i \\ \mathbf{x}_i^0 &= \mathbf{x}_{i,0} \\ \mathbf{x}_i^K &= \mathbf{x}_{i,f} \end{aligned}$$

Before passing to the algorithm of Sequential Convex Programming, it is necessary to make some clarifications. Problem 5 is written in the context of a de-centralized strategy. This implies that the  $i$ -th spacecraft optimizes its own trajectory regardless of the position and/or velocity of others. This strategy, which is more suitable in the case where the satellites of the formation are all equipped with the same computational resources, does not consider the optimization of the formation as a single entity which is what we would be most interested in. In fact, if instead of the cost-function  $\min_{\mathbf{u}_i} \sum_{k=0}^{K-1} \|\mathbf{u}_i^k\|_2$  we had  $\min_{[\mathbf{u}_1, \dots, \mathbf{u}_N]} \sum_{i=1}^N \sum_{k=0}^{K-1} \|\mathbf{u}_i^k\|_2$ , where  $N$  is the number of spacecrafts, the optimization would choose a path that would minimize the overall fuel consumption. This, as demonstrated in [44], results in a more efficient use of the fuel consumption, so it can be affirmed that, if a satellite can be endowed with a high-performances data handling system, this solution is to prefer wrt to de-centralized one. The detailed definition of the centralized optimal problem is given in Appendix D. Concerning Problem 4, there is not a particular distinction between centralized and de-centralized strategy. In fact, there is not coupling between the various rotational optimization problems of the formation (the coupling for translational case is given by the CA constraint), making each satellite rotational state independent from those of other spacecrafts.

### 6.3 Sequential Convex Programming (SCP)

Several approximations were introduced during the convexification of Problem 1. First, the introduction of initial guess trajectories  $\hat{\mathbf{x}}_i$  for linearization can lead to significant errors. Moreover, if the initial trajectories deviate a lot from the real

ones, the constraint on the CA may result in the elimination of solutions that could in reality satisfy the minimum distance criterion and consequently the solution thus obtained would deviate even further from the optimal one. In order to solve this problem, the Sequential Convex Programming (SCP) method is used. As the name suggests, SCP involves a sequential and iterative resolution of the problem, trying to refine the solution more and more until a certain accuracy is satisfied. The idea behind SCP is simple, if  $\mathbf{x}_{i,m-1}$  represents the solution of the problem at (m-1)-th iteration, it is possible to use this solution as the new reference trajectory for iteration (m)-th  $\hat{\mathbf{x}}_i = \mathbf{x}_{i,m-1}$ . At this point, one criterion is needed to stop the iterative process. The most used and the most intuitive would be to stop the process in the case in which the new iteration does not differ more than a predetermined quantity from the previous one, this can be written through the following equation

$$\|\mathbf{x}_{i,m}^k - \mathbf{x}_{i,m-1}^k\|_\infty < \epsilon \quad \forall k = 0, \dots, K \quad (6.9)$$

where  $\epsilon$  is a constant and it is chosen depending on the desired accuracy.

It is now possible to write a pseudo-algorithm for SCP in order to clarify the optimization process. It is reported in case of de-centralized strategy but the centralized case is simple to derive.

**Algorithm 1:** Sequential Convex Programming

---

```

 $\hat{\mathbf{x}}_i^k \leftarrow \mathbf{0}_{6 \times 1}$  or  $\mathbf{x}_{i,initial}^k \quad \forall i, k$ 
 $\mathbf{x}_{i,0}^k \leftarrow$  solution to Problem 5 excluding CA constraint  $\quad \forall i, k$ 
 $\hat{\mathbf{x}}_i^k \leftarrow \mathbf{x}_{i,0}^k \quad \forall i, k$ 
 $\mathcal{G} := \{1, \dots, N\}$ 
 $m \leftarrow 1$ 
while  $\mathcal{G} \neq \emptyset$  do
  forall  $i \in \mathcal{G}$  do
     $\mathbf{x}_{i,m}^k \leftarrow$  solution of the Problem 5  $\quad \forall k$ 
  end
  forall  $i \in \mathcal{G}$  do
     $\hat{\mathbf{x}}_i^k \leftarrow \mathbf{x}_{i,m}^k \quad \forall k$ 
  end
   $\mathcal{H} := \{1, \dots, N\}$ 
  forall  $i \in \mathcal{G}$  do
    if  $\|\mathbf{x}_{i,m}^k - \mathbf{x}_{i,m-1}^k\|_\infty < \epsilon \quad \forall k$  and  $\|C(\mathbf{x}_{i,m}^k - \mathbf{x}_{j,m}^k)\|_\infty \geq R_{col} \quad \forall k, j \in \mathcal{H}$ 
      then
        Remove  $i$  from  $\mathcal{G}$ 
      end
    end
  end
   $m \leftarrow m + 1$ 
end
 $M \leftarrow m$ 
 $\mathbf{x}_{i,M}^k$  is the SCP solution to Problem 5

```

---

Algorithm 1 allows to obtain more precise results wrt solving only once Problem 5. After calculating these trajectories, Problem 4 can be solved for controlling rotational motion with higher precision. The problem of this method is that it does not consider unmodeled disturbances or errors in the application of control. In fact, having no external measurements Algorithm 1 still represents an open-loop control. This can lead to non-negligible errors in the reached final state. In order to close the loop, the method of Closed Loop control with Sequential Convex Programming (CL-SCP) will be described in the following section.

## 6.4 Closed Loop Control with Sequential Convex Programming (CL-SCP)

The concept behind (CL-SCP) algorithm is very simple and is based on classical characteristics of a feedback control loop. If relative measurements are available,

it is possible to re-initialize Algorithm 1 by using the measurements as initial state vectors. This is equal to closing the control loop as in a feedback controller. If the re-initialization is applied several times during the maneuvers the final result will be more accurate. If we call  $k_0$  the instant at which the re-initialization is applied and  $K_H$  the optimization horizon of the single CL-SCP iteration, it is possible to rewrite Problem 5 by considering re-initialization as

---

**Problem 6** *Translational case, De-centralize Convex Optimal Control for CL-SCP*

$$\min_{\mathbf{u}_i} \sum_{k=k_0}^{K-1} \|\mathbf{u}_i^k\|_2$$

subject to

$$\begin{aligned} \dot{\mathbf{x}}_i^{k+1} &= A_i^k \mathbf{x}_i^k + B_i^k \mathbf{u}_i^k + c_i^k & k &= k_0, \dots, K-1 \\ \|\mathbf{u}_i^k\|_2 &\leq U_{\max} & k &= k_0, \dots, K-1 \\ (\bar{\mathbf{x}}_i^k - \bar{\mathbf{x}}_j^k)^T C^T C (\mathbf{x}_i^k - \bar{\mathbf{x}}_j^k) &\geq R_{\text{col}} \|C (\bar{\mathbf{x}}_i^k - \bar{\mathbf{x}}_j^k)\|_2 & k &= k_0, \dots, k_0 + K_H \quad j = 1, \dots, N \quad j \neq i \\ \mathbf{x}_i^0 &= \mathbf{x}_{i,\text{actual}} \\ \mathbf{x}_i^K &= \mathbf{x}_{i,f} \end{aligned}$$


---

where  $\mathbf{x}_{i,\text{actual}}$  is the measured state at  $k_0$ . It is clear how Problem 6 is simpler to solve. In particular, the most time-consuming part of optimal control is due to CA constraints, in Problem 6 the constraints are considered only up to  $k_0 + K_H$ , while it is evident that the control input has to be calculated in all the time span  $K$  which is the instant at which the final position  $\mathbf{x}_{i,f}$  has to be reached.

In case of  $k_0 + K_H > K$  Problem 6 is not defined and in this case Problem 5 can be used to complete the maneuvers. It can be remarked that the smaller is the horizon  $K_H$  the more the trajectory followed will be optimal but the greater will be the computational effort. The choice of  $K_H$  depends also on the total time used for the correction  $t_f$  and will always be dictated by a trade-off between precision and available computational resources. In Figure 7.16 the working principle of CL-SCP method is shown. In particular, it is possible to see how closing the loop improves the accuracy (Figure 7.16 (Right)) by re-calculating the new trajectory by measuring the actual state.

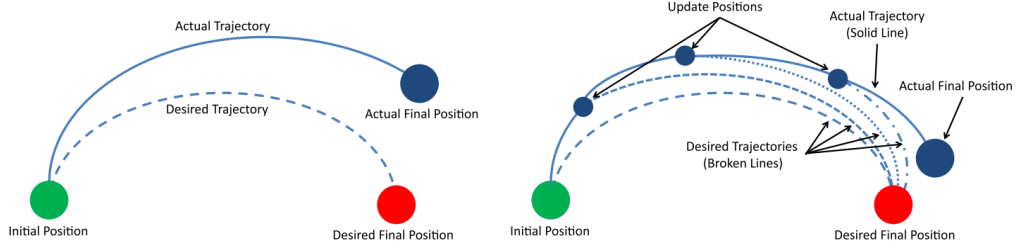


**Figure 6.2:** *Left:* Trajectory given by SCP . *Right:* Trajectory given by CL-SCP, [44]

For sake of completeness the algorithm of CL-SCP is presented in Algorithm 2.

---

**Algorithm 2:** CL-SCP

---

$k_0 \leftarrow 0$

**while**  $k_0 + K_H \leq K$  **do**

    Solve Problem 6 using Algorithm 1

    Store  $\mathbf{x}_i^k \quad \forall i, k = k_0, \dots, k_0 + K_H$

    Store  $\mathbf{u}_i^k \quad \forall i, k = k_0, \dots, k_0 + K_H - 1$

$k_0 \leftarrow k_0 + K_H$

**end**

Solve Problem 5 using Algorithm 1

Store  $\mathbf{x}_i^k \quad \forall i, k = k_0, \dots, K$

Store  $\mathbf{u}_i^k \quad \forall i, k = k_0, \dots, k_0 + K - 1$

---

## 6.5 Reconfigurability

As discussed in Chapter. 1, Reconfigurability property is one of the main advantage of Formation Flying. We can distinguish two different kinds of reconfiguration

- reconfiguration aiming at restoring the initial configuration that has undergone drift due to differential accelerations
- reconfiguration aiming at changing the actual configuration of the formation into another for needs dictated by the mission

Both of them can involve all the spacecrafts of the formation (total reconfiguration) or a number  $N_r \leq N$  of them (partial reconfiguration). The first typology does not involve particular other considerations than those made above. In fact, once it is decided that one or more satellites in the formation should undergo correction maneuvers, Problem 5 in de-centralized or centralized strategy can be solved through Algorithm 1 or 2

The second typology is more complicated. In fact, if the formation has to reach another configuration the decision-making process that assigns a satellite from the

previous configuration a place in the new one can lead to several problems. The first is that the place assignment may not take into account possible crossings between trajectories. This aspect is very critical, even if by using the CA constraint a certain safety margin is already obtained. The second aspect is to try to figure out which satellite of the old formation should go to occupy a given place in the new one so that the total fuel consumption is minimized. In particular, it is clear that if old configuration has  $N$  satellites and the new one foresees only  $N_r$  satellites, there are  $NN_r$  possible place assignments.

This problem can be solved with a second optimization whose the optimization variable is the  $NN_r$  dimensional vector

$$\mathbf{y} = [y_{11}, \dots, y_{1,N_r}, y_{2,1}, \dots, y_{NN_r}]^T$$

where  $y_{il}$  is a boolean variable which indicates if  $i$ -th satellite of old configuration should go to  $l$ -th place of the new one ( $y_{il} = 1$ ) or not ( $y_{il} = 0$ ). It is possible to underline that the fact that  $\mathbf{y}$  is a vector of booleans creates an additional complication. In fact, optimizing  $\mathbf{y}$  means solving an integer optimization problem. This type of problem can be easily solved in the case of linear optimization, in which both the constraints and the objective function are linear functions, on the contrary the problem can become much more difficult in the case in which the problem presents non-linearities in one of the equations that describe it. Before defining the optimization problem, a discussion on the constraints  $\mathbf{y}$  must respect follows. There are two main evident constraints which applies in this situation.

The first is the so-called *final state condition* [44] which dictates that the  $l$ -th place of the new configuration may be occupied by one and only one spacecraft from the old formation. In addition, it binds at least one satellite of the formation to occupy the  $l$ -th place, so that no free places remain in the new configuration. This condition can be expressed by the following equations

$$\begin{aligned} y_{11} + \dots + y_{i1} + \dots + y_{N1} &= 1 \\ \vdots & \\ y_{1l} + \dots + y_{il} + \dots + y_{Nl} &= 1 \\ \vdots & \\ y_{1N_r} + \dots + y_{iN_r} + \dots + y_{NN_r} &= 1 \end{aligned} \quad \left\{ \begin{array}{l} i = 1, \dots, N \\ l = 1, \dots, N_r \end{array} \right. \quad (6.10)$$

This constraint avoids that more than one satellites occupy a given place, this prevents also from possible collision.

The second constraint is called *exclusion condition*. This condition dictates that  $i$ -th spacecraft can occupy at most one place of the new configuration. It can be written as

$$\begin{aligned}
 & y_{11} + \cdots + y_{1l} + \cdots + y_{1N_r} \leq 1 \\
 & \vdots \\
 & y_{i1} + \cdots + y_{il} + \cdots + y_{iN_r} \leq 1 \\
 & \vdots \\
 & y_{N1} + \cdots + y_{Nl} + \cdots + y_{NN_r} \leq 1
 \end{aligned}
 \quad \left\{ \begin{array}{l} i = 1, \dots, N \\ l = 1, \dots, N_r \end{array} \right. \quad (6.11)$$

Having in mind Equations 6.10 and 6.11, is now possible to present the complete problem. Both in centralized strategy or in de-centralized one, the cost-function considering the reconfiguration problem can be expressed as

$$\sum_{i=1}^N \sum_{l=1}^{N_r} \sum_{k=0}^{K-1} y_{il} \|\mathbf{u}_{il}^k\|_2 \quad (6.12)$$

Where variables  $\|\mathbf{u}_{il}\|$  represent the control inputs for placing the  $i$ -th spacecraft in the  $l$ -th place of the new configuration and they have to respect the same constraints presented in Problem 5 for no-assignment optimization problem. Thus, the complete optimization problem becomes

**Problem 7** *Translational case, reconfiguration Optimal Control*

$$\min_{\mathbf{y}} \sum_{i=1}^N \sum_{l=1}^{N_r} \sum_{k=0}^{K-1} y_{il} \|\mathbf{u}_{il}^k\|_2$$

subject to

*Equation 6.10*

*Equation 6.11*

$$\begin{aligned} \dot{\mathbf{x}}_{il}^{k+1} &= A_{il}^k \mathbf{x}_{il}^k + B_{il}^k \mathbf{u}_{il}^k + c_{il}^k & k = 0, \dots, K-1 \quad i = 1, \dots, N \\ & & l = 1, \dots, N_r \\ \|\mathbf{u}_{il}^k\|_2 &\leq U_{\max} & k = 0, \dots, K-1 \quad i = 1, \dots, N \\ & & l = 1, \dots, N_r \\ (\bar{\mathbf{x}}_{il}^k - \bar{\mathbf{x}}_j^k)^T C^T C (\mathbf{x}_{il}^k - \mathbf{x}_j^k) &\geq R_{\text{col}} \|C (\bar{\mathbf{x}}_{il}^k - \bar{\mathbf{x}}_j^k)\|_2 & k = 0, \dots, K \quad i = 1, \dots, N \\ & & j = 1, \dots, N \quad j \neq i \\ \mathbf{x}_{il}^0 &= \mathbf{x}_{i,0} & i = 1, \dots, N \quad l = 1, \dots, N_r \\ \mathbf{x}_{il}^K &= \mathbf{x}_{i,l,f} & i = 1, \dots, N \quad l = 1, \dots, N_r \end{aligned}$$

where  $\mathbf{x}_{il}$  underlines the reconfiguration of  $i$ -th spacecraft in  $l$ -th place while  $\mathbf{x}_{i,l,f}$  represents final state in case the  $i$ -th satellite is assigned to  $l$ -th place of the new configuration. The presented problem is not easy to solve, mainly because of the presence of the optimization variable  $\mathbf{y}$ . It is possible to find the solution through the exploitation of a genetic algorithm (GA) [44]. It extracts samples of  $\mathbf{y}$  (a population) which satisfy all the constraints, and then it evaluates the cost-function these realizations create. Then, it takes the subpopulation composed of the  $\lambda$  samples that have the lowest cost-function values and averages them. At the next iteration it creates new samples using the average computed at the previous iteration. This method can be very effective because it may allow not to evaluate all possible combinations of place assignments, but does not guarantee that the solution found is actually the global minimum. In this work, it was preferred to use another method to find the optimal  $\mathbf{y}$ . This method is based on the following observations:

- Considering the physics of the problem, the cost of the maneuver that brings the  $i$ -th satellite to the  $l$ -th position is independent of the variable  $y_{il}$ .
- Convex optimization allows the cost of this assignment to be obtained in extremely small time periods

So, if in a vector  $\boldsymbol{\xi} = [\xi_{11}, \dots, \xi_{1N_r}, \xi_{2,1}, \dots, \xi_{NN_r}]^T$  we save all the costs for placing  $i$ -th satellite in  $l$ -th position derived by Problem 5, then it is possible to reduce the Problem 7 into a linear optimization problem for which there are several and very performing solvers. In fact, observing that Equations 6.10 and 6.11 represent linear constraints and  $\boldsymbol{\xi}$  vector of constants is the so-called weights vector, the Problem 7 can be written also as

---

**Problem 8** *Translational case, reconfiguration Integer Linear Programming*

$$\min_{\mathbf{y}} \boldsymbol{\xi}^T \mathbf{y}$$

subject to

$$\begin{aligned} y_{11} + \dots + y_{i1} + \dots + y_{N1} &= 1 \\ \vdots \\ y_{1l} + \dots + y_{il} + \dots + y_{Nl} &= 1 \\ \vdots \\ y_{1N_r} + \dots + y_{iN_r} + \dots + y_{NN_r} &= 1 \end{aligned} \quad \left\{ \begin{array}{l} i = 1, \dots, N \\ l = 1, \dots, N_r \end{array} \right.$$
  

$$\begin{aligned} y_{11} + \dots + y_{1l} + \dots + y_{1N_r} &\leq 1 \\ \vdots \\ y_{i1} + \dots + y_{il} + \dots + y_{iN_r} &\leq 1 \\ \vdots \\ y_{N1} + \dots + y_{Nl} + \dots + y_{NN_r} &\leq 1 \end{aligned} \quad \left\{ \begin{array}{l} i = 1, \dots, N \\ l = 1, \dots, N_r \end{array} \right.$$

---

This problem is solved very quickly through solvers that implement techniques such as branch and bound, greedy algorithms, cutting planes etc...[1]. The most interesting thing is that it allows to find the global optimum unlike the GA which, according to the problem, may have difficulties in convergence. The only negative aspect of applying this methodology is the calculation of the vector of weights  $\boldsymbol{\xi}$ , in fact it is required to calculate the cost of maneuvering to place the satellite  $i$ -th in all possible  $N_r$  places. This aspect is strongly mitigated by the speed of the convex programming. In fact, in [10] reference is made to possible applications of convex

programming in the case of hundreds, or even thousands of satellites in reasonable times. Hence, as long as  $NN_r$  is kept in the order of  $10^3$  Problem 8 can be solved. There is another major advantage in solving Problem 8 rather than Problem 7. In fact, the GA, as explained above, creates a population of vectors  $\mathbf{y}$ . To calculate the cost of each realization, Problem 5 is solved for each satellite whose  $y_{il} = 1$ . If within the same population it often happens that  $y_{il} = 1$ , the algorithm calculates several times the same cost, which is absolutely inefficient since this cost is a constant given an initial and a final position. It is therefore very likely, that if the GA fails to converge correctly, Problem 5 is solved a number of times greater than  $NN_r$ . For these reasons GA should be used only for very large problems.

# Chapter 7

## Numerical Results and Discussion

This chapter aims at presenting some test cases simulations based on the methods and algorithms presented in Chapter 6. In particular, Proportional Derivative and Optimal 6DoF controls will be compared in order to verify anticipations made regarding fuel consumption, precision. Concerning Optimal control. simulations of different strategies (centralized, de-centralize, SCP only and CL-SCP) will be presented to show different performances in terms of accuracy, computational time and fuel efficiency. Finally, an example of partial re-configuration in de-centralized strategy will be reported. In the first section, common parameters used for all simulations are presented, while specific parameters are described for each simulation in the relative section.

### 7.1 Common Parameters

Common parameters involve the initial conditions of the leader spacecraft which are reported in Table7.1

|          |                         |
|----------|-------------------------|
| $a$      | $6.94761 \times 10^6 m$ |
| $e$      | 0.01                    |
| $i$      | $97^\circ$              |
| $\Omega$ | $270^\circ$             |
| $\omega$ | $70^\circ$              |
| $\nu$    | $0^\circ$               |

**Table 7.1:** Initial Orbital Parameters of the Leader spacecraft, control simulations

The simulations have been carried out on different configurations, parameters relative to each one of these configurations will be detailed in the next sections. In

all cases, the formation is composed by spacecrafts with the same initial inertial properties and dimensions (cubic satellites have been considered) which are detailed in Table 7.2

|                |                     |   |
|----------------|---------------------|---|
| Initial mass   | $m_0$               | 20 kg   |
| Inertia matrix | $\mathbf{J}_{G,BF}$ | $diag([7.2, 7.2, 7.2]) \text{ kg} \cdot \text{m}^2$ |
| Length         | $a$                 | 0.3 m   |

**Table 7.2:** Initial inertial properties and dimensions

All simulations have been carried out considering un-modeled perturbations. In fact, even if the propagation model used is very accurate, it doesn't account for less important perturbations. In addition, when the control inputs are applied, they could be subject to variations wrt the calculated values because of misalignment of the actuators, dynamics of the actuators, coupling between translational and rotational effects etc.. These effects are taken into account by considering the applied control inputs as gaussian random variables with properties detailed in Table 7.3 which also reports actuators saturation values

|                                   |                              |                                    |
|-----------------------------------|------------------------------|------------------------------------|
| Force actuator saturation         | $F_{i,max} \ i = x, y, z$    | 1 N                                |
| Control force average             | $\mu_F$                      | 0 N                                |
| Control force standard deviation  | $\sigma_F$                   | $2 \times 10^{-2} \text{ N}$       |
| Torque actuator saturation        | $\tau_{i,max} \ i = x, y, z$ | 1 N · m                            |
| Control torque average            | $\mu_\tau$                   | 0 N · m                            |
| Control torque standard deviation | $\sigma_\tau$                | $10^{-4} \text{ N} \cdot \text{m}$ |

**Table 7.3:** Actuators properties

As far as the propulsion system is concerned, in the simulations a cold gas system with an  $I_{sp} = 70 \text{ s}$  has been considered to control the translational dynamics, while as far as the rotational one is concerned, the control is done by reaction wheels whose dynamics is neglected and whose only parameter considered is the maximum torque they can generate (as in Table 7.3). For completeness, the equations used to calculate fuel consumption during control maneuvers are reported below

$$\Delta m = m_b(1 - e^{-\frac{\Delta V}{I_{sp}g_0}})$$

where  $m_b$  is the mass of the spacecraft before the maneuver,  $g_0 = 9.80665 \frac{\text{m}}{\text{s}^2}$  is a constant and  $\Delta V$  is calculated as

$$\Delta V = \int_{t_0}^{t_1} \frac{\|\mathbf{F}_c(t)\|}{m(t)}$$

where  $[t_0, t_1]$  is the interval of time of control maneuver,  $\|\mathbf{F}_c(t)\|$  is the control force and  $m(t)$  is the mass of the spacecraft.

Finally, all simulations consider all perturbations presented in Chapter 3 if not otherwise specified.

## 7.2 Drift Correction

In this simulation, a Helix configuration composed by seven spacecrafts (leader included) has been propagated in free-flying configuration until a condition activates the control loop. It is possible to adopt different criteria to activate control algorithms, the one chosen in this work activates the control loop when the euclidean distance of a generic follower wrt the leader is higher than a predetermined value. This value depends on the configuration and on the maximum admissible drift the formation can undergo while remaining operational. Another possible criterion would consider a limit on the proximity of the spacecrafts of the formation by activating the loop when the distance between two spacecrafts is lower than a predetermined quantity in order to avoid collisions.

The Drift correction simulation has been chosen to show differences between methods presented in Chapter 6, in particular, the same configuration has been controlled in 6DoF with the PD controller, with the optimal controller centralized architecture in SCP and in de-centralized architecture both in SCP and CL-SCP. The initial conditions of the spacecrafts of the formation are dictated by the propagation in uncontrolled mode until the control algorithm is activated by the criterion explained above, while the final relative positions are the same as reported in Table 7.4 and initial relative velocities have been found with 5.25 for improving stability. Concerning rotational motion, also in this case the initial state depends on the history of perturbations acting during the propagation while the final state is the same for all the spacecrafts and considers an Earth pointing direction for attitude and  $\boldsymbol{\omega}_{BF} = \mathbf{0}$ .

|                    |       |
|--------------------|-------|
| $a \cdot \delta i$ | 100 m |
| $a \cdot \delta e$ | 200 m |
| $\alpha_1$         | 9°    |
| $N$                | 7     |

**Table 7.4:** Helix final parameters for drift correction simulation.

### 7.2.1 PD Controller

In Table 7.5, the gains used for this simulation are reported

|                       |                                  |                 |
|-----------------------|----------------------------------|-----------------|
| Position Gain         | $k_{p,i} \ i = 1, \dots, N$      | $0.1 \ N/m$     |
| Velocity Gain         | $k_{v,i} \ i = 1, \dots, N$      | $5 \ Ns/m$      |
| Quaternion Gain       | $k_{q,i} \ i = 1, \dots, Nm$     | $0.1 \ Nm$      |
| Angular Velocity Gain | $k_{\omega,i} \ i = 1, \dots, N$ | $0.1 \ Nms/rad$ |

**Table 7.5:** PD gains definition

Since the transfer function of the system is quite complicated, the gains used have been chosen having as objective the convergence of the control law. It is clear that more accurate synthesis methodologies could be studied but such a study would be outside the scope of interest of this study. For simplicity all the crossed gains have been set to zero ( $k_{f,ij} = 0 \ N/m$  and  $k_{\tau,ij} = 0 \ Nm$ ). In Figure 7.1 it is possible to visualize the trajectories followed by spacecrafts in case of PD controller. The final position required is highlighted in red and it is visible that the target position state has been correctly reached. If one looks carefully at the figure, one can perceive how the trajectories of the satellites have a not very smooth shape, this is an indication of the fact that the control applies instantaneous manoeuvres based on the value of the sensors received in real-time and is therefore unable to predict the trend in future instants. In order to have quantitative information, it is possible to display the convergence history in (Figures 7.2 and 7.3).

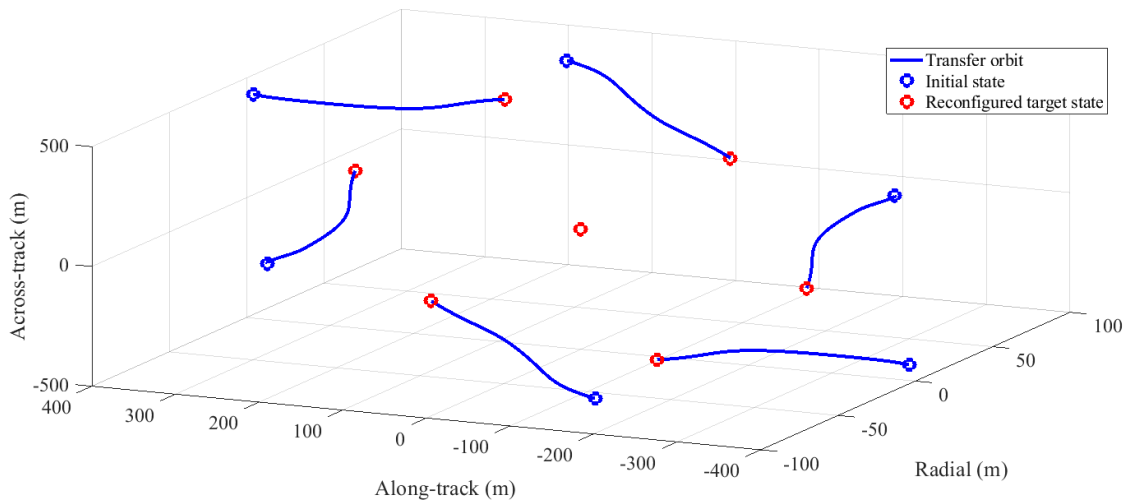


**Figure 7.1:** Trajectories drift correction PD controller

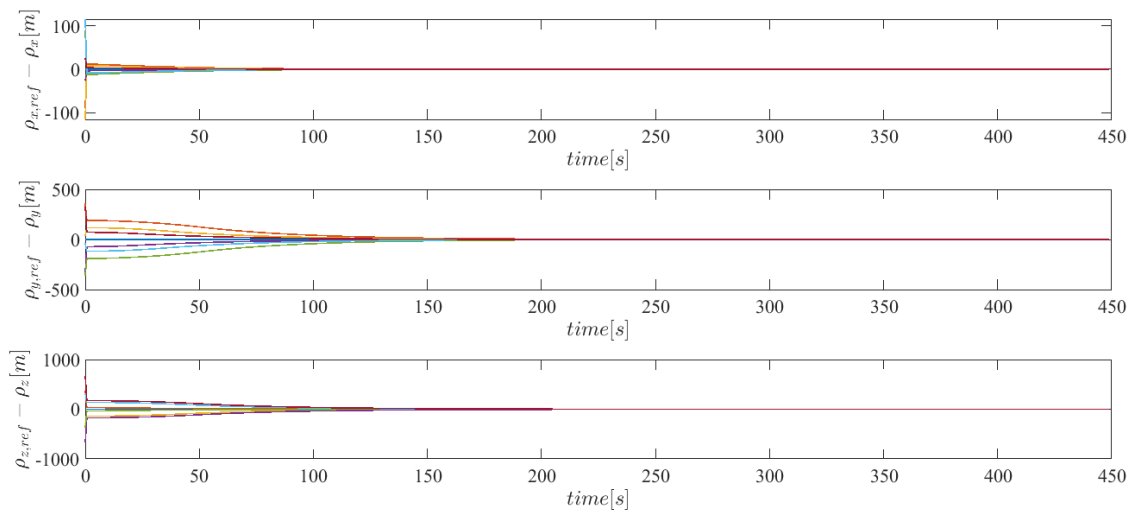


**Figure 7.2:** Position errors history drift correction PD controller

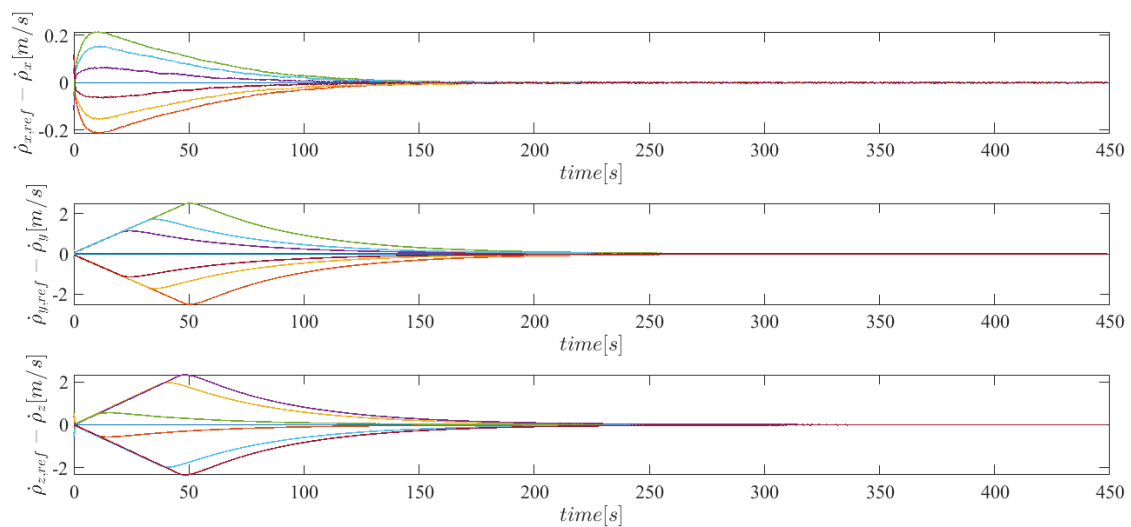


**Figure 7.3:** Velocity errors history drift correction PD controller

The convergence behaviour is quite good, it is possible to see how the position errors are almost zero after 150 s, while the velocity errors after 200 s. It is also evident how the convergence rate decreases in last part of the maneuver because of small errors between reference state and the real one. This behaviour is obtained thanks to control forces reported in Figure 7.4. It is evident how the control is saturated in the initial phases of the maneuver, this is in agreement with what was anticipated in the Chapter 5, i.e. this kind of control tends to have very high input forces. It is worthy to underline the symmetric behaviour of control forces, this is due to the inherent symmetry of the initial helix configuration. Finally, it is very important to

point out that the forces required in the radial direction are lower than in the other two directions, this aspect validates what was seen in the stability Chapter 5.

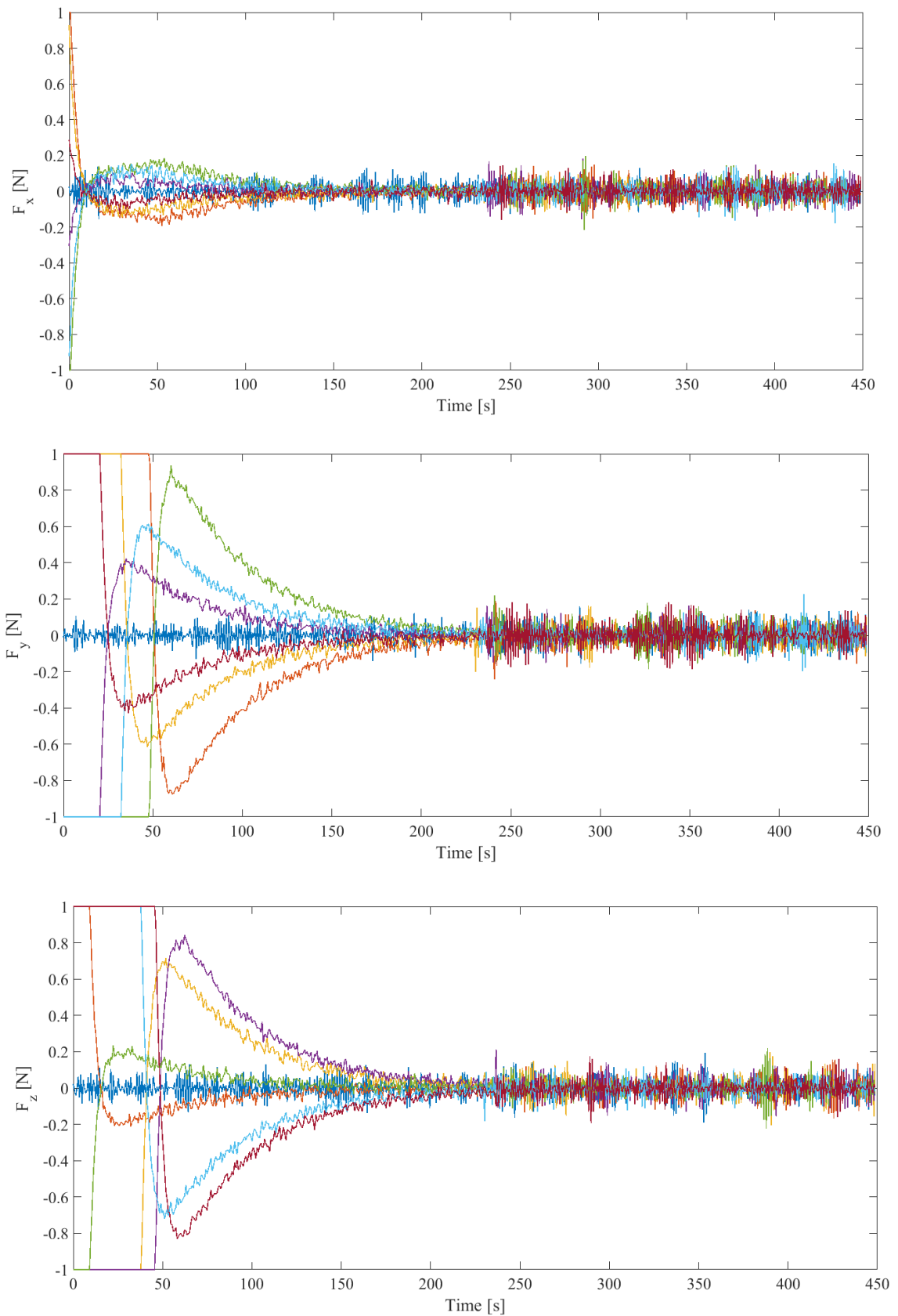


**Figure 7.4:** Actuation Forces drift correction PD controller

Concerning rotational motion, Figure 7.6 shows the history of versor  $\hat{z}_{BF}$  of each spacecrafts and the final target state, while Figure 7.5 presents a zoom in the neighborhood of a spacecraft. It is clear how, at the end of the simulation, versors  $\hat{z}_{BF}$  are correctly oriented towards the radial direction (Earth pointing direction). The results are verified through the plots describing the attitude and angular velocity errors (Figures 7.7 and 7.8). It should be noted that the rotational dynamics is slower to converge with the parameters chosen. Moreover, it presents strong oscillations about the final target showing a more unstable behavior than the translational case. This aspect could be corrected by decreasing the gains  $k_q$  and  $k_\omega$ , but in this way the convergence will be slowed down further. Ultimately, it is a matter of making a trade-off between convergence speed and stability.

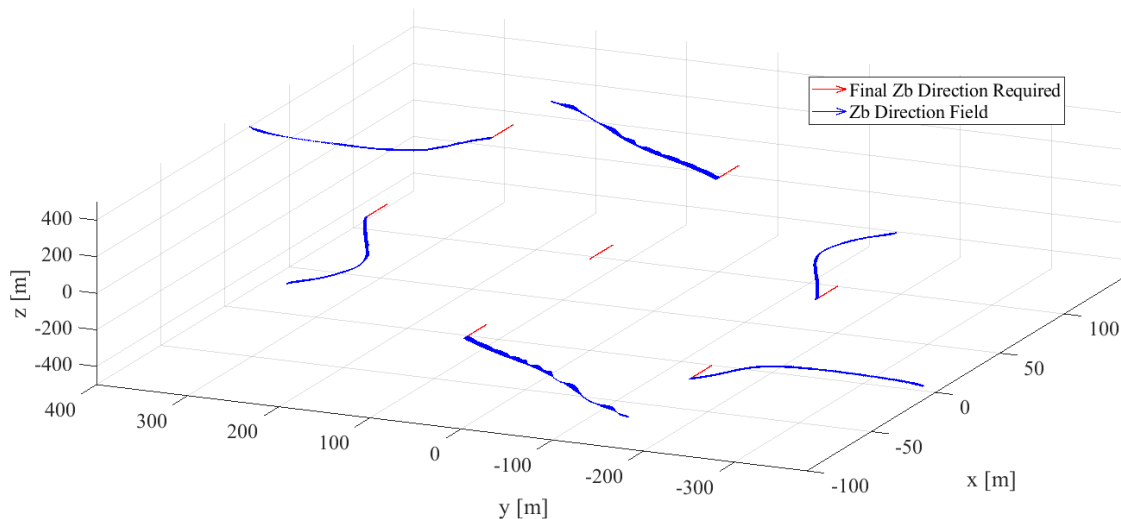


**Figure 7.5:**  $\hat{z}_{BF}$  field drift correction PD controller

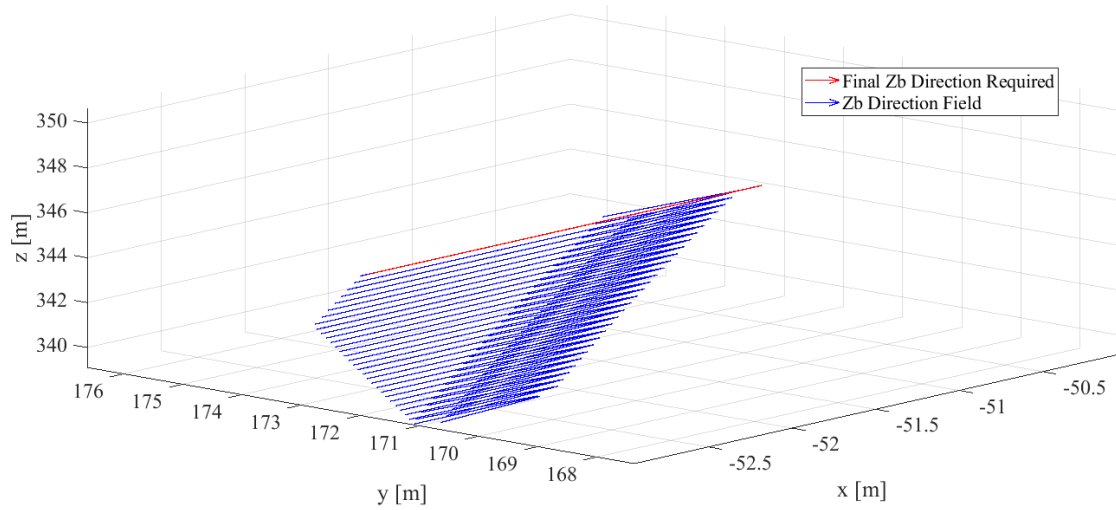


**Figure 7.6:**  $\hat{z}_{BF}$  field drift correction PD controller (detail)

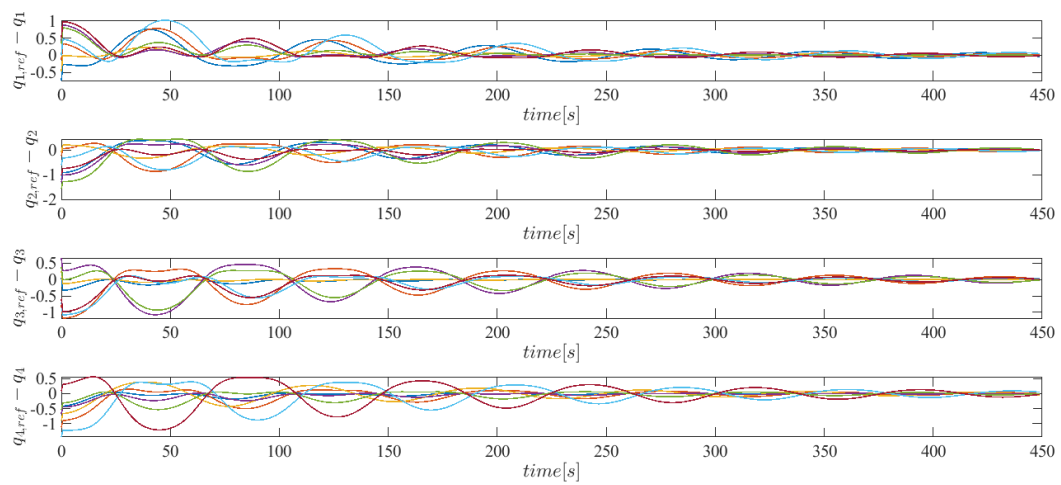


**Figure 7.7:** Quaternion errors history drift correction PD controller

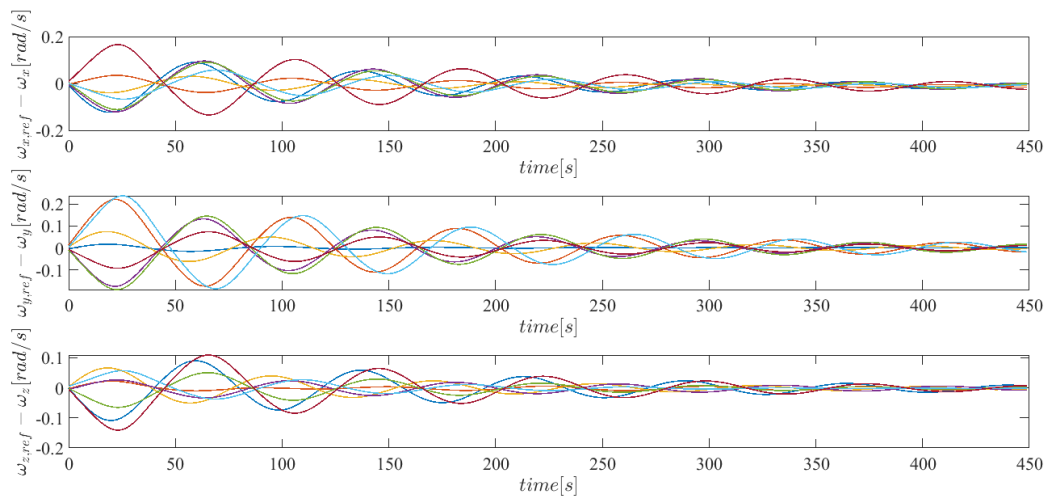


**Figure 7.8:** Angular velocity errors history drift correction PD controller

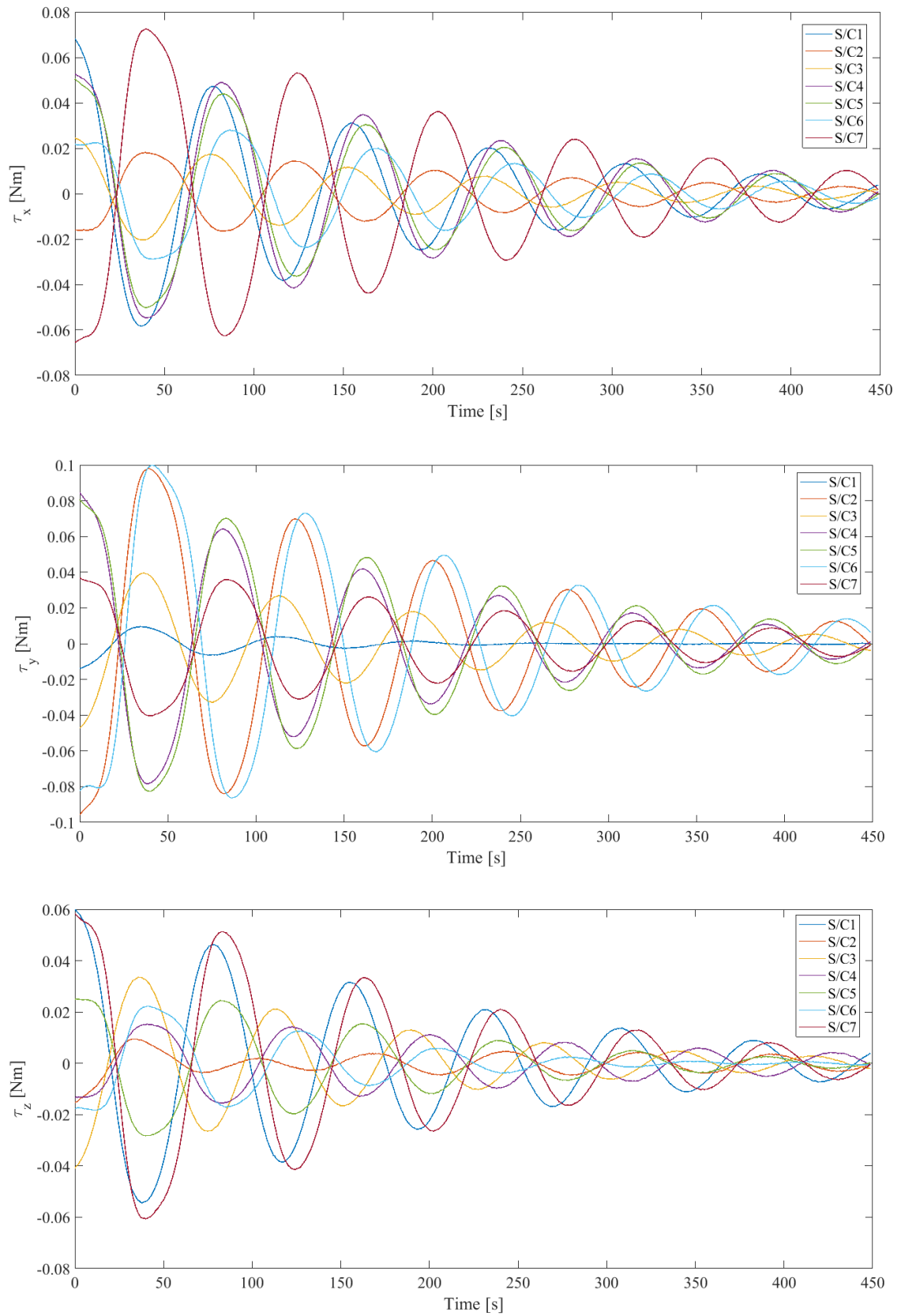


**Figure 7.9:** Actuation Torques drift correction PD controller

The  $\Delta m_{tot}$  fuel consumption of the entire formation for the maneuver is  $\Delta m_{tot} = 1.10427 \text{ kg}$ . Considering the initial mass of the spacecrafts it can be noticed that it corresponds to an average of  $\Delta m_{av} = 0.184045 \text{ kg}$  per satellite which is not negligible (0.920225% of the initial mass).

### 7.2.2 Optimal Controller de-centralized SCP

The parameters used for all Optimal control simulations are reported in Table 7.6.

|                              |                        |  |
|------------------------------|------------------------|--|
| Final time                   | $t_f$                  | $0.05T_0 \text{ s}$                          |
| Number of points             | $K$                    | 100  |
| Stopping criterion           | $\epsilon$             | $10^{-2}$                                    |
| Minimum distance             | $R_{col}$              | $20 \text{ m}$                               |
| Initial guess trajectories   | $\bar{\mathbf{x}}_i^k$ | free-flying leader trajectory $\forall i, k$ |
| Initial guess control inputs | $\bar{\mathbf{u}}_i^k$ | $0 \forall i, k$                             |

**Table 7.6:** SCP simulation parameters

In Figure 7.10 optimal trajectories as calculated by Optimal controller in de-centralized strategy using sequential convex programming are calculated. It is visible how in this case the trajectories have a different shape wrt PD controller, they try to use the dynamics in order to save fuel thus resulting in more homogeneous and smoother paths. These trajectories are obtained through control forces presented in Figure 7.11. It is visible how the control forces are one order of magnitude lower than PD controller case. Again, the control forces remain symmetrical with respect to the time axis. One aspect in common with the PD controller is that both are able to identify the least need for control along the radial direction by predicting smaller control forces  $F_x$  than in the other two directions.

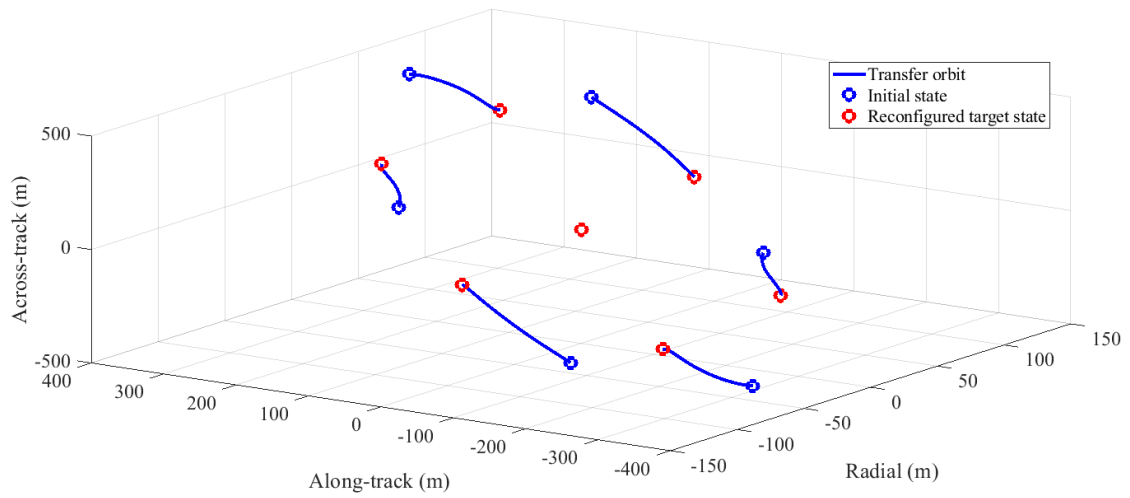


**Figure 7.10:** Trajectories drift correction Optimal controller de-centralized SCP

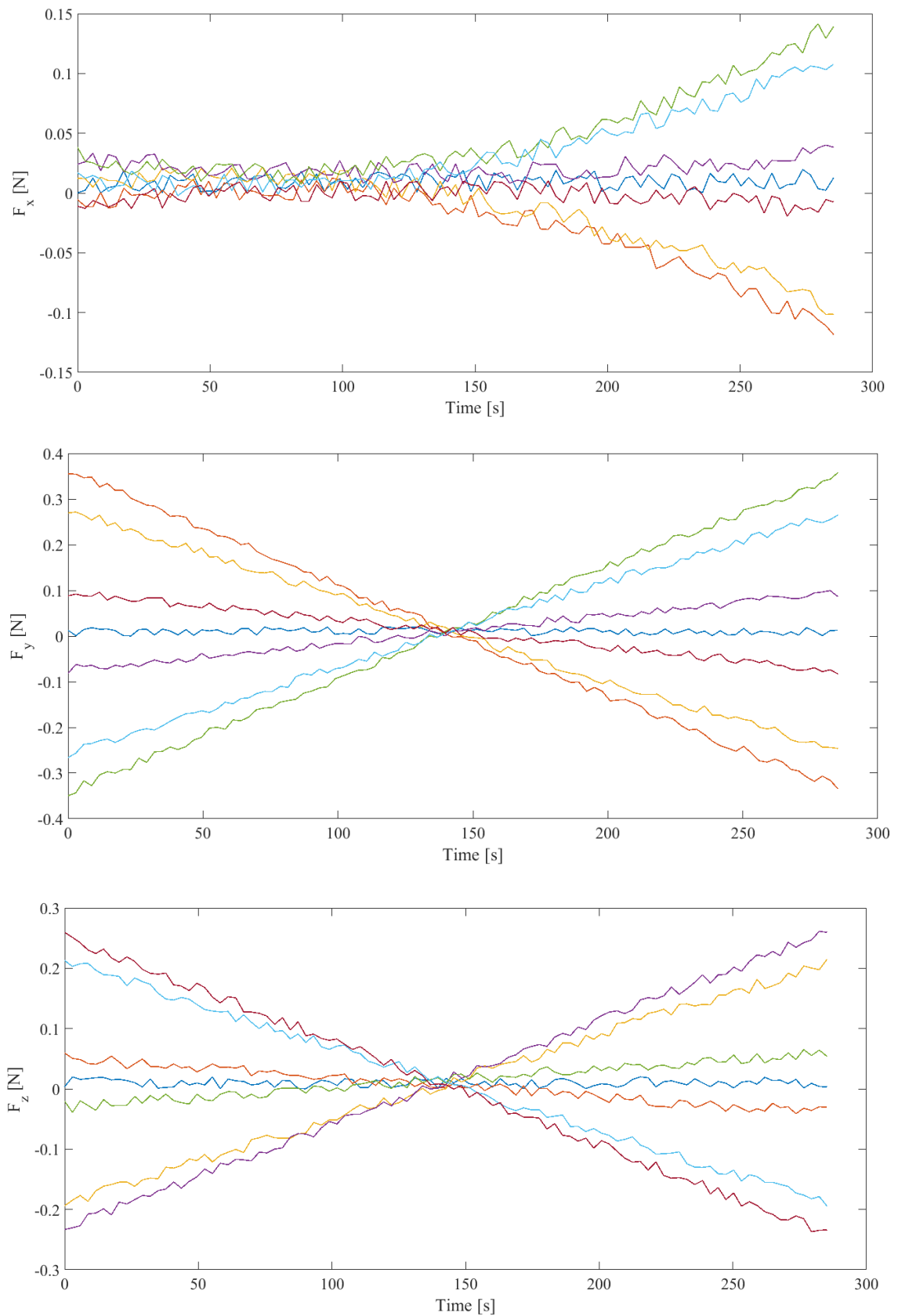


**Figure 7.11:** Actuation Forces drift correction Optimal controller de-centralized SCP

In this case the total fuel consumption is  $\Delta m_{tot} = 0.613562 \text{ kg}$ , while the average is  $\Delta m_{av} = 0.102260 \text{ kg}$ . It is already evident that the control forces obtained by the optimal controller allow to perform the same correction with less fuel consumption. A more in-depth comparative analysis will be done in a later section.

### 7.2.3 Optimal Controller centralized SCP

The centralized architecture simulation has been effectuated in order to analyse the effects of adopting a different architecture. The simulation solves the Problem reported in Annex. D. In Figure 7.12 the calculated trajectories are reported. It is visible how they are very similar to the de-centralized case, they both present the smoothness of Optimal control trajectories. Analogous behaviour could be expected in control forces which are reported in Figure 7.13.

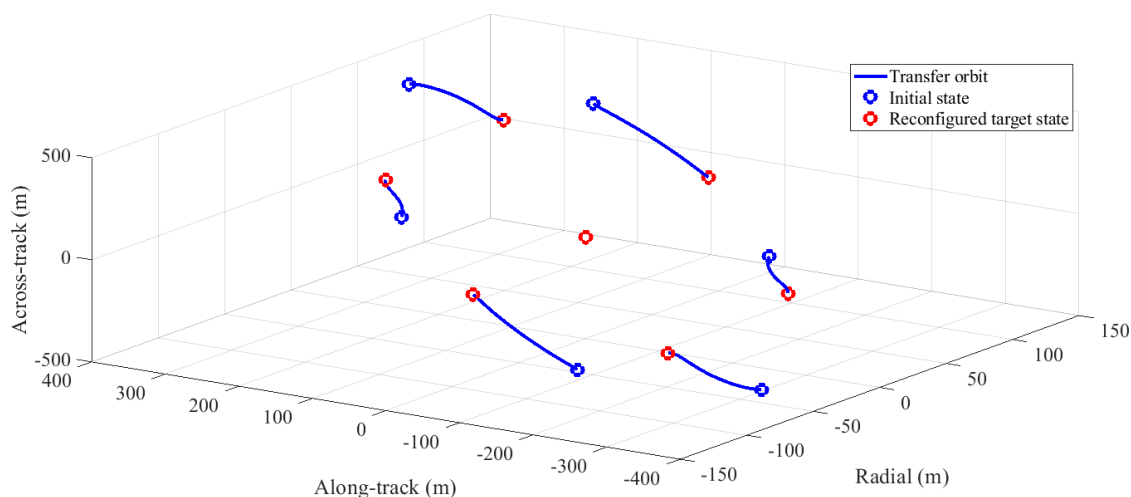


**Figure 7.12:** Trajectories drift correction Optimal controller centralized SCP

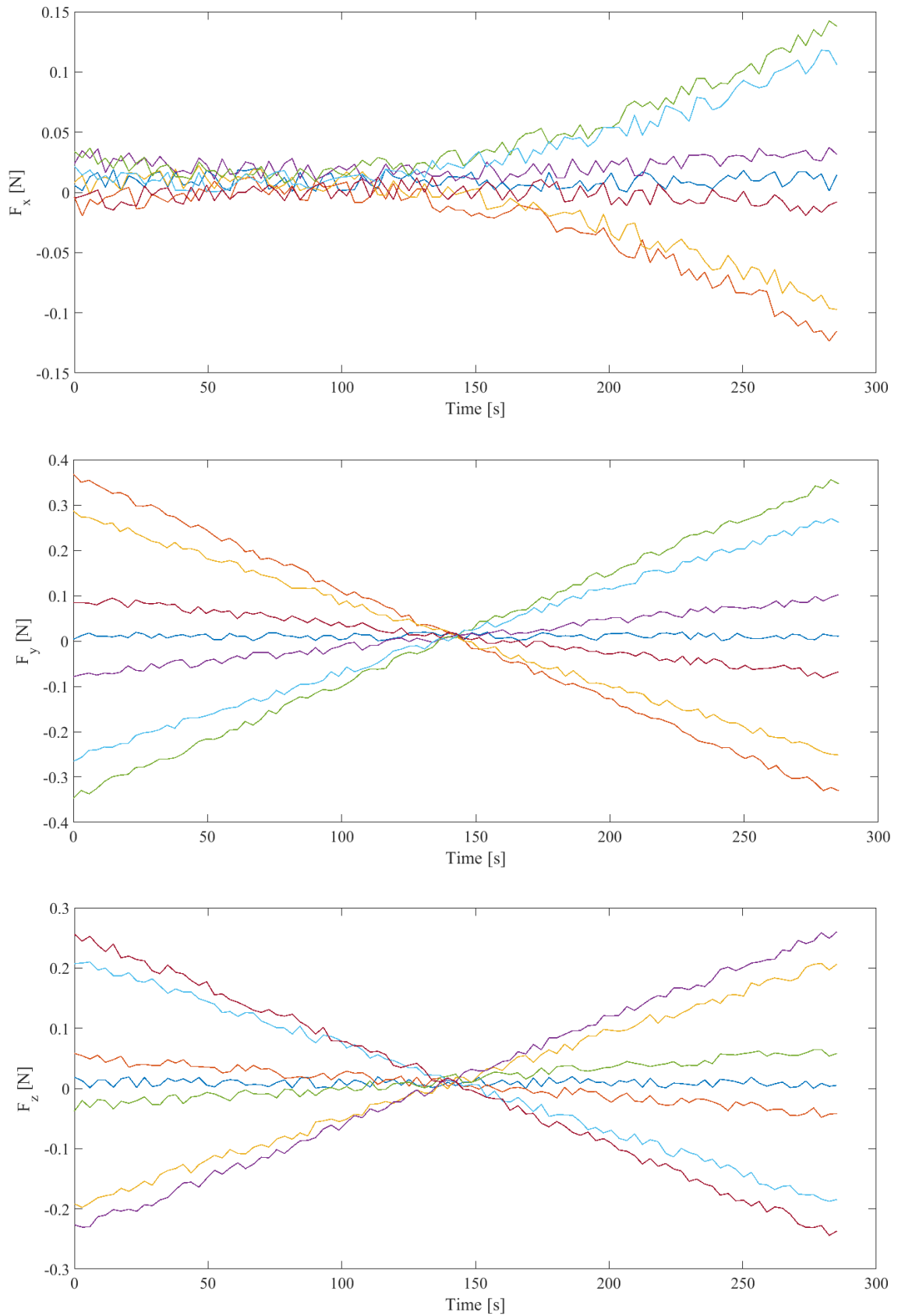


**Figure 7.13:** Actuation Forces drift correction Optimal controller centralized SCP

Regarding convergence behaviour there are not relevant remarks. What is more interesting is the total fuel consumption and the actuation forces reported in Figure 7.13. Total fuel consumption is of  $\Delta m_{tot} = 0.404724 \text{ kg}$  (smaller than the de-centralized case). Regarding computational times, Table 7.7 indicates the CPU time taken to find the final trajectories. It should be noted that in the de-centralized case, the value shown in the table is the average computation time taken by a single satellite. In fact, the total time of the simulation, which is carried out for the entire formation, has been divided by the number of satellites that make up the formation. It is evident how de-centralized strategy allows to calculate trajectories in a shorter interval of time, underlying that the choice of the architecture is dictated by a trade-off between fuel consumption and computational resources.

|                        |            |
|------------------------|------------|
| Centralized strategy   | 115.7343 s |
| De-entralized strategy | 26,3616 s  |

**Table 7.7:** Computational times comparison

In this case total fuel consumption is  $\Delta m_{tot} = 0.404724 \text{ kg}$ .and the average is  $\Delta m_{av} = 0.067454 \text{ kg}$ .

#### 7.2.4 Optimal Controller de-centralized CL-SCP

Parameters used for this simulation are the same of the Table 7.6 and only the definition of the CL-SCP horizon  $K_H = 12$  was added. Similarly to previous cases, in Figure 7.14 the trajectories calculated through CL-SCP method are shown. In Figure 7.15, control input forces are reported for completeness, not showing any particular appreciable difference from previous optimal control cases.

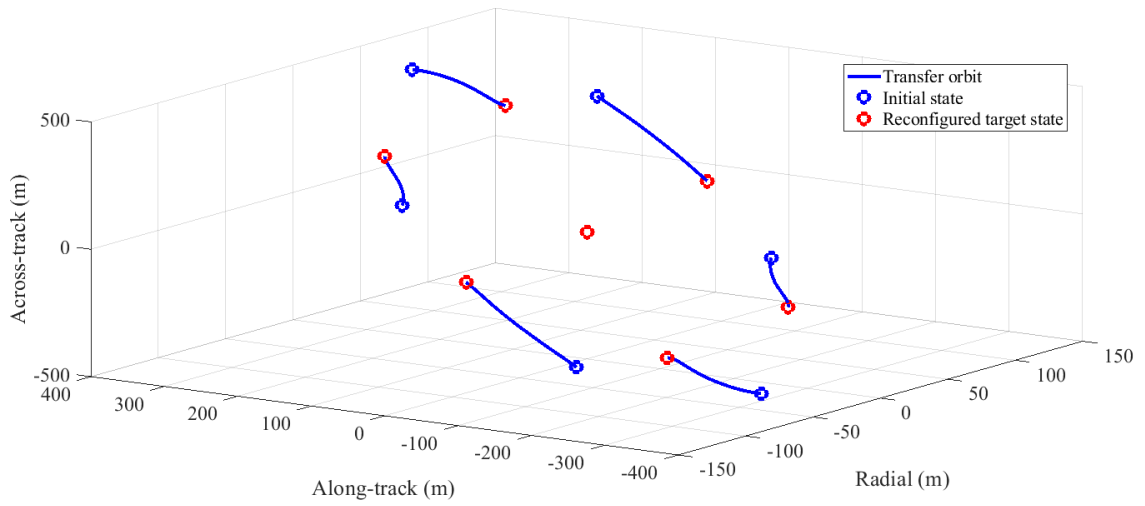


**Figure 7.14:** Trajectories drift correction Optimal controller de-centralized CL-SCP

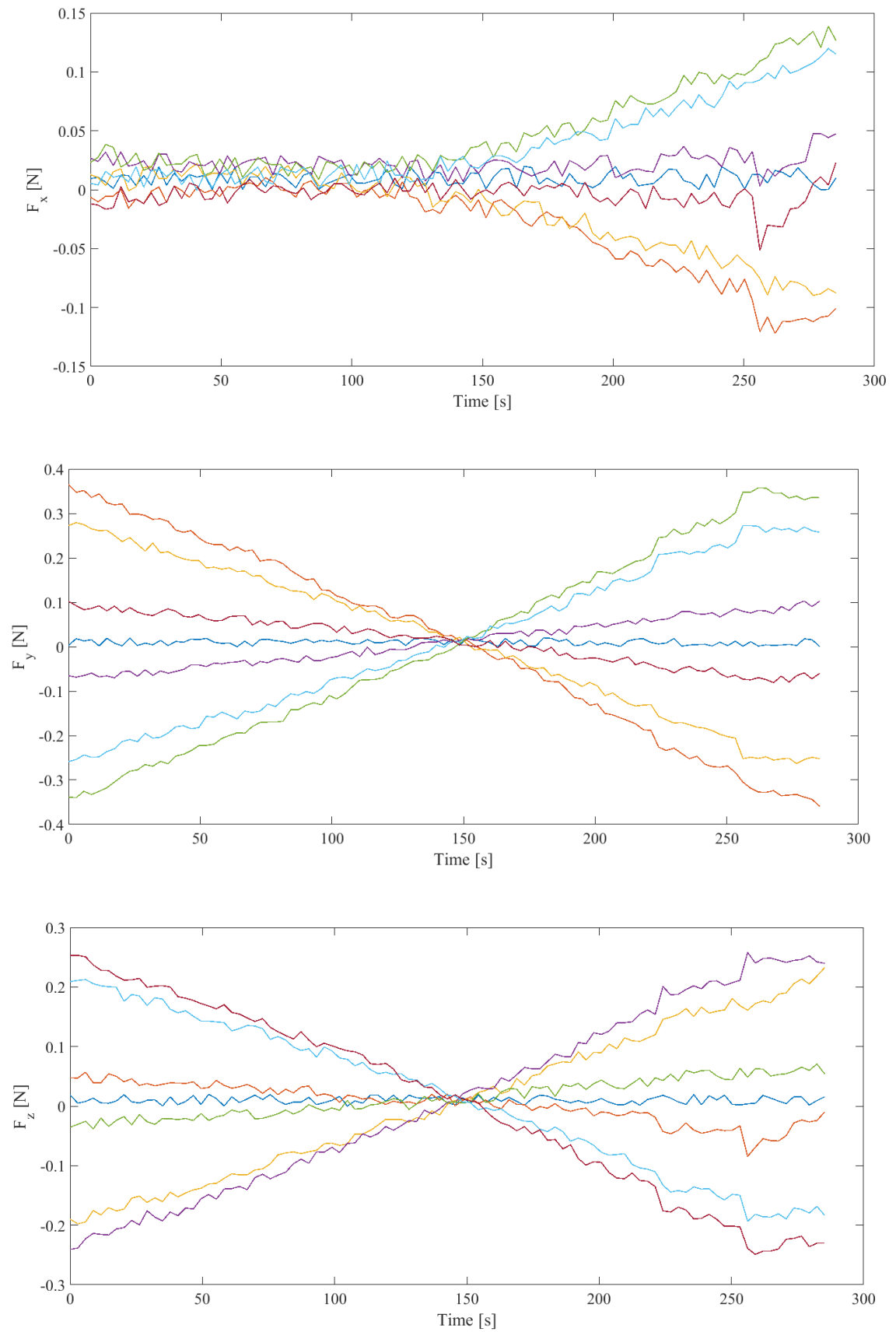


**Figure 7.15:** Actuation Forces drift correction Optimal controller de-centralized CL-SCP

The most interesting thing is that in this case the final position error has been reduced wrt the Open Loop case. This is the main reason why an Open Loop control system cannot meet the accuracy requirements of the mission. Figures 7.16 and 7.17 show qualitatively a comparison in  $xy$  plane between de-centralized OL and CL strategies. It is clear how the final position obtained through the closed loop strategy is nearer to the required one for all the spacecrafts. These results will be also quantitatively analyzed in the next section.

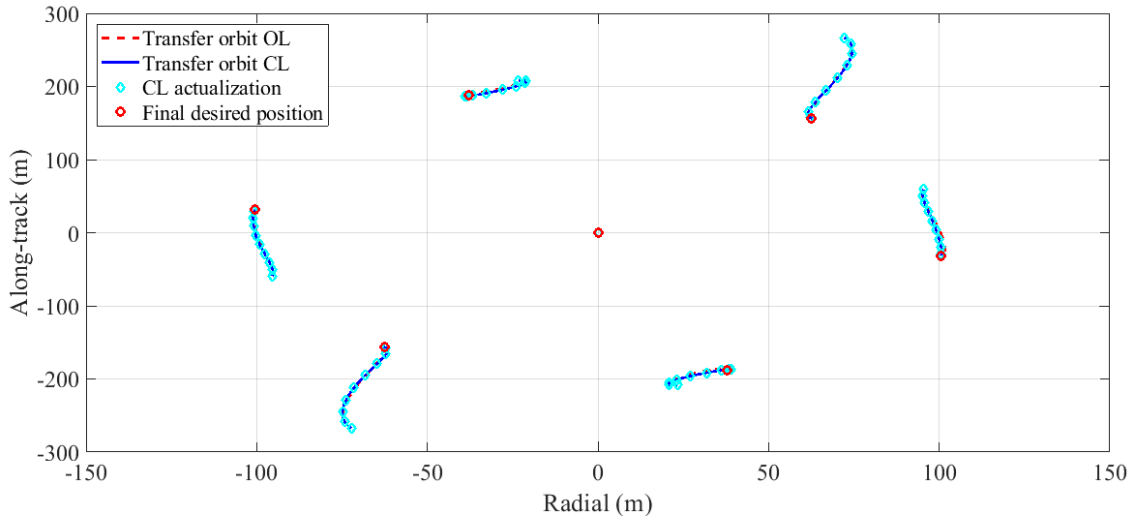


**Figure 7.16:**  $xy$  trajectories comparison between SCP and CL-SCP

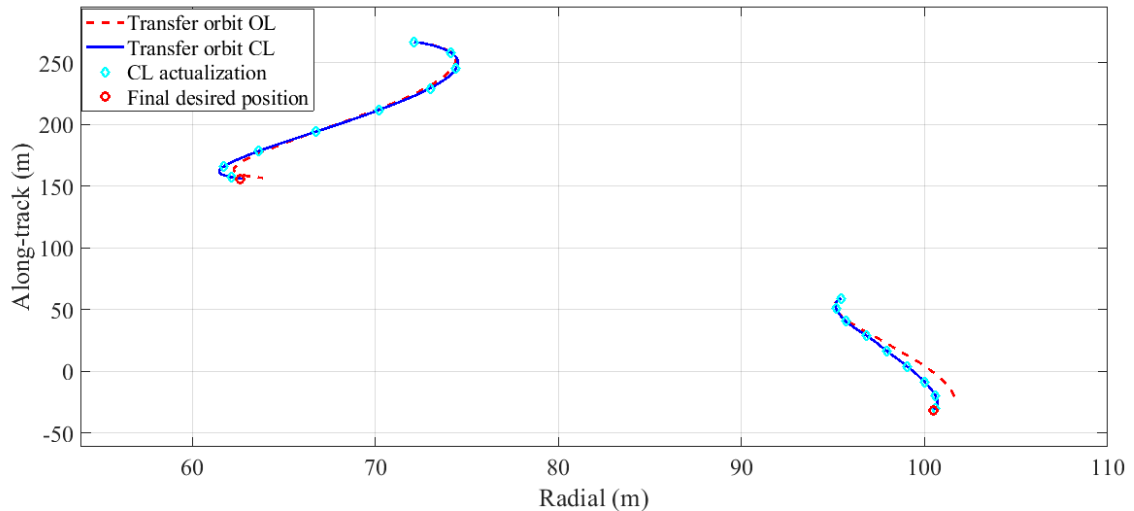


**Figure 7.17:**  $xy$  trajectories comparison between SCP and CL-SCP (detail)

Concerning rotational motion, Figures 7.18, 7.19, 7.20 and Figure 7.21 report the  $\hat{z}_{BF}$  versor field, the evolution of the quaternions and angular velocities and the

control torques obtained through the Optimal control algorithm.

From Figure 7.18, it is already possible to see how the satellites  $\hat{z}_{BF}$  versors converge to the required attitude without oscillations, unlike the PD controller. This result is further confirmed by the Figures 7.19 and 7.20 which present smoother curves that converge homogeneously to the reference quantities. It is also interesting to note that in this case the angular velocities are always an order of magnitude smaller than in the case of the PD controller anticipating the lower intensity of the control torques. In fact, in Figure 7.21 it is immediately visible how also in this case the profiles of control torques are more homogeneous and above all are of the order of  $10^{-3} Nm$ , proving the effective optimization of the rotational trajectories.

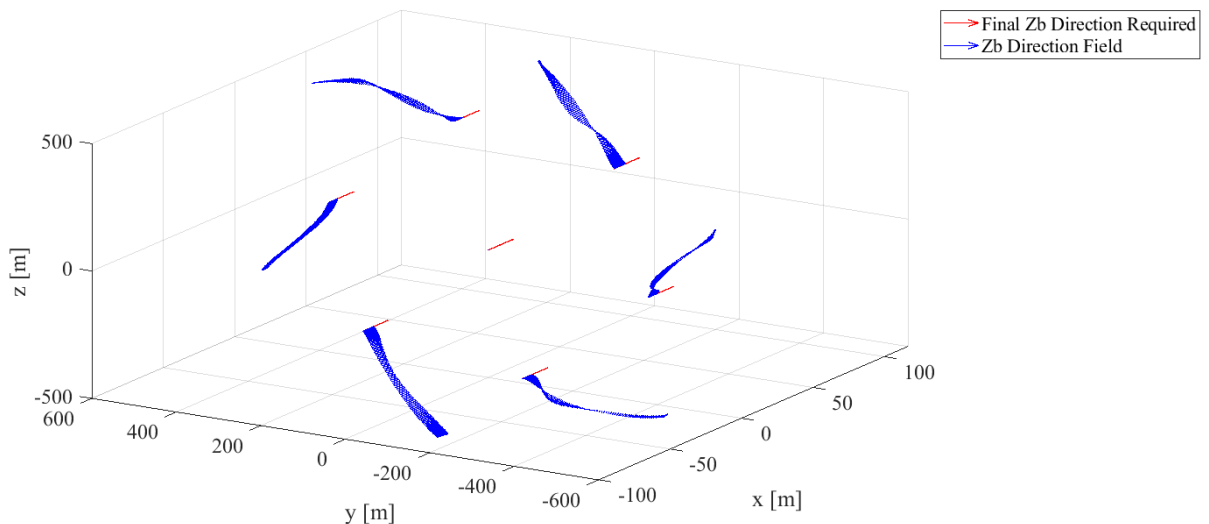


**Figure 7.18:**  $\hat{z}_{BF}$  field drift correction Optimal controller CL-SCP

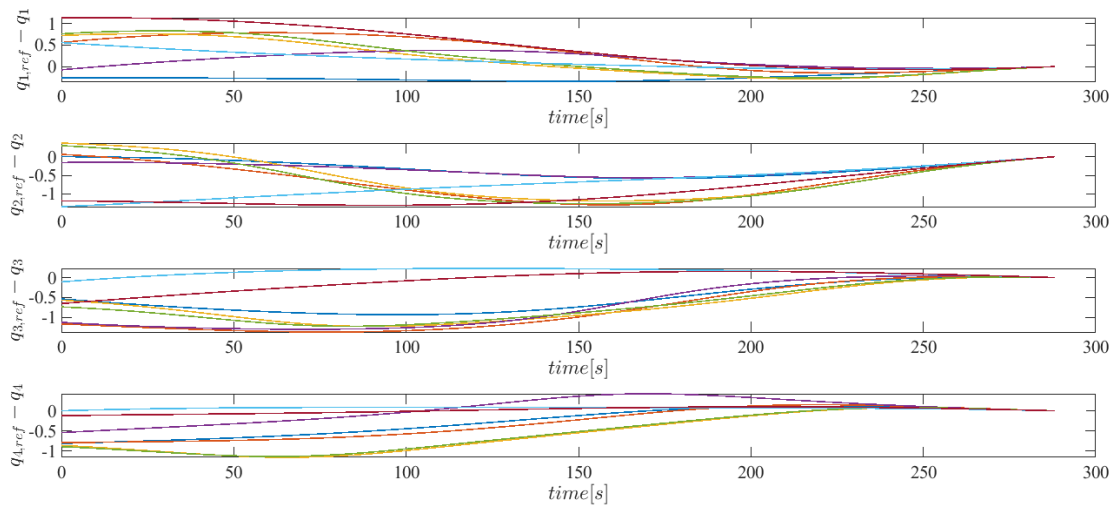


**Figure 7.19:** Quaternion errors history drift correction Optimal controller CL-SCP

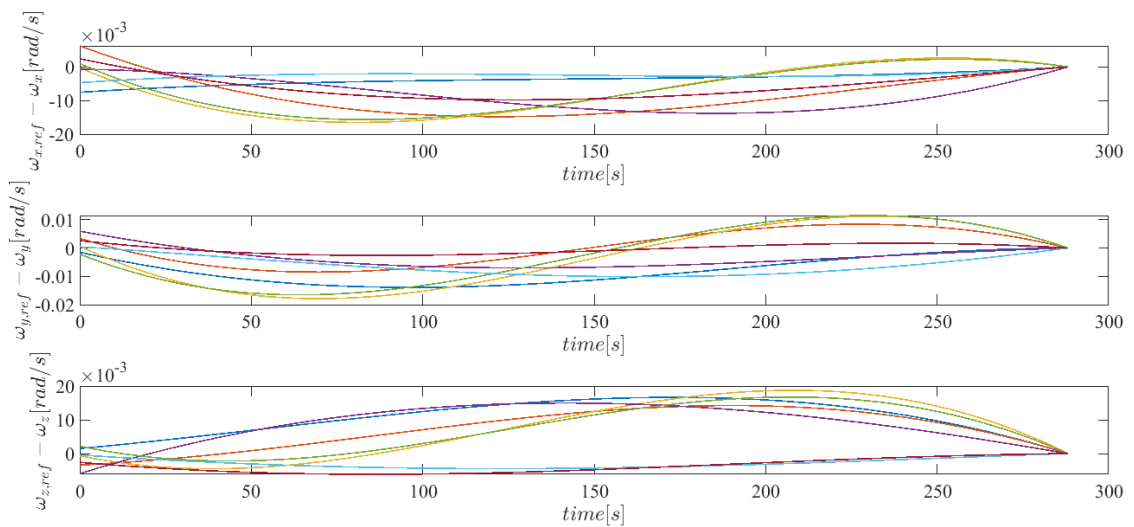


**Figure 7.20:** Angular velocity errors history drift correction Optimal controller CL-SCP

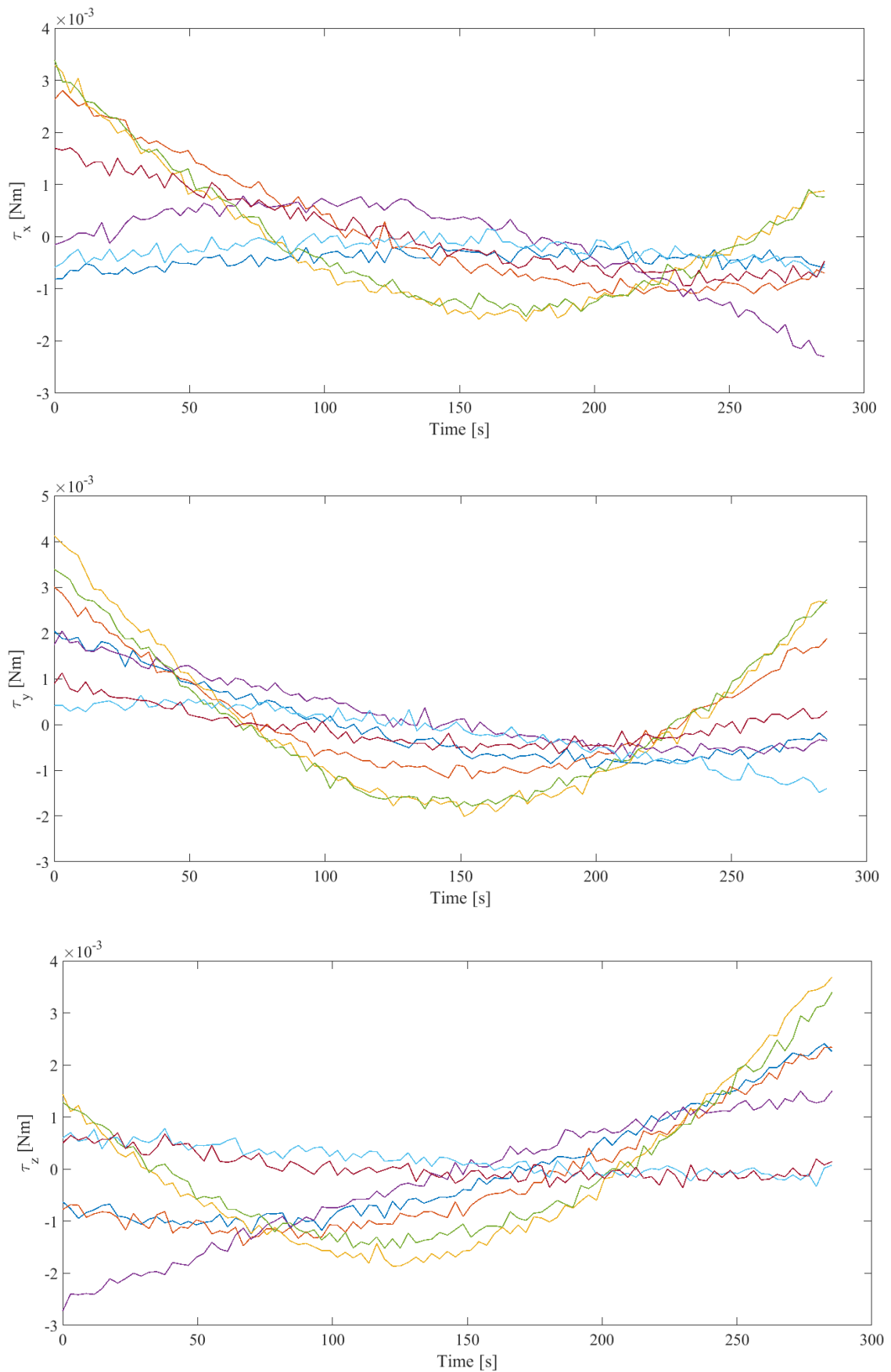


**Figure 7.21:** Actuation Torques drift correction Optimal controller CL-SCP

Regarding fuel consumption this simulation presents  $\Delta m_{tot} = 0.439086 \text{ kg}$  and the average is  $\Delta m_{av} = 0.073181 \text{ kg}$ .

### 7.3 Discussion

It is now possible to make a discussion about the results that have just been found in the case of correcting drifts of the initial configuration. In particular, it is possible to compare the different methodologies applied considering the accuracy with which the final target state was reached and the fuel consumption of the manoeuvre. In terms of accuracy, this work has rather focused on the analysis of reaching the final position of the spacecrafts (same considerations can be done with velocities, quaternions and angular velocities). The metric chosen for this comparison is the euclidean distance between the final position of the spacecraft and the desired final position

$$\Delta\rho = \sqrt{(\Delta\rho_{x,ref} - \Delta\rho_x)^2 + (\Delta\rho_{y,ref} - \Delta\rho_y)^2 + (\Delta\rho_{z,ref} - \Delta\rho_z)^2}$$

In Table 7.8 the results of this quantity for each simulations have been reported in terms of maximum position error and the average one. It is evident that the optimal control cases in de-centralized and non-centralized SCP are the worst cases. This result was predictable considering that they are Open-Loop methodologies that do not consider external measures, so linearization errors and unmodeled perturbations have more important effects. As far as the PD controller is concerned, it is worth noting that the differences in position and velocity are 0.05 since this is the stopping criterion of the algorithm, which therefore makes it easier to reach the final state with more precision at the expense of a greater use of fuel. Finally, it is important to underline how the closing of the loop in the case of Optimal control has gained an order of magnitude in reaching the final position. The final error is due to the fact that at a certain point the remaining part of the instants in which the optimal calculation is performed is smaller than the horizon  $K_H$ , so the last part of the trajectories is propagated without further updating the initial states through the measurements. The precision with which the final state is reached is very important because the stability of the configuration depends on it. If the final conditions have been imposed in such a way that the satellites are placed in  $J_2$  invariant orbits, an error in position or velocity with respect to these conditions will cause a higher drift rate and consequently a greater need for corrections.

|         |                  |            |                  |
|---------|------------------|------------|------------------|
| PD      | $\Delta\rho$ [m] | OC dec SCP | $\Delta\rho$ [m] |
| Maximum | $\leq 0.05$      | Maximum    | 8.6289           |
| Average | $\leq 0.05$      | Average    | 4.52795          |

|            |                  |               |                  |
|------------|------------------|---------------|------------------|
| OC cen SCP | $\Delta\rho$ [m] | OC dec CL-SCP | $\Delta\rho$ [m] |
| Maximum    | 4.7097           | Maximum       | 0.7887           |
| Average    | 3.3175           | Average       | 0.6207           |

**Table 7.8:** Final position errors drift corrections simulations

In Table 7.9, the fuel consumption of each simulation has been reported in terms of total mass used by the whole formation  $\Delta m_{tot}$ , the average one  $\Delta m_{av}$  and the percentage of the average mass wrt the initial one  $\Delta m_{\%av} = \Delta m_{av}/m_0 \cdot 100$ . It is possible to notice that the case of PD controller is prohibitive. With a single maneuver, each satellite on average uses almost 10% of the initial mass. This implies that a small number of corrections can be made, thus reducing the life of the mission. The case of de-centralized Optimal control behaves better. For the same maneuver it consumes almost half of the mass, showing how the optimization algorithm is able to find fuel saving solutions. The de-centralized strategy finds however a sub-optimal solution since each satellite does not know a priori the position of the other spacecrafts, which instead the centralized strategy does. In fact, if only one spacecraft could calculate all the trajectories, it would be able to plan the control forces in order to avoid collisions in a preventive way. The centralized strategy reduces by one third the fuel used by the PD controller, but it has still the problem of accuracy. A good compromise is the de-centralized strategy in closed-loop. In fact, it increases the accuracy of the system but at the expense of greater fuel use than the simple de-centralized strategy. This is due to the fact that the actual trajectory followed by the spacecrafts is not the one calculated by Optimal control, and consequently, a trajectory that requires more corrections (sub-optimal trajectory).

| Case          | $\Delta m_{tot}$ [kg] | $\Delta m_{av}$ [kg] | $\Delta m_{\%av}$ |
|---------------|-----------------------|----------------------|-------------------|
| PD            | 1.10427               | 0.184045             | 0.920225          |
| OC dec SCP    | 0.410259              | 0.0683765            | 0.3418825         |
| OC cen SCP    | 0.404724              | 0.067454             | 0.33727           |
| OC dec CL-SCP | 0.439086              | 0.073181             | 0.365905          |

**Table 7.9:** Fuel consumption summary drift corrections simulations

Ultimately, the best compromise is the case of decentralized Optimal control in CL, since, although it makes use of more fuel than the open-loop (but less than the PD controller), it allows to improve the accuracy which leads to greater stability of the

formation so requiring less frequent correction maneuvers.

## 7.4 Closed-Loop Partial reconfiguration

This simulation aims at showing a test case solution to Problem 8 in order to better understand the relationships between quantities involved in partial reconfiguration. The algorithm has been applied in conjunction with the optimal controller in de-centralized strategy in the context of Sequential Convex Programming. Initial configuration was composed by seven satellites flying in Helix configuration (Table 5.5) which have been partially re-configured in a four satellites Cartwheel-Pendulum configuration (Table 5.12). First of all, the weights vector  $\boldsymbol{\xi}$  has been calculated by solving  $NN_r = 28$  ( $N = 7$  and  $N_r = 4$ ) optimal control problems. The value of the objective function to place the  $i$ -th spacecraft of old configuration in  $l$ -th place of new one, which are a measure of fuel consumption for the maneuvers, has been stored as the  $\xi_{il}$  component. Problem 8 has finally been solved in very short time with function *intlinprog*. The solution  $\mathbf{y}$  of this test case is the following

$$\mathbf{y} = [[1, 0, 0, 0], [0, 1, 0, 0], [0, 0, 0, 1], [0, 0, 0, 0], [0, 0, 1, 0], [0, 0, 0, 0], [0, 0, 0, 0]]$$

its physical meaning is reported in Table 7.10 which indicates, through a satellite ID, which place of the new configuration has been assigned to the spacecraft of the old formation.

| Old configuration ID | New configuration ID |
|----------------------|----------------------|
| 1                    | 1                    |
| 2                    | 2                    |
| 3                    | 4                    |
| 5                    | 3                    |

**Table 7.10:**  $\mathbf{y}$  physical meaning

The spacecrafts not present in the table are those which have not been assigned to any place of the new configuration, so they've been propagated in a free-flying mode.

In Figure 7.22 it is possible to visualize the re-configuration trajectories while the fuel consumption of each spacecraft and the total has been reported in Table 7.11

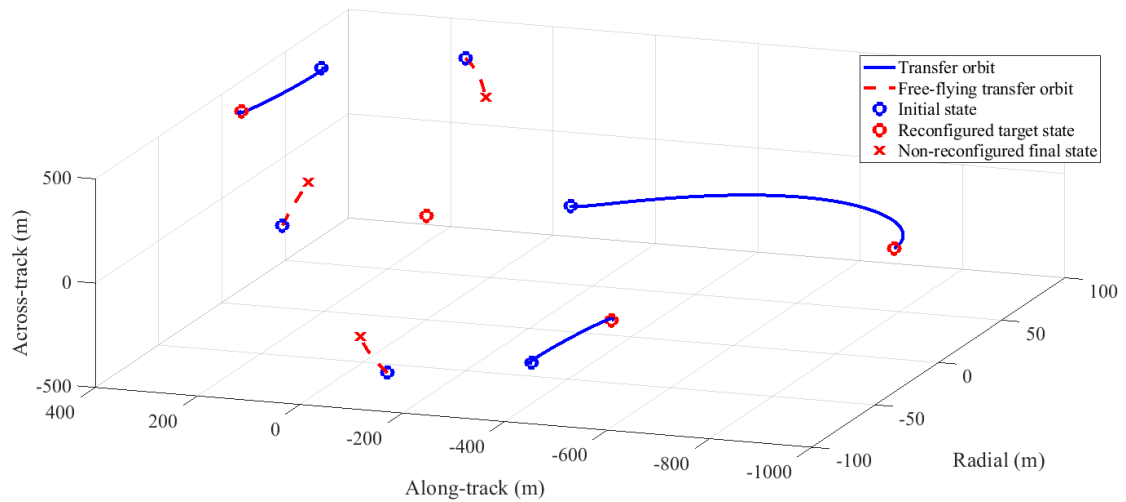


**Figure 7.22:** Trajectories partial re-configuration Optimal controller de-centralized SCP

In Figure 7.23 input control forces are reported. It is easy to see how the control forces were applied to only three spacecrafts of the previous formation (the leader does not apply correction forces since it is in the same place in both configurations). The two satellites that were reconfigured in Cross-Track Pendulum configuration exhibit similar behaviors in all three directions both in terms of trend and orders of magnitude. The satellite that has been reconfigured in Interferometric-Cartwheel configuration presents instead more intense control forces reaching saturation in the along-track direction. These trends depend very much on the initial and final configurations and it is possible to reduce the fuel consumption by reducing the distances involved.

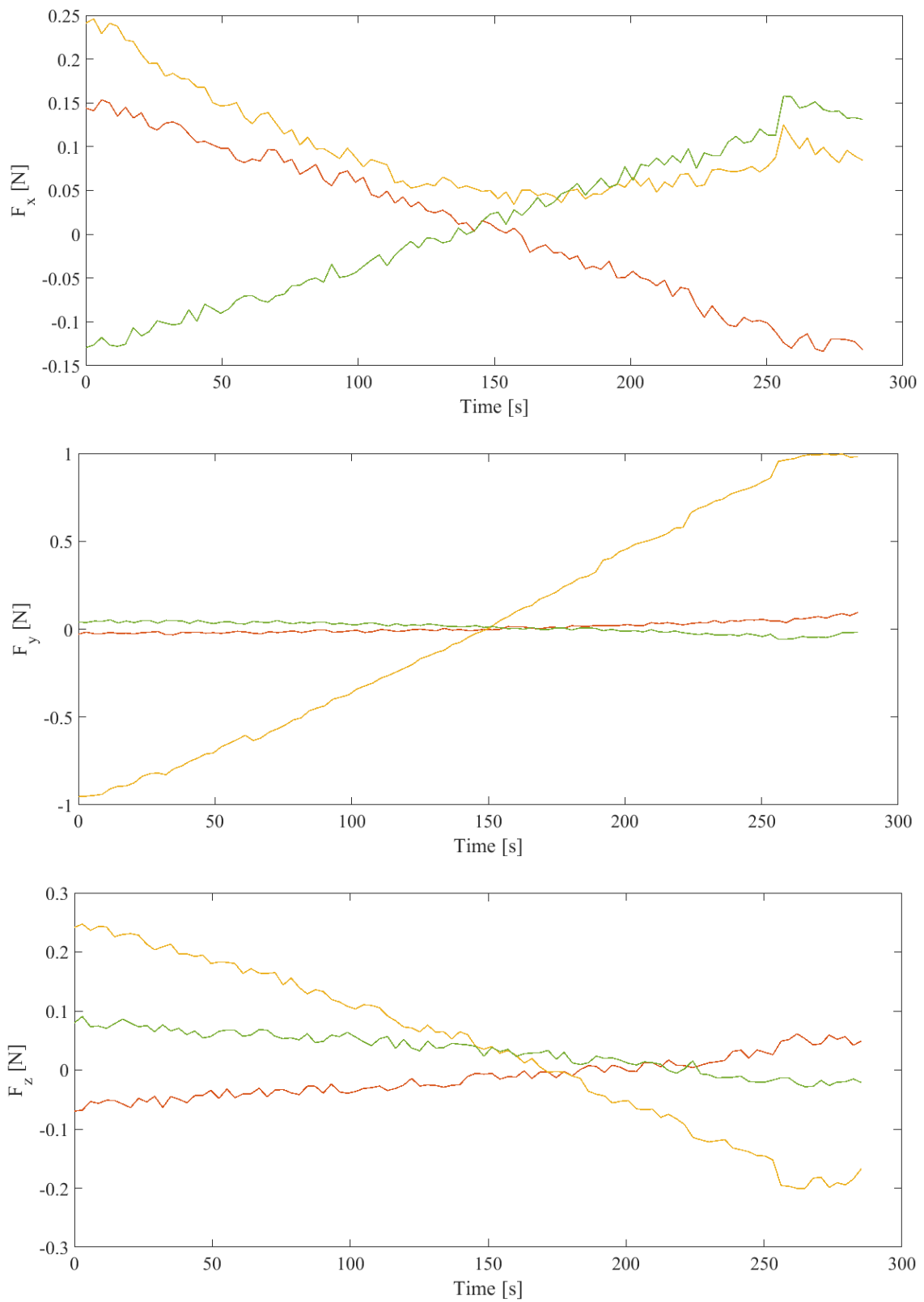


**Figure 7.23:** Actuation Forces partial re-configuration Optimal controller de-centralized SCP

| Spacecraft ID | $\Delta m$ [kg] |
|---------------|-----------------|
| 1             | 0               |
| 2             | 0.03601         |
| 3             | 0.23867         |
| 5             | 0.03916         |
| Total         | 0.31384         |

**Table 7.11:** Fuel consumption partial re-configuration

As stated in Chapter 6, Problem 8 can be also used if an optimal total re-configuration is required. In fact, it can happen that after many orbits, drifts are so high that the actual configuration is very different from the initial one. This implies that, in case we want to correct the current configuration bringing it back to the initial one, the assignment of the places that involves the re-location of the spacecraft  $i$ -th in its initial position may not be the optimal one, that is, there could be a spacecraft closer to the position  $i$ -th of the initial configuration which would use less fuel to occupy it. This is true if the spacecrafts are all the same and interchangeable.

Figure 7.24 shows the consequences of not using the optimal reassignment algorithm. After many orbits the configuration turns out to be very different from the initial one, if each satellite would be assigned to the place it had in the initial configuration, many crossings (possibility of collisions) and higher fuel consumption could occur. The optimal re-configuration algorithm allows to solve this problem by reassigning the seats in such a way that these aspects are taken into account, obtaining the trajectories shown in the previous sections.

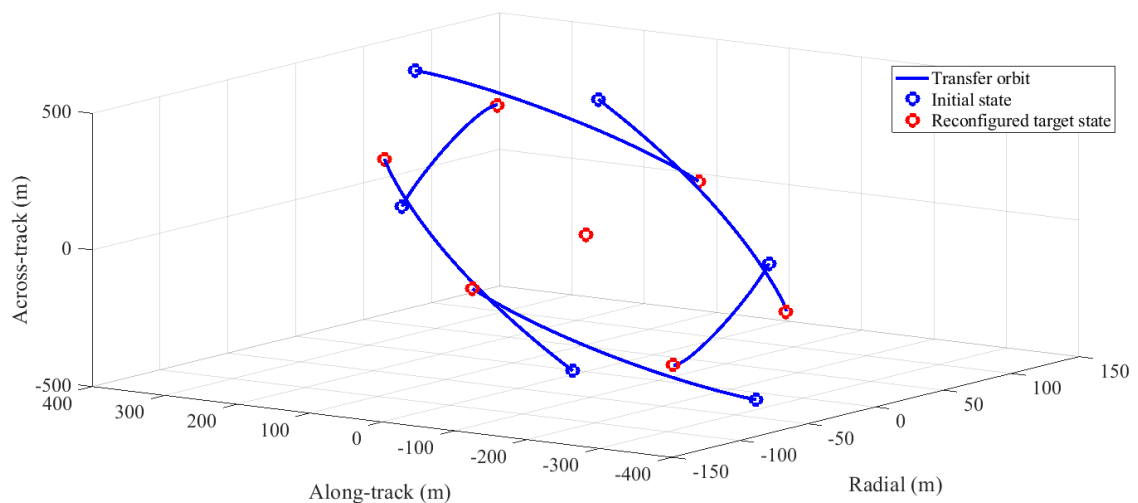


**Figure 7.24:** Trajectories drift correction non-optimal places assignment

# Chapter 8

## Conclusions and Future Work

### 8.1 Research Outcome and Discussion

This research tries to give a complete overview on formation flying. The main aspects of this kind of systems have been presented starting from the requirements the propagation model should have in order to properly deal with relative dynamics to the control of the formation by using two different controllers. Problems related to the management of such a system, like fuel consumption and computational cost, gave a definite direction to the discussion that had as main objective to present the state of the art of methods that try to mitigate such problems. In particular, the study of formation stability, which led to the synthesis of initial conditions that guarantee the smallest possible drift, is essential for a long duration missions and for a higher quality of data taken. Despite the importance of the study of stability, it has been seen that it is not sufficient to eliminate the drift of the followers with respect to the leader, so it is necessary to provide strategies for active control of the formation. There are an infinite number of possible control techniques. In this work, the attention has been brought to the Proportional Derivative controller and the Optimal controller, since each of them has characteristics useful in the case under consideration. In particular, the PD is simple to implement and does not need a lot of computing power, so it can be easily implemented in real-time systems, but unfortunately it does not optimize fuel consumption which is very important for this kind of applications. It is worth pointing out that a PID (Proportional Integral Derivative controller) is usually the most used controller in this kind of applications because of its ability to reduce any static errors in the steady-state phase to zero. In this work, the simplest PD has been adopted in order to avoid an in-depth synthesis of the integration constants of the controller, this aspect could be treated in future developments of this work. This last aspect is instead taken into account by the op-

timal control whose purpose is to calculate the control inputs in order to minimize a given objective function. Normal methods of solving a non-linear optimization problem would take too long to find the solution if computational capabilities are limited. It is for this reason that, in order to be able to implement optimal computation in autonomous systems, the problem has been convexified and finally solved in very limited time through Sequential Convex Programming. While the PD controller is intrinsically a Closed-Loop controller, optimal controller does not normally take into account possible external measures with which the boundary conditions of the problem to be solved can be updated. In order to increase its effectiveness, optimal control was periodically solved using external measures obtained from a propagation of the full non-linear dynamics with the control actions computed in the previous iteration. Both methods gave satisfying results in terms of accuracy even in cases where unmodeled perturbations and in general external disturbances act on the system. Finally, the problem of total or partial optimal re-configuration was addressed. This aspect makes this system particularly flexible and suitable for those missions that aim to take data of different types. It has been noted, as one could already imagine, that the re-configuration maneuver is usually more expensive than a simple control maneuver (i.e. Station Keeping maneuver, Collision Avoidance maneuver etc...). However, it must be underlined that this cost depends on multiple variables, first of all, the starting and final configurations and the dimensions that characterize these configurations (relative positions and velocities). It is also important to underline that the type of architecture chosen for the mission, is closely linked to the choice of algorithm for the calculation of formation control that must also be based on the type of sensors and communication system with which the formation spacecrafts are equipped.

## 8.2 Future Works

This thesis has treated the problem in its entirety in order to get an overall idea of the different steps that lead to the design of a system of the general. It is evident how several aspects can be further investigated. Other types of control could be treated in such a way as to be able to make several comparisons with the methods used in this work. This study could be done by varying the number and type of sensors on board so that a more complete picture can be obtained that considers the limitations related to physical reality, such as the visibility between satellites and the rate of information exchange between satellites.

It would be interesting to see how the system behaves when one has sensors that derive relative quantities with respect to the leader and other spacecraft, in partic-

ular how to mitigate sensor-related errors using filtering systems such as Kalman's, and especially how these estimates vary as position and number of sensors vary.

An important analysis would include the evaluation of the system performance if some of the system quantities are considered as random variables. For example, to understand what the error of the system would be if an error was made in the estimation of the mass of each satellite. Clearly, the Monte Carlo method would allow such an analysis to be carried out, but would entail a great computational cost. Other methodologies that allow an analysis of this problem would include the use of mapping through Taylor series approximations up to an arbitrary order by exploiting the results of Differential Algebra [41]. Such a methodology would also allow the optimal trajectory to be calculated in very small times if an error in the initial or final state, or any other magnitude that is part of the optimization, starts from the nominal optimal trajectory.

A very interesting study would involve Machine Learning algorithms for estimating relative position and velocity if satellites are equipped with dedicated cameras. This very recent study would be part of the more general branch called *Video-Based Autonomous Navigation* on which nowadays many researchers are developing more and more performing methods. The most critical aspect of this study would be to find a large dataset with which to train the Machine Learning model. However, the size and computational resources of the individual spacecrafts should be able to perform the required calculations, in addition it would be necessary to perform an extensive study of model interpretability so that the probability of error in the estimate is minimized.

# Bibliography

- [1] Programmazione lineare intera. <http://www.diag.uniroma1.it/~or/meccanica/cap12.pdf>.
- [2] Spacecraft orbit state. <http://gmat.sourceforge.net/docs/nightly/html/SpacecraftOrbitState.html>.
- [3] Bonnard B. and Caillaud J. Introduction to nonlinear optimal control. *Advanced Topics in Control Systems Theory*, 2006.
- [4] Tapley B.D., Watkins M.M., Ries J.C., Davis G.W., Eanes R.J., Poole S.R., Rim H.J., Schutz B.E., Shum C.K., Nerem R.S., Lerch F.J., Marshall J.A., Klosko S.M., Pavlis N.K., and Williamson R.G. The joint gravity model 3. *Journal of Geophysical Research*, 1996.
- [5] ADCS For Beginners. Earth centered inertial frame. <https://adcsforbeginners.wordpress.com/tag/earth-centred-inertial-frame/>.
- [6] Webster Cash, Stephen Kendrick, Charley Noecker, John Bally, Julia DeMarines, James Green, Phillip Oakley, Ann Shipley, Scott Benson, Steve Oleson, et al. The new worlds observer: the astrophysics strategic mission concept study. In *UV/Optical/IR Space Telescopes: Innovative Technologies and Concepts IV*, volume 7436, page 743606. International Society for Optics and Photonics, 2009.
- [7] Morgan D., Chung S., and Hadaegh F.Y. Model predictive control of swarms of spacecraft using sequential convex programming. *Journal of Guidance, Control, and Dynamics*, 37(6):1725–1740, 2014.
- [8] Morgan D., Chung S., Blackmore L., Acikmese B., Bayard D., and Hadaegh F.Y. Swarm-keeping strategies for spacecraft under  $j_2$  and atmospheric drag perturbations. *American Institute of Aeronautics and Astronautics*, 2021.

- [9] Zhang R. et al. Study of satellite shadow function model considering the overlapping parts of earth shadow and moon shadow and its application to gps satellite orbit determination. *Adv. Space Res.*, 2018.
- [10] Tassi F. and Quadrelli M.B. Lagrangian and eulerian multi-scale control of a distributed multibody robotic system. Master's thesis, Politecnico di Milano, 2018.
- [11] Fasano G. and D'Errico M. Modeling orbital relative motion to enable formation design from application requirements. *Celest Mech Dyn Astr*, pages 113–139, 2009.
- [12] Jacazio G. and Piombo B. *Meccanica applicata alle macchine*. Levrotto & Bella, 1994.
- [13] Krieger G., Moreira A., Fiedler H., Hajnsek I., Werner M., Younis M., and Zink M. Tandem-x: A satellite formation for high-resolution sar interferometry. *IEEE Transactions on Geoscience and Remote Sensing*, 2007.
- [14] Xu G. and Wang D. Nonlinear dynamic equations of satellite relative motion around an oblate earth. *Journal of Guidance, Control, and Dynamics*, Vol. 31, No. 5, pages 1521–1524, 2008.
- [15] Skinner G.K., Arzoumanian Z., Cash W.C., Gehrels N., Gendreau K.C., Gorenstein P., Krizmanic J.F., Miller M.C., Phillips J.D., Reasenberg R.D., et al. The milli-arc-second structure imager (massim): a new concept for a high angular resolution x-ray telescope. In *Space Telescopes and Instrumentation 2008: Ultraviolet to Gamma Ray*, volume 7011, page 70110T. International Society for Optics and Photonics, 2008.
- [16] Curtis H.D. *Orbital Mechanics for Engineering Students*. Elsevier - Butterworth-Heinemann, 2010.
- [17] Qureshi R. H. Cooley S. D. Hughes, S. P. and J. J. Parker. Verification and validation of the general mission analysis tool (gmat). In *AIAA/AAS astrodynamics specialist conference*, page 4151, 2014.
- [18] Sullivan J., Grimberg S., and D'Amico S. Comprehensive survey and assessment of spacecraft relative motion dynamics models. *Journal of Guidance, Control, and Dynamics*, pages 1837–1859, 2017.
- [19] Kechichian J.A. Motion in general elliptic orbit with respect to a dragging and precessing coordinate frame. *The Journal of the Astronautical Sciences*, pages 25–45, 1998.

- [20] Alfriend K., Vadali S.R., Gurfil P., How J., and Breger L. *Spacecraft Formation Flying. Dynamics, Control and Navigation*. 2010.
- [21] Carrer L., Bovolo F., and Bruzzone L. Distributed radar sounder: A novel concept for subsurface investigations using sensors in formation flight. *IEEE Transactions on Geoscience and Remote Sensing, Vol. 57, No. 12*, 2019.
- [22] Grant M. and Boyd S. Cvx: Matlab software for disciplined convex programming, version 2.1, 2014.
- [23] Singgih Pulukadang M. <https://www.slideshare.net/AmitRastogi11/synthetic-aperture-radar>.
- [24] Szmuk M. and Acikmese B. Successive convexification for 6-dof mars rocket powered landing with free-final-time. *2018 AIAA Guidance, Navigation, and Control Conference, Kissimmee, FL*, 2018.
- [25] Szmuk M., Acikmese B., Andrew W. Berning Jr., and Huntington G. Successive convexification for fuel-optimal powered landing with aerodynamic drag and non-convex constraints. *2016 AIAA Guidance, Navigation, and Control Conference, San Diego, CA*, 2016.
- [26] Valli M., Armellin R., Di Lizia P., and Lavagna M.R. Nonlinear mapping of uncertainties in celestial mechanics. *Journal of Guidance, Control, and Dynamics, Vol. 36, No. 1*, 2013.
- [27] Quadrelli M.B. Modeling and dynamics of tethered formations for space interferometry. *11th AAS/AIAA Space Flight Mechanics Meeting, Santa Barbara, California, Oct. 2000*, 2000.
- [28] Quadrelli M.B. Modeling and dynamics of tethered formations for space interferometry. *Paper AAS 01-231*, 2001.
- [29] Quadrelli M.B. Dynamics and control of novel orbiting formations with internal dynamics. *Journal of the Astronautical Sciences, Vol. 51, No.3, pp.319-337*, 2003.
- [30] Quadrelli M.B. Effect of distributed rod and string flexibility on formation dynamic stability. *Journal of the Astronautical Sciences, Vol. 51, No.3, pp.339-357*, 2003.
- [31] Quadrelli M.B., Ono M., and Jain A. Modeling of active tether system concepts for planetary exploration. *Acta Astronautica*, 2016.

- [32] Quadrelli M.B., Basinger S., Palacios D., and Arumugam D. Control of granular imaging systems. *AIAA SPACE 2015 Conference and Exposition*, 2015.
- [33] Montenbruck O., Lutz F., and Gill E. *Satellite Orbits: Model, Methods and Applications*. Springer, 2000.
- [34] Di Lizia P., Armellin R., Morselli A., and Bernelli-Zazzera F. High order optimal feedback control of space trajectories with bounded control. *Acta Astronautica*, 2013.
- [35] Di Lizia P., Armellin R., Bernelli-Zazzera F., and Berz M. High order optimal control of space trajectories with uncertain boundary conditions. *Acta Astronautica*, 2013.
- [36] Gurfil P. and Kholoshevnikov K.V. Manifolds and metrics in the relative spacecraft motion problem. *Journal of Guidance, Control, and Dynamics*, vol. 29, no. 4, pp. 1004–1010, 2006.
- [37] Lopez-Dekker P., Krieger G., and Moreira A. *Multistatic Radar Systems*. Springer, 2012.
- [38] Hughes P.C. *Spacecraft Attitude Dynamics*. John Wiley, 1986.
- [39] Mazouz R. and Quadrelli M.B. Convex optimization guidance for precision landing on titan. *AIAA Scitech 2021 Forum*, 2021.
- [40] Mazouz R., Quadrelli M.B., and Beauchamp R. Dynamics and optimal control for free-flight and tethered arrays in low earth orbit. 2021.
- [41] Morselli A. Wittig A. Massari M. Di Lizia P. Armellin R. Rasotto, M. and G. Ortega. Differential algebra space toolbox for nonlinear uncertainty propagation in space dynamics. 2016.
- [42] Sharing Earth Observation Resources. Prisma (prototype research instruments and space mission technology advancement). <https://earth.esa.int/web/eoportal/satellite-missions/p/prisma-prototype>.
- [43] Bevilacqua S. and Quadrelli M.B. Model derivation and dynamics propagation of multi-body tethered systems. Master’s thesis, Politecnico di Milano, 2018.
- [44] Sarno S., Guo G., D’Errico M., and Gill E. A guidance approach to satellite formation reconfiguration based on convex optimization and genetic algorithms. *Adv. Space Res.*, 2020.

- [45] Segal S., Carmi A., and Gurfil P. Stereovision-based estimation of relative dynamics between noncooperative satellites: Theory and experiments. *IEEE Transactions on Control Systems Technology*, 2013.
- [46] Segal S. and Gurfil P. Effect of kinematic rotation-translation coupling on relative spacecraft translational dynamics. *Journal of Guidance, Control, and Dynamics*, vol. 32, no. 3, pp. 1045–1050, 2009.
- [47] Schuldt T. An optical readout for the lisa gravitational reference sensor. 2010.
- [48] Gim D. W. and Alfriend K.T. State transition matrix of relative motion for the perturbed noncircular reference orbit. *Journal of Guidance, Control, and Dynamics* Vol. 26, No. 6, 2003.
- [49] Zhong W. and Gurfil P. Mean orbital elements estimation for autonomous satellite guidance and orbit control. *J. of Guidance, Control, and Dynamics*, vol. 36, no. 6, pp. 1624–1641, 2013.
- [50] Clohessy W.H. and Wiltshire R.S. Terminal guidance system for satellite rendezvous. *Journal of the Aerospace Sciences*, 27(9):653–658, 1960.
- [51] Wikiwand. Magnetospheric multiscale mission. [https://www.wikiwand.com/en/Magnetospheric\\_Multiscale\\_Mission](https://www.wikiwand.com/en/Magnetospheric_Multiscale_Mission).
- [52] Yue X., Wang X., and Dai H. A simple time domain collocation method to precisely search for the periodic orbits of satellite relative motion. *Mathematical Problems in Engineering*, 2014, 2014.
- [53] Xing Y., Cao X., Zhang S., Guo H., and Wang F. Relative position and attitude estimation for satellite formation with coupled translational and rotational dynamics. *Acta Astronautica*, 2010.

# Appendix A

## Model Validation

This appendix is intended to give an idea of the level of accuracy of the dynamic propagation model that was used for all simulations, by comparing it with NASA General Mission Analysis Tool (GMAT). In particular, the effects of the perturbations will be seen individually in order to verify their absolute goodness, in fact, in the case in which we put in a single graph the effect of  $J_2$  and solar pressure, the second would not be visible since its effect is of some order of magnitude less than the first. In any case, only the effects on the semi-major axis, eccentricity and inclination are shown to avoid an excessive number of images. The only remark involves the Drag perturbation. In fact, the GMAT tool does not present the possibility to use the Harris-Priester density model, so the comparison has been made with the Jacchia model. It is possible to see that although the density models are different, the difference between the two models remains very small. In Figures. A.1, A.2,A.3,A.4,A.5, the comparisons of the following cases are given:

- Only Gravity Potential (up to grade 4 order 4).
- Only Drag
- Only Solar Pressure
- Only Third-body perturbation (Sun and Moon)

The initial conditions of the satellite are those reported in Table. 5.1.

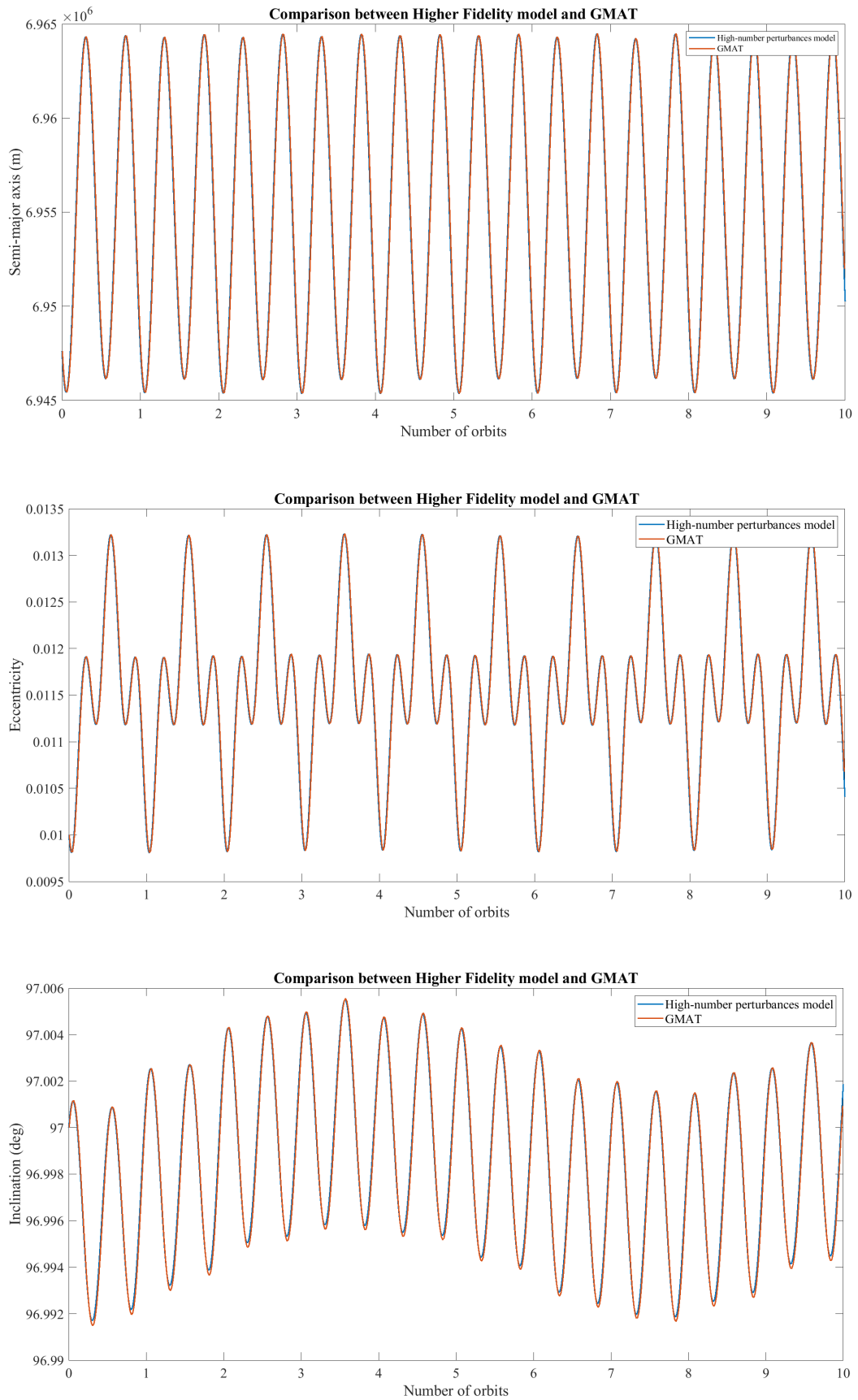


**Figure A.1:** GMAT comparison, Gravitational Potential (up to grade 4 order 4)

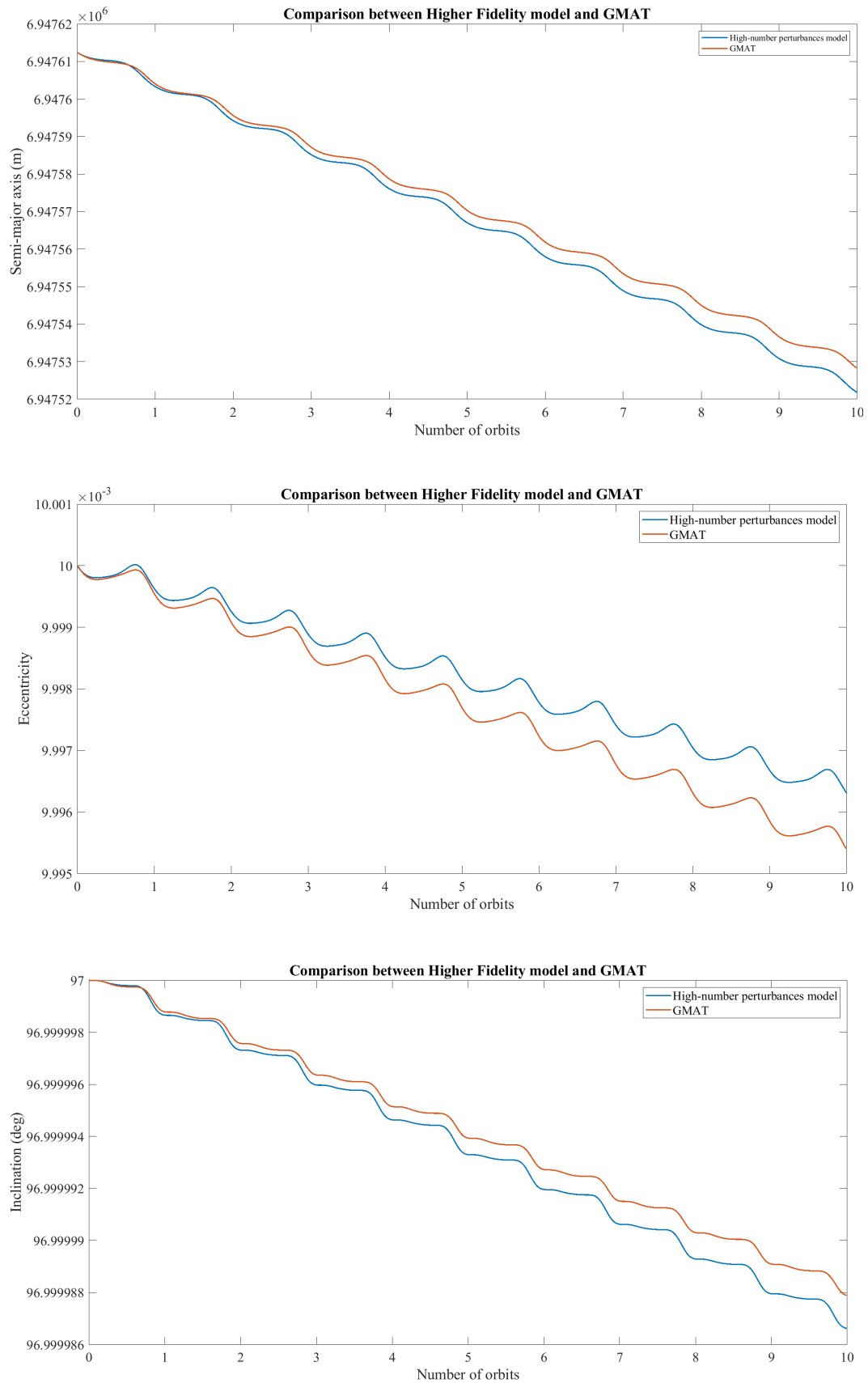


Figure A.2: GMAT comparison, Drag (*HarrispriestervsJacchia*)

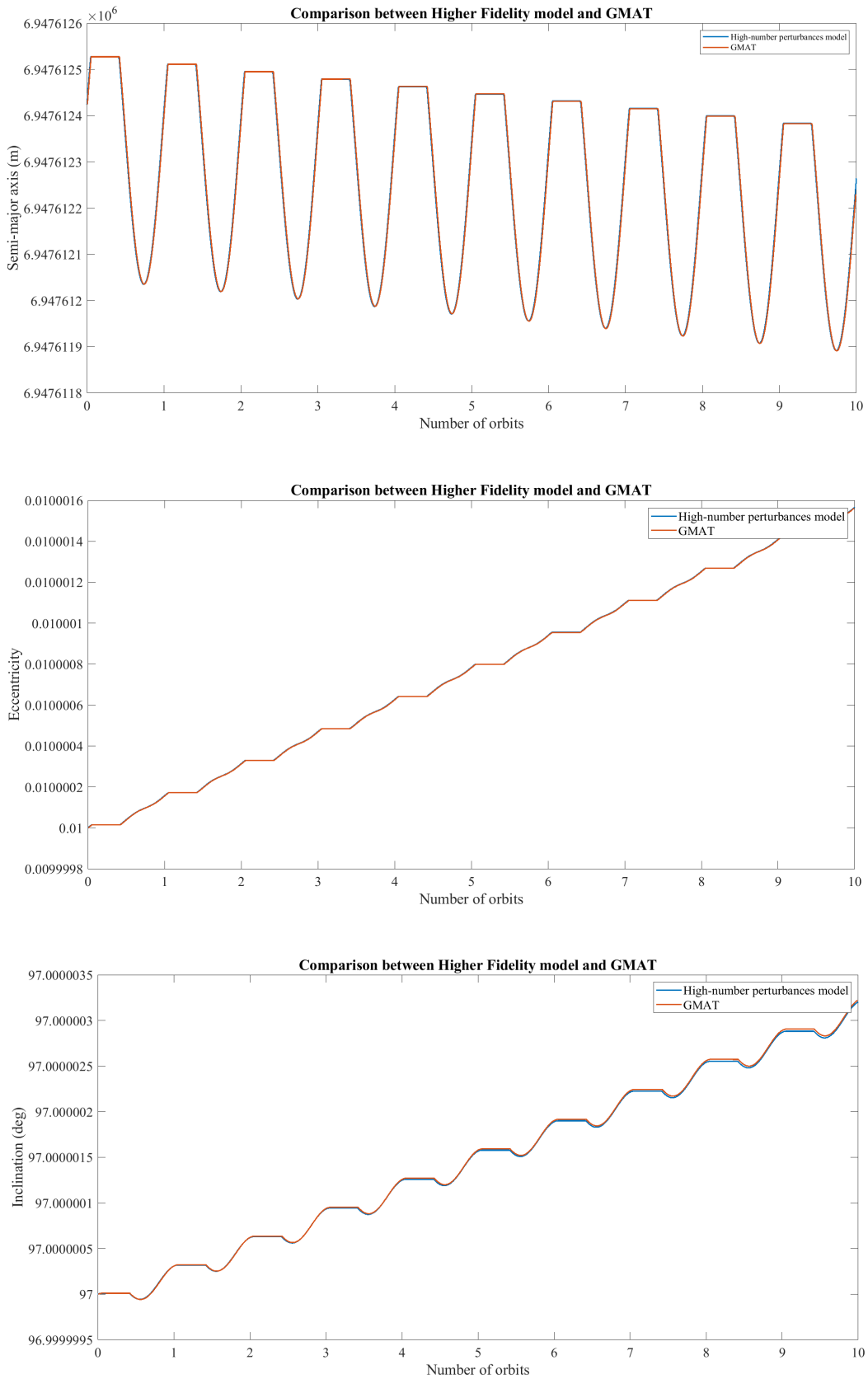


Figure A.3: GMAT comparison, Solar Pressure

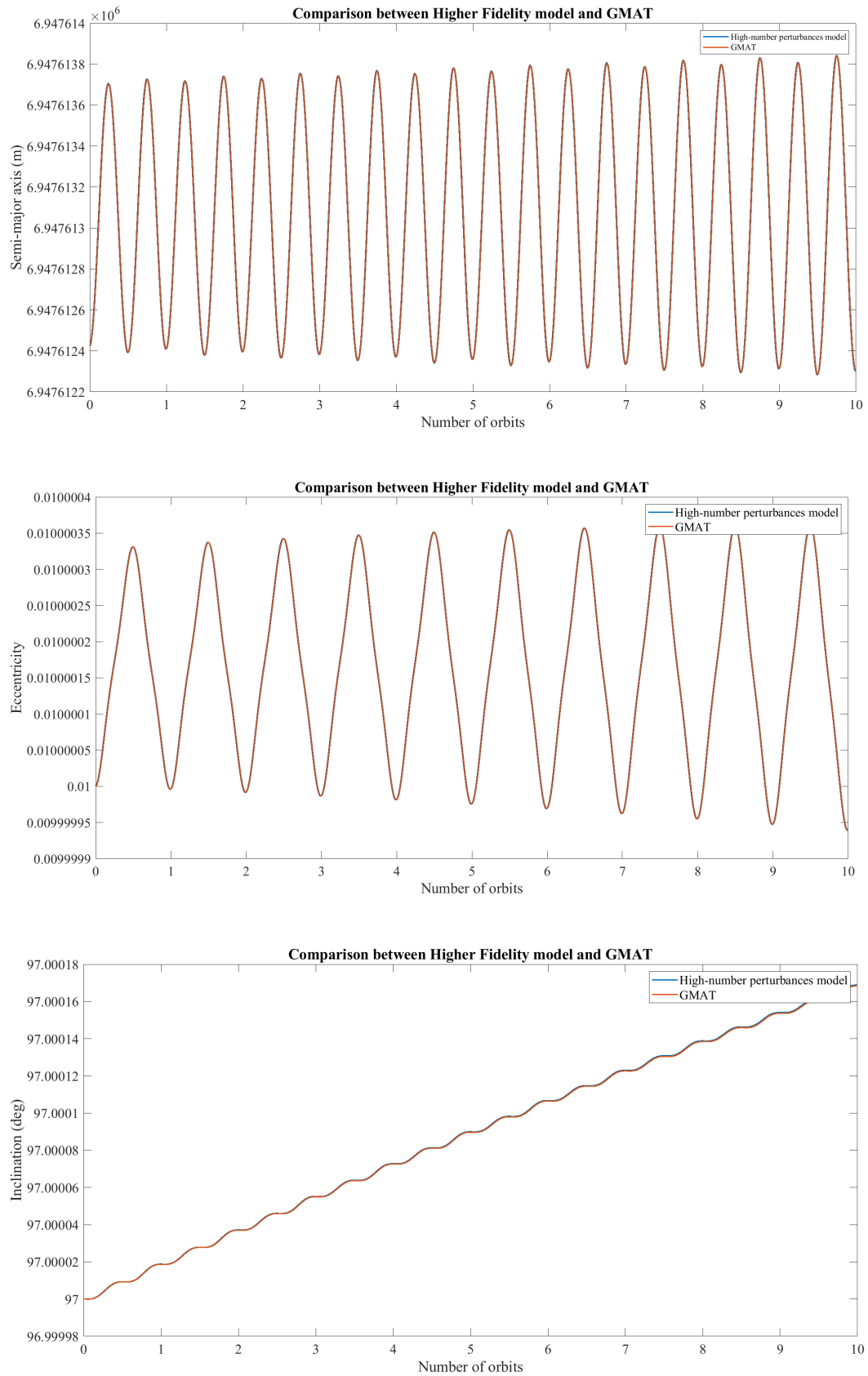


Figure A.4: GMAT comparison, Third-body (Moon)

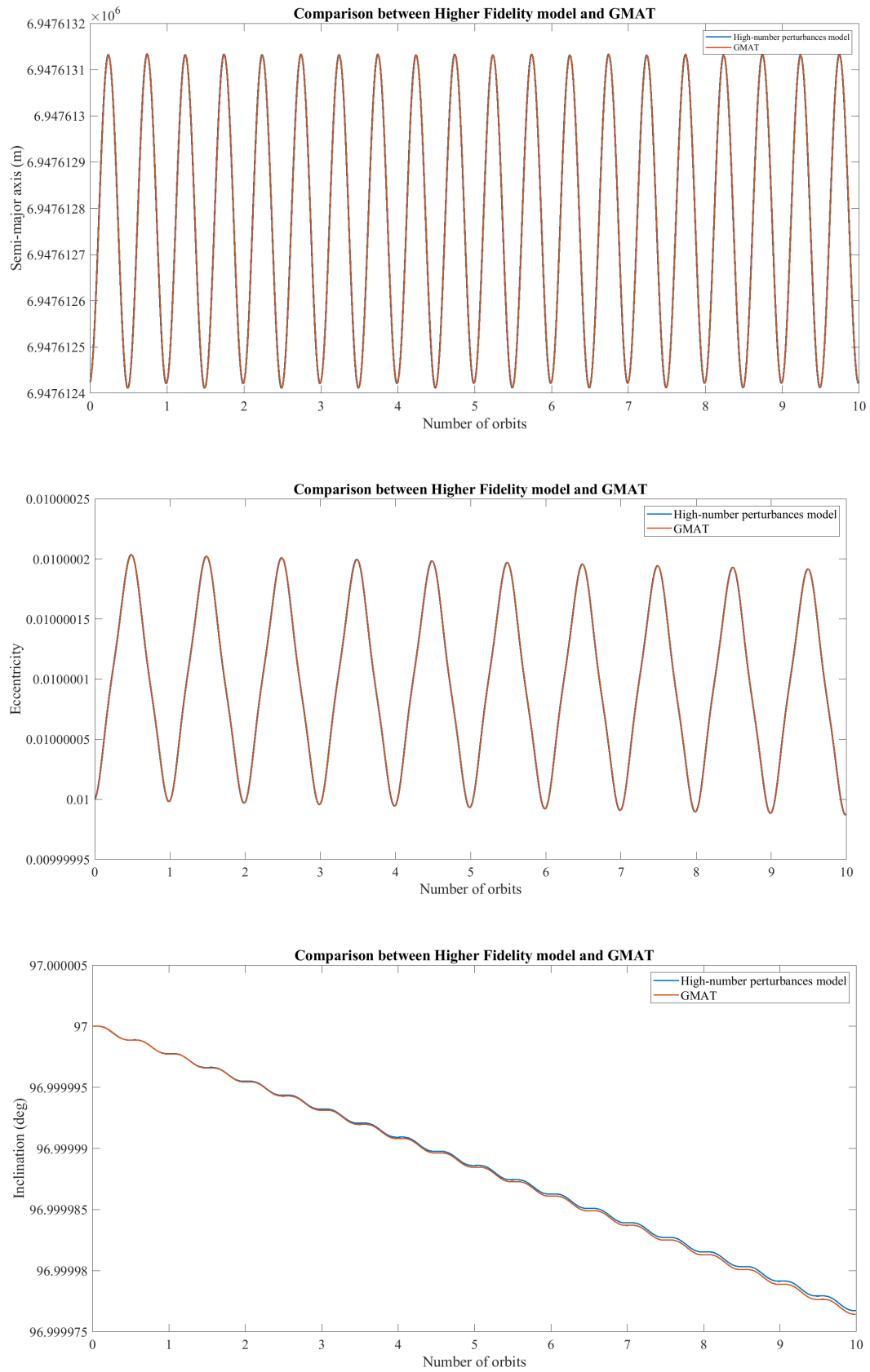


Figure A.5: GMAT comparison, Third-body (Sun)

# Appendix B

## Relative Motion under $J_2$ perturbation

Satellite motion around an oblate Earth has analytical solution. Considering a spacecraft subject only to  $J_2$  perturbation, its motion can be described through the following equations [14]

$$\begin{aligned} \dot{r} &= v_x \\ \dot{v}_x &= -\frac{\mu}{r^2} + \frac{h^2}{r^3} - \frac{k_{J_2}}{r^4} (1 - 3s_i^2 s_\theta^2) \\ \dot{h} &= -\frac{k_{J_2} s_i^2 s_{2\theta}}{r^3} \\ \dot{\theta} &= \frac{h}{r^2} + \frac{2k_{J_2} c_i^2 s_\theta^2}{hr^3} \\ \dot{i} &= -\frac{k_{J_2} s_{2i} s_{2\theta}}{2hr^3} \\ \dot{\Omega} &= -\frac{2k_{J_2} c_i s_\theta^2}{hr^3} \end{aligned} \tag{B.1}$$

where  $s_x = \sin x$ ,  $c_x = \cos x$ ,  $k_{J_2} = \frac{3J_2 \mu R_e^2}{2}$ ,  $R_e$  is the radius of the Earth,  $h$  is the angular momentum of the spacecraft,  $r$  is its distance from the center of the Earth,  $v_x$  is the radial velocity,  $i$  the inclination of the orbit,  $\theta$  the argument of latitude of the orbit and  $\Omega$  the RAAN. Equations. B.1 have been used only to propagate the orbit of the LVLH frame. The main reason is that, for this simple case, analytical solutions for angular velocity and acceleration of the frame subject to  $J_2$  exist, if we write the LVLH components of these quantities the following equations hold

$$\begin{aligned}
 \omega_x &= -\frac{k_{J2}s_2i s_\theta}{hr^3} \\
 \omega_y &= 0 \\
 \omega_z &= \frac{h}{r^2} \\
 \alpha_x = \dot{\omega}_x &= -\frac{k_{J2}s_2i c_\theta}{r^5} + \frac{3v_x k_{J2}s_2i s_\theta}{r^4 h} - \frac{8k_{J2}^2 s_i^3 c_i s_\theta^2 c_\theta}{r^6 h^2} \\
 \dot{\omega}_y &= 0 \\
 \alpha_z = \dot{\omega}_z &= -\frac{2hv_x}{r^3} - \frac{k_{J2}s_i^2 s_2\theta}{r^5}
 \end{aligned} \tag{B.2}$$

Equations. B.2 prove necessary to solve Equations. 4.15 describing relative motion wrt the LVLH frame.

# Appendix C

## Centralized Optimal Problem

In the centralized strategy, the translational problem is very similar to the decentralized case. The difference is that, in this case the optimization variable comprises all the spacecrafts of the formation. As done in Chapter. 6, if we call  $\mathbf{Z}_i = [(\mathbf{x}_i^0)^T, \dots, (\mathbf{x}_i^K)^T, (\mathbf{u}_i^0)^T, \dots, (\mathbf{u}_i^{K-1})^T]^T$  the  $i$ -th optimization variable referring to the  $i$ -th spacecrafts, the centralized problem can be reformulated using the new optimization variable defined as  $\mathbf{Z} = [\mathbf{Z}_1^T, \dots, \mathbf{Z}_N^T]^T$ , being  $N$  the number of spacecrafts. It is clear that this approach greatly increases the number of elements to be optimized, but the speed of convex programming ensures that this does not result in an excessive increase in the time required for resolution. The centralized problem just reduces to a concatenation of all constraints of each spacecraft but with a different cost-function. In fact, the main goal of this approach is that of optimizing the overall consumption as a formation, this can be done by using the following cost-function  $\min_{[\mathbf{u}_1, \dots, \mathbf{u}_N]} \sum_{i=1}^N \sum_{k=0}^{K-1} \|\mathbf{u}_i^k\|_2$ . The optimization problem is summarized as follows

---

**Problem** *Translational case, Centralized Convex Optimal Control*

$$\min_{[\mathbf{u}_1, \dots, \mathbf{u}_N]} \sum_{i=1}^N \sum_{k=0}^{K-1} \|\mathbf{u}_i^k\|_2$$

subject to

$$\begin{aligned} \dot{\mathbf{x}}_i^{k+1} &= A_i^k \mathbf{x}_i^k + B_i^k \mathbf{u}_i^k + c_i^k & k = 0, \dots, K-1 \quad i = 1, \dots, N \\ \|\mathbf{u}_i^k\|_2 &\leq U_{\max} & k = 0, \dots, K-1 \quad i = 1, \dots, N \\ (\bar{\mathbf{x}}_i^k - \bar{\mathbf{x}}_j^k)^T C^T C (\mathbf{x}_i^k - \mathbf{x}_j^k) &\geq R_{\text{col}} \|C (\bar{\mathbf{x}}_i^k - \bar{\mathbf{x}}_j^k)\|_2 & k = 0, \dots, K \quad i = 1, \dots, N \\ && j = 1, \dots, N \quad j \neq i \\ \mathbf{x}_i^0 &= \mathbf{x}_{i,0} & i = 1, \dots, N \\ \mathbf{x}_i^K &= \mathbf{x}_{i,f} & i = 1, \dots, N \end{aligned}$$

---

# Appendix D

## Test case: Optimal control high-number of satellites

For completeness, in this section a case of drift correction maneuver through Optimal control de-centralized SCP strategy of 80 satellites without unmodeled perturbation is discussed. The simulation involves a Helix configuration in the same manner as presented in Chapter 7. In this case, the final parameters of the helix are reported in Table.D.2 which shows how the quantities  $a \cdot \delta i$  and  $a \cdot \delta e$  have been increased in order to take into account the high number of satellites that would otherwise be too close. The parameters used for Optimal control algorithm are summarized in Table. D.1.  $K$  has been reduced in order to respect RAM limit imposed by MATLAB and to improve computational speed. Figure. D.1 shows the trajectories followed by the spacecrafts while control forces are reported in Figure. D.4. For completeness, also the convergence in position and velocities are reported in Figures. D.2 and D.3. Fuel consumption is instead shown in Table.D.3. The Optimal control with SCP allows to obtain results even in cases where the formation is composed of a high number of satellites. It should be noted, however, that in the centralized case, as the number of satellites increases, more computing power is required, in such cases a de-centralized architecture should be preferred despite the higher fuel consumption.

|                              |                        |  |
|------------------------------|------------------------|--|
| Final time                   | $t_f$                  | $0.05T_0$ s                                  |
| Number of points             | $K$                    | 20   |
| Stopping criterion           | $\epsilon$             | $10^{-2}$                                    |
| Minimum distance             | $R_{col}$              | 5 m  |
| Initial guess trajectories   | $\bar{\mathbf{x}}_i^k$ | free-flying leader trajectory $\forall i, k$ |
| Initial guess control inputs | $\bar{\mathbf{u}}_i^k$ | 0 $\forall i, k$                             |

**Table D.1:** SCP simulation paramters

|                    |       |
|--------------------|-------|
| $a \cdot \delta i$ | 200 m |
| $a \cdot \delta e$ | 800 m |
| $\alpha_1$         | 9°    |
| $N$                | 80    |

**Table D.2:** Helix final parameters for drift correction 80 satellites simulation.

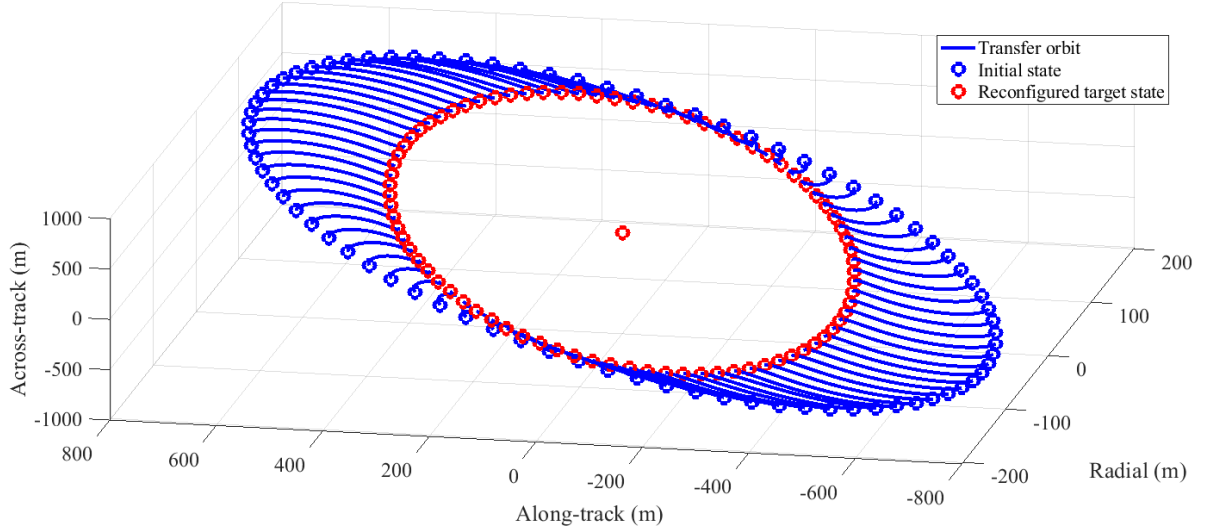


**Figure D.1:** Trajectories 80 satellites Optimal controller de-centralized SCP

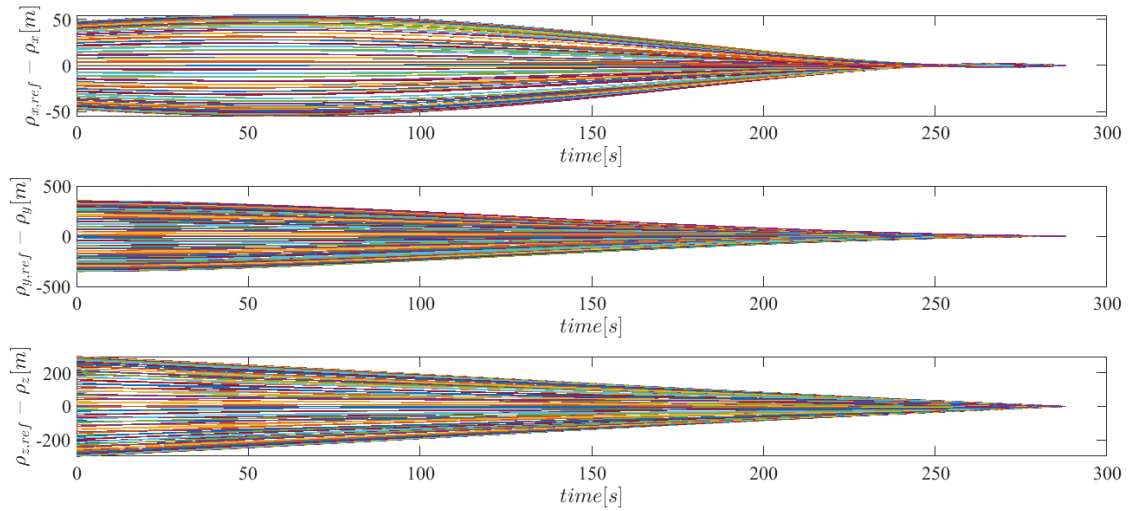


**Figure D.2:** Position errors history drift correction 80 satellites Optimal controller de-centralized SCP

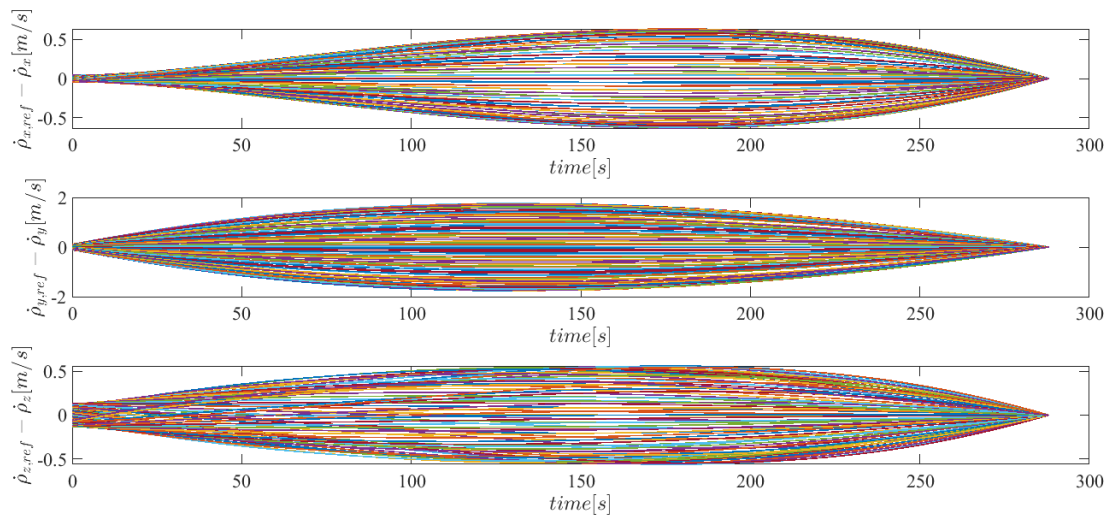


**Figure D.3:** Velocity errors history drift correction 80 satellites Optimal controller decentralized SCP

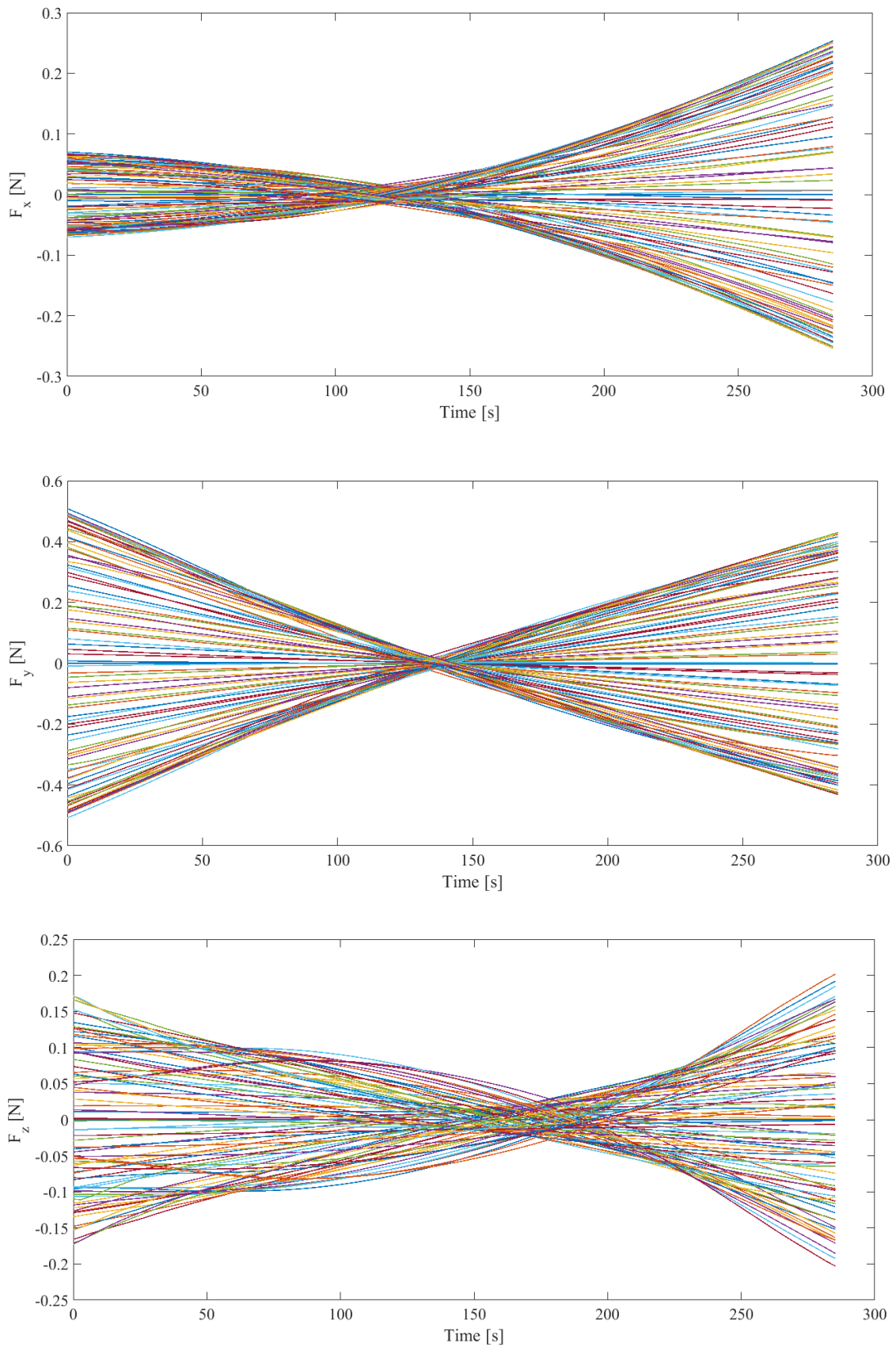


**Figure D.4:** Actuation Forces drift correction 80 satellites Optimal controller decentralized SCP

| Case       | $\Delta m_{tot}$ [kg] | $\Delta m_{av}$ [kg] | $\Delta m_{\%av}$ |
|------------|-----------------------|----------------------|-------------------|
| OC dec SCP | 5.6743                | 0.07092875           | 0.35464375        |

**Table D.3:** Fuel consumption summary drift corrections 80 satellites simulations